Doctorate program in Biomedical Engineering

Department of electronic engineering

Temporal and frequency differentiation of healthy and pathological lung tissue through minimally invasive electrical impedance spectroscopy.

Doctoral Thesis by compendium of publications

Georgina Company Se

May 2023

Directors

Dr. Eng. Lexa Nescolarde Selva

Dr. Eng. Ramon Bragós Bardia

ABSTRACT

Respiratory diseases, along with heart diseases, are the most prevalent in the world. The acquisition of lung samples, acquired through different procedures through bronchoscopy, is essential for a correct diagnosis of the disease. This sampling is relatively simple for central lesions of the bronchial trunk. However, for peripheral lesions it is not so easy to access the sample and ensure that it is taken at the point previously identified using medical imaging techniques. By measuring bioimpedance, which allows obtaining the passive electrical properties of biological tissue, it is intended to evaluate differences in lung tissue according to its state (cancerous, fibrotic, pneumonic, healthy or emphysematous) in order to confirm the appropriate location for taking pathological samples, such as performing a biopsy. In order to obtain the highest differentiation between the different states of the tissue, first of all a study is carried out on the measurement method that allows a greater differentiation between healthy tissue and bronchial tissue. The possibility of implementing the 3-electrode method to replace the 4-electrode method, used in preliminary measurements, is evaluated, since it provides practical advantages. Subsequently, due to the great dispersion of the measurements within the same type of tissue among the different patients, the implementation of a calibration method, already used for cardiac applications, is studied. This method consists of using a measurement made in the main bronchus to calibrate the measurements of the lung parenchyma, thus reducing the effect of geometric differences between patients. Next, the thesis presents the global study on the differentiation between the different types of lung tissue with a population of 102 patients on whom 116 measurements have been performed. Finally, the implementation of machine learning classification algorithms for the real-time classification of measurements is studied in a complementary way in order to help in the correct location of the bronchoscope to take samples of pathological tissue, thus improving the efficiency of bronchoscopy, with the limitations of the low number of measurements. The results of the different studies show that the 3-electrode measurements improve the differentiation and/or separation between tissues compared to the 4-electrode method. In turn, the calibration of the measurements using a sample taken from the bronchus decreases the intragroup dispersion and, consequently, increases the intergroup separation, which improves the differentiation capacity. On the other hand, the differentiation of the tissues (using the 3-electrode method and after the subsequent

calibration of the measurements) evaluating the two most discriminatory frequencies, shows significant differences between those pathologies that entail an increase in tissue density (neoplasm, fibrosis and pneumonia) and those tissues that carry a greater amount of air in the lungs compared to the previous ones and/or destruction of tissue (healthy, emphysema). Thus, significant differences are found in the four impedance parameters analyzed [module ($|Z|$), phase angle (PA), resistance (R) and reactance (Xc)] between: neoplasm and pneumonia ($p < 0.05$); neoplasm and healthy tissue ($p < 0.001$); neoplasm and emphysema ($p < 0.001$); fibrosis and healthy tissue ($p < 0.001$) and pneumonia and healthy tissue ($p < 0.01$). There are also significant differences in $|Z|$, R and Xc between fibrosis and emphysema ($p < 0.05$) and in $|Z|$ and R between pneumonia and emphysema ($p < 0.05$). Finally, after the implementation of different classification algorithms, the results show great accuracy when it comes to classifying and detecting a sample of neoplasm tissue, and allow separating some pathologies not detected with classical statistical methods. In conclusion, the implementation of bioimpedance measurements through bronchoscopy can improve clinical diagnosis, since it is capable of discriminating between different types of tissue in a minimally invasive way. However, for the combined use with Artificial Intelligence techniques, the number of measures should be increased for a greater training of the algorithms and the possible implementation in the interventional pulmonology units of the departments of respiratory medicine.

RESUMEN

Las enfermedades respiratorias, junto con las enfermedades cardíacas, son las más prevalentes en el mundo. La adquisición de muestras pulmonares, adquiridas mediante distintos procedimientos a través de broncoscopia, es esencial para un correcto diagnóstico de la enfermedad. Este muestreo es relativamente sencillo para lesiones centrales del tronco bronquial. Sin embargo, para las lesiones periféricas no es tan sencillo acceder a la muestra y asegurar que se toma en el punto previamente identificado mediante técnicas de imagen médica. Mediante la medición de bioimpedancia, que permite obtener las propiedades eléctricas pasivas del tejido biológico, se pretende evaluar diferencias en el tejido pulmonar de acuerdo con su estado (canceroso, fibrótico, neumónico, sano o enfisematoso) con la finalidad de confirmar la localización adecuada para la toma de muestras patológicas, tales como la realización de una biopsia. Con el fin de obtener la mayor diferenciación entre los distintos estados del tejido, en primer lugar se realiza un estudio sobre el método de medida que permite una mayor diferenciación entre tejido sano y tejido bronquial. Se evalúa la posibilidad de implementar el método de 3-electrodos para reemplazar al de 4-electrodos, utilizado en mediciones preliminares, ya que aporta ventajas de tipo práctico. Posteriormente, debido a la gran dispersión de las medidas dentro de un mismo tipo de tejido entre los distintos pacientes, se estudia la implementación de un método de calibración, ya usado para aplicaciones cardíacas. Este método consiste en la utilización de una medida realizada en el bronquio principal para calibrar las medidas del parénquima pulmonar, reduciendo así el efecto de las diferencias geométricas entre pacientes. A continuación, la tesis presenta el estudio global sobre la diferenciación entre los distintos tipos de tejido pulmonar con una población de 102 pacientes sobre los que se han llevado a cabo 116 medidas. Finalmente, se estudia, de forma complementaria, la implementación de algoritmos de clasificación de machine learning para la clasificación en tiempo real de las medidas con el fin de ayudar en la correcta localización del broncoscopio para tomar muestras del tejido patológico, mejorando así la eficacia de la broncoscopia, con las limitaciones propias del bajo número de medidas.

Los resultados de los distintos estudios muestran que las medidas a 3 electrodos mejoran la diferenciación y/o separación entre tejidos respecto al método de 4 electrodos. A su vez, la calibración de las medidas usando una muestra tomada en el bronquio disminuye

la dispersión intragrupo y, en consecuencia, aumenta la separación intergrupal, lo que mejora la capacidad de diferenciación. Por otro lado, la diferenciación de los tejidos, (empleando el método de 3 electrodos y tras la posterior calibración de las medidas) evaluando las dos frecuencias más discriminatorias, muestra diferencias significativas entre aquellas patologías que conllevan un aumento en la densidad del tejido (neoplasia, fibrosis y neumonía) y aquellos tejidos que conllevan una mayor cantidad de aire en los pulmones respecto a los anteriores y/o destrucción de tejido (sano, enfisema). De esta forma, se encuentran diferencias significativas en los cuatro parámetros de impedancia analizados [módulo ($|Z|$), fase (PA), resistencia (R) y reactancia (Xc)] entre: neoplasia y neumonía ($p < 0.05$); neoplasia y tejido sano ($p < 0.001$); neoplasia y enfisema ($p < 0.001$); fibrosis y tejido sano ($p < 0.001$) y neumonía y tejido sano ($p < 0.01$). También se encuentran diferencias significativas en $|Z|$, R y Xc entre fibrosis y enfisema ($p < 0.05$) y en $|Z|$ y R entre neumonía y enfisema ($p < 0.05$).

Por último, tras la implementación de diferentes algoritmos de clasificación, los resultados muestran una gran eficacia a la hora de clasificar y detectar una muestra de tejido neoplásico, y permiten separar algunas patologías no detectadas con métodos estadísticos clásicos.

En conclusión, la implementación de mediciones de bioimpedancia mediante broncoscopia, puede mejorar el diagnóstico clínico, puesto que es capaz de discriminar entre distintos tipos de tejido de forma mínimamente invasiva. Sin embargo, para el uso combinado con técnicas de Inteligencia Artificial, se debe aumentar la muestra de las medidas para un mayor entrenamiento de los algoritmos y la posible implementación en las unidades de neumología intervencionista de los departamentos de medicina respiratoria.

RESUM

Les malalties respiratòries, juntament amb les malalties cardíaques, són les més prevalents al món. L'adquisició de mostres pulmonars, adquirides mitjançant diferents procediments a través de broncoscòpia, és essencial per a un diagnòstic correcte de la malaltia. Aquest mostreig és relativament senzill per a lesions centrals del tronc bronquial. Tot i això, per a les lesions perifèriques no és tan senzill accedir a la mostra i assegurar que es pren en el punt prèviament identificat mitjançant tècniques d'imatge mèdica. Mitjançant la mesura de bioimpedància, que permet obtenir les propietats elèctriques passives del teixit biològic, es pretén avaluar diferències en el teixit pulmonar d'acord amb el seu estat (cancerós, fibròtic, pneumònic, sa o emfisematós) amb la finalitat de confirmar la localització adequada per a la presa de mostres patològiques, com ara la realització d'una biòpsia. Per tal d'obtenir la diferenciació més gran entre els diferents estats del teixit, en primer lloc es realitza un estudi sobre el mètode de mesura que permet una major diferenciació entre teixit sa i teixit bronquial. S'avalua la possibilitat d'implementar el mètode de 3-elèctrodes per reemplaçar el de 4-elèctrodes, utilitzat en mesures preliminars, ja que aporta avantatges de tipus pràctic. Posteriorment, a causa de la gran dispersió de les mesures dins un mateix tipus de teixit entre els diferents pacients, s'estudia la implementació d'un mètode de calibratge ja utilitzat per a aplicacions cardíaques. Aquest mètode consisteix en la utilització d'una mesura realitzada al bronqui principal per calibrar les mesures del parènquima pulmonar, reduint així l'efecte de les diferències geomètriques entre pacients. Tot seguit, la tesi presenta l'estudi global sobre la diferenciació entre els diferents tipus de teixit pulmonar amb una població de 102 pacients sobre els quals s'han dut a terme 116 mesures. Finalment, s'estudia, de forma complementària, la implementació d'algoritmes de classificació de Machine Learning per a la classificació en temps real de les mesures per tal d'ajudar a la correcta localització del broncoscopi per prendre mostres del teixit patològic, millorant així l'eficàcia de la broncoscòpia, amb les limitacions pròpies del baix nombre de mesures. Els resultats dels diferents estudis mostren que les mesures a 3 elèctrodes milloren la diferenciació i/o separació entre teixits respecte al mètode de 4 elèctrodes. Alhora, el calibratge de les mesures utilitzant una mostra presa en el bronqui disminueix la dispersió intragrup i, en conseqüència, augmenta la separació intergrupal, cosa que millora la capacitat de diferenciació. D'altra banda, la diferenciació dels teixits, (utilitzant el mètode de 3

elèctrodes i desprès del calibratge posterior de les mesures) evaluant les dues freqüències més discriminatòries, mostra diferències significatives entre aquelles patologies que comporten un augment en la densitat del teixit (neoplàsia , fibrosi i pneumònia) i aquells teixits que comporten una major quantitat d'aire als pulmons respecte als anteriors i/o destrucció de teixit (sa, emfisema). D'aquesta manera, es troben diferències significatives als quatre paràmetres d'impedància analitzats [mòdul ($|Z|$), fase (PA), resistència (R) i reactància (Xc)] entre: neoplàsia i pneumònia ($p < 0.05$); neoplàsia i teixit sa ($p < 0.001$); neoplàsia i emfisema ($p < 0.001$); fibrosi i teixit sa ($p < 0.001$) i pneumònia i teixit sa ($p < 0.01$). També es troben diferències significatives a $|Z|$, R i Xc entre fibrosi i emfisema ($p < 0.05$) i a $|Z|$ i R entre pneumònia i emfisema ($p < 0.05$). Per acabar, desprès de la implementació de diferents algoritmes de classificació, els resultats mostren una gran eficàcia a l'hora de classificar i detectar una mostra de teixit neoplàsic, i permeten separar algunes patologies no detectades amb mètodes estadístics clàssics. En conclusió, la implementació de mesures de bioimpedància mitjançant broncoscòpia pot millorar el diagnòstic clínic, ja que és capaç de discriminar entre diferents tipus de teixit de manera mínimament invasiva. No obstant això, per a l'ús combinat amb tècniques d'intel·ligència artificial, cal augmentar la mostra de les mesures per a un entrenament més gran dels algoritmes i la possible implementació en les unitats de pneumologia intervencionista dels departaments de medicina respiratòria.

ACKNOWLEDGMENTS

I would like to begin by thanking each and every one of the patients for their collaboration and willingness to participate in the study. To all of them, most of whom were nervous and worried, without you this study would not have been possible. I take with me each of the stories that you told before the test and I take with me all the anecdotes that you have given me during your visit to the interventional pulmonology area.

I would also like to thank all the people that has take part in this thesis:

To Marta Navarro, Margarita Robles and Laura Romero, nurses and assistant in the bronchoscopy unit, for their kindness and willingness to help in any way necessary. They made me feel like one of the team.

To Dr. Virginia Pajares and Dr. Alfons Torrego for allowing me to take the bioimpedance measurements and for their implication in the study.

To Professor Javier Rosell and Professor Pere Riu for their collaborations and contributions to the research papers published in this thesis.

To Alfonso Mendez for being an invaluable mentall support during the thesis. Thank you for all the conversations we have had during these almost 4 years in the laboratory and for all the good times you have given me.

I would like to express my greatest gratitude to my two thesis directors:

To Professor Ramon Bragós, for being there for anything needed during the development of this thesis, no matter what time or day it was and for his absolutely dedication to the project.

Specially thanks to Dr. Lexa Nescolarde for her absolutely dedication to my thesis. This thesis could not have been possible without her. For teaching me her technical knowledge in statistics and also on how to write research articles but also for her knowledge of life. She has become a benchmark for me.

Finally, I would like to thank all my family for their invaluable support during all the development of the thesis and for always believing in me.

TABLE OF CONTENTS

TABLE OF FIGURES

CHAPTER 1: INTRODUCTION AND THEORETICAL BACKGROUND

1. THESIS OVERVIEW

1.1.Problem statement

Respiratory diseases are among the most prevalent illnesses worldwide, along with heart complications. Moreover, each year an estimated 3 million people die due to respiratory disease complications, making respiratory diseases the third leading cause of death worldwide [1].

The diagnosis of lung diseases is performed through multiple approaches. Pulmonary function tests evaluate lung capacities and volumes in order to discriminate between obstructive and restrictive pulmonary diseases [2]. Medical images offer the possibility to observe structural and functional abnormalities [3].

The most used imaging technique system is the radiography (X-ray). However, X-ray is a low contrast imaging technique [4], hindering the detection of abnormal anatomical structures [5]. Its low resolution and its 2D character limits the capacity to detect tumours or nodules, either benign or malign [6]. The diagnosis through X-ray imaging has been improved through high-resolution computed tomography (CT) used to evaluate abnormalities in the lung parenchyma [7]. This technique is considered to be the standard for the diagnostic of lung cancer [6] despite an increase of radiation dose to the patient. Moreover, the radiation necessary to be administrated in these types of images makes difficult the follow-up of a particular disorder [8]. Molecular images such as positron emission tomography (PET) gives metabolic information making possible a more accurate diagnostic [6]. Lung diseases often present identical or similar symptoms and the different pathologies are only differentiable when they are in an advanced stage. The problem arises when the objective is to differentiate between pathologies in an initial state, increasing the accuracy of the diagnostic. The combination of positron emission tomography with computed tomography (PET/CT) allows a better nodule distinction.

The diagnosis through PET/CT often leads to false negative cases. In addition to the false negative cases, the metastasis propagation velocity can also be misinterpreted if, at the first moment, the tumour presents a low consumption rate of the radio tracer. In the same way that there is the possibility to make a diagnostic of false negatives there is also the possibility to make a diagnostic of false positives detecting infections and inflammations with a high glucose metabolic rate. These cases make necessary the need of a more accurate diagnostic [6].

Imaging techniques are complementary to a third method of diagnostic, bronchoscopies. Flexible bronchoscopies have limited value in the obtention of peripheral tissue lesions.

With endobronchial involvement, the selection of the biopsy site is relatively simple. The necessity of confirmation that the biopsy location is correct in peripheral lesions leads to the development of other techniques such as virtual bronchoscopy (VB), radial endobronchial ultrasound (r-EBUS), electromagnetic navigation (EMN) and ultrathin bronchoscopes. However, the diagnostic using these techniques remains suboptimal [9], [10].

One possible strategy to improve lung disease diagnosis and tissue sample is through the measure of the lung tissue bioimpedance. Electric impedance tomography (EIT) is an imaging technique which consists on the mapping of the immittance distribution in a layer of tissue. The acquisition is performed through multiple skin surface electrodes in which current is successively injected through electrode pairs and the voltage between the other electrodes is recorded. However, it is a poor resolution imaging technique and therefore, not suitable for tumour detection [11].

The hypothesis is that electrical impedance spectroscopy (EIS) obtained in-situ through a catheter introduced with a bronchoscope would be another possible way to differentiate lung tissue states among different pathologies. This technique could be used for tissue characterisation having the possibility to detect changes in the pulmonary structure minimally-invasively for the detection of abnormalities which would complement the actual diagnosis systems.

1.2. Objectives

Motivated by the ideas exposed in the summary above, the **main purpose** of the thesis is to validate the abovementioned hypothesis by applying electrical impedance spectroscopy to obtain bioimpedance measurements of lung tissue to perform lung tissue differentiation based on the different tissue states (**Article 3**). The pathologies included are neoplasm, fibrosis, pneumonia and emphysema. In addition, healthy lung tissue is also included in the study. The bioimpedance measurements are acquired through a bronchoscopy process, introducing a catheter through the working channel of the bronchoscope. Prior to bronchoscopy, radiological images (CT or PET/CT) are acquired to confirm diagnosis and know the pathology location and diagnosis of lung neoplasm is confirmed by biopsy.

Subsequently, in order to achieve the main objective of the thesis different goals are planned:

1.   Find the best electrode configuration that allows a good tissue differentiation while maintaining the practicality of the technique for the clinicians (**Article 1**). A comparison of the ability to differentiate lung tissue by using the 4-electrode method and the 3-electrode method is conducted.

2.   Study the implementation of a calibration method to reduce data variability and increase the tissue state separation capability. The calibration method, already used in cardiac applications, consists of using a measurement of bioimpedance performed in a known position in the bronchi to calibrate all the lung measurements. The objective of the calibration is to eliminate the geometrical differences among subjects and measurements (**Article 2**).

Finally, in order to improve real-time diagnosis and help for a better sample location accuracy, the following additional objective is defined:

1.   Implement machine learning classification algorithms to perform tissue characterization through impedance measurements. (**Non-published results**).

1.3. Thesis framework and outline

The present PhD thesis has been developed in the Electronic and Biomedical Instrumentation group, from the department of Electronic Engineering of the Polytechnic University of Catalonia of Barcelona together with the Interventional Pulmonology Unit of the Respiratory Medicine Department of the "Hospital de la Santa Creu i Sant Pau" of Barcelona.

The study was initiated in the frame of the research project: Z-LUNG, "Biopsia electrónica de tejido pulmonar in-vivo basada en espectroscopia de impedancia eléctrica" (RTI2018-098116-B-C21).

The theoretical background of the thesis is presented in Chapter 2 with a summary of the main concepts of lung physiology together with a description of the pathologies included in the study. Moreover, the procedures performed in bronchoscopy prior or after the acquisition of bioimpedance measures are also described. Furthermore, an introduction of the main concepts of bioimpedance analysis is also performed including a review of the studies already published regarding the use of electrical impedance spectroscopy, with emphasis in lung measurements, for clinical purposes. Finally, a brief description of the machine learning concept and the algorithms applied is also presented.

In chapter 2 to 4 the three articles published during the development of the thesis are presented. The first article (Chapter 2) makes a comparison regarding the capacity to differentiate among different tissue states between the 4-electrode method and the 3-electrode method to acquire bioimpedance data and perform tissue differentiation. Also, the advantages or disadvantages of using one method or another in the clinical process of bronchoscopy are discussed. In Chapter 3, the second article of the thesis analyzes the implementation of a calibration method for the bioimpedance measurements to increase tissue differentiation by reducing data variability among samples belonging to the same tissue group and increasing the differentiation capability among tissue states. The third article of the thesis presented in Chapter 4 performs tissue differentiation using electrical impedance spectroscopy measurements (frequency range: 1 kHz to 1MHz) among neoplasm, fibrosis, pneumonia, healthy lung tissue and emphysema by selecting the most discriminative frequencies. It also performs a discriminant analysis to complement the tissue differentiation statistics. In Chapter 5 the still non-published results regarding the

use of machine learning algorithms for tissue classification based on the minimally-invasive electrical impedance spectroscopy measurements are presented.

In Chapter 6 the discussion of the main results and conclusions of the thesis are presented.

In addition, in the Annexes section, a list of the conference papers and articles directly or non-directly derived from the thesis but published during the development of the thesis is also presented.

2. THEORETICAL BACKGROUND

2.1. Anatomy and physiology of lungs

The lungs are the principal organs involved in the respiratory process. While the right lung is divided into three lobules (upper, middle and lower) the left lung is only divided into upper and lower lobes. Each of the lobes are, in turn, divided into bronchopulmonary segments which are regions that are supplied by specific tertiary bronchus and arteries. The right lung has 10 bronchopulmonary segments while the left lung has only eight (**Fig. 1**) [12].

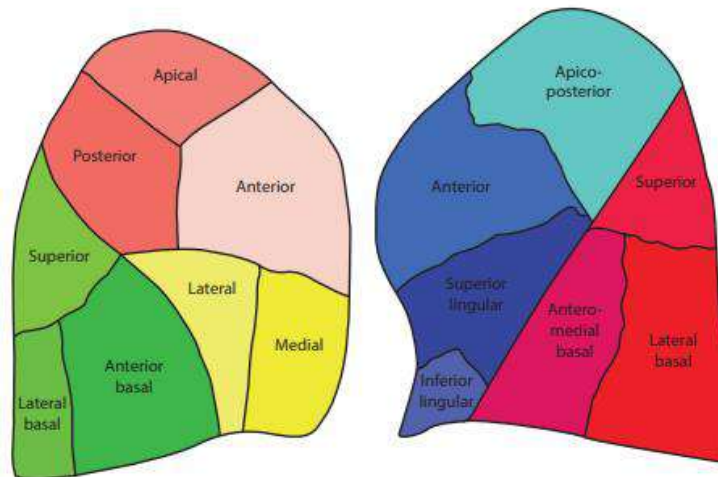**Figure 1.** Distribution of the bronchopulmonary segments [12].

The airways of the lungs, structured in a complex array of duct networks, allow the gas exchange process. They are constituted by the trachea, which divides into multiple bronchial generations that end up in the alveoli. At the end of the trachea the carina is found and divides into the left and right principal bronchi, being the left one larger than

the right. The right principal bronchi further divides into the upper and intermediate lobe bronchi while the left principal bronchus divides into the upper and lower lobe bronchus (**Fig. 2**) [12]. Bronchi divides further into the bronchioles, the terminal bronchioles, the respiratory bronchioles, the alveolar ducts and end in the alveolar ducts, after undergoing twenty-three divisions [13].

What makes the difference between bronchi and bronchioles is that the first one presents a diameter of more than 0.1 cm while bronchioles have a diameter lower than that value.

From trachea to terminal bronchioles is the region known as conducting airways while the respiratory bronchioles, alveolar ducts and alveolar sacs constitute the respiratory zone. The function of the conducting airways is to transport the air and protect the lung from the contaminant substances that are inhaled during the respiratory process. The respiratory zone is the place where the gas exchange occurs. Lungs can contain 300 million alveoli and 140 m^2 of gas exchange alveolar surface on average. The respiratory zone is divided in multiple acinus, which is an anatomic unit that consists on different respiratory bronchioles, alveolar ducts and alveoli, which are supplied by s single terminal bronchiole [13].

The airways are formed by different types of tissue. In contact to the lumen of the airways there is the mucosa and the submucosa, which are separated by a basement membrane. The mucosa is composed principally by epithelial cells. In the submucosa smooth muscle and connective tissue can be found. Finally, a fibrocartilaginous layer containing the cartilage rings (that have a support function of the airways) is found surrounding the submucosa [14]. The bronchial epithelium cells include pseudostratified ciliated columnar epithelial cells, interspersed globet cells, neuroendocrine cells and underlying basal cells. Globet cells are in charge of mucous secretion for trapping inhaled particles and ciliated cells guides the mucous and particles to the pharynx to be eliminated. Basal cells, present in bronchi are in charge of regenerating damaged bronchial mucosa. Neuroendocrine cells are in charge in the ventilation/perfusion regulation. In bronchioles, Clara cells replace globet cells which detoxify inhaled toxins and participate in the regeneration of bronchial epithelium which is damaged [13].
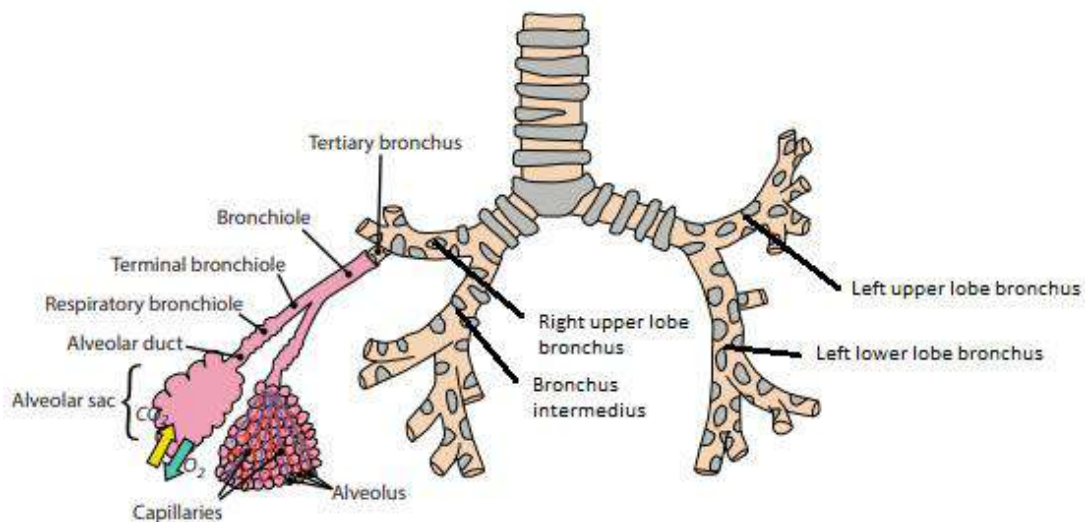
Figure 2. Airway divisions [12].

Type I and II pneumocytes are present in the alveolar sacs. The first ones facilitate the gas exchange process. The second ones secrete surfactant which prevent alveoli from collapse at low intra-alveolar pressures [13].

Moreover, the lungs are vascularized organs in order to deliver deoxygenated blood to the alveoli for gas exchange process. The main pulmonary artery, originated at the right ventricle, divides into the left and right pulmonary arteries. In the same way as the bronchus splits into next generations, smaller generations of arteries are originated from the divisions of the left and right pulmonary arteries following the same paths as the bronchus and bronchioles. After the gas exchange process, the different capillaries join together to form the pulmonary veins [12].

2.2. Lung diseases and diagnosis techniques

The lungs are vulnerable to injury due to environmental factors causing multiple forms of cell damage that leads to lung disorders. Multiple disorders can be developed in lung tissue. However, pathologies not analyzed in this thesis will not be explained in this section.

2.2.1. Emphysema

Emphysema is a chronic obstructive pulmonary disease (COPD) together with chronic bronchitis developed as a result of a chronic inflammation and characterized by an airflow

limitation in a forced expiration [13]. COPD caused more than 3 million death in 2012 worldwide which represented the 6% of the global deaths. Moreover, it is estimated that by 2030 the number of death due to COPD will rise to 4.5 million. Nowadays it is the third leading cause of death around the world. More specifically, it is estimated that in United States the percentage of population suffering from emphysema is between 4 and 5% in males and between the 1 and 3% in females.

Emphysema is characterized by an irreversible destruction of the alveolar walls and the terminal bronchioles. This destruction leads to an enlargement of the airspace (**Fig. 3**) producing an air accumulation due to the destruction of the elastic tissue. Emphysema is also characterized by a decreased gas exchange capacity [12], [15]. The major problem in emphysema is the loss of elastic recoil, thus decreasing the capacity of expelling the air in expiration [14], [15]. Progressive hypoxia and dyspnea are produced as a result of the loss of alveolar surface area and its capillary bed for the gas exchange process [15].
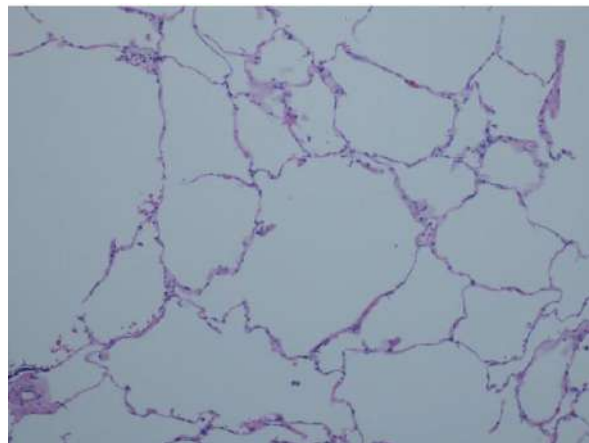
Figure 3. Tissue structure of emphysematous lung [12].

After the apparition of symptom related to COPD (chronic cough, sputum production and dyspnea), the diagnosis of emphysema begins with a detailed history of the patient with the focus on the exposition to toxic substances such as smoke. After that, spirometry is necessary to confirm the diagnosis in which the volume of air exhaled in the first second of expiration (FEV_1) is compared to the total volume of exhaled air (force vital capacity, FVC) obtaining the ratio FEV_1/FVC. A ratio lower than 0.7 is diagnostic of airflow obstruction [12]. After spirometry, pulmonary function tests evaluate the disease severity to guide therapy by measuring lung volumes. In COPD patients, an increase in the residual volume (RV) is sign of hyperinflation of the lungs. Moreover, the diffusion

capacity of carbon monoxide (DLCO) is used to evaluate the alveolar-capillary interface efficacy of gas exchange. DLCO is reduced in emphysema but is not altered in chronic bronchitis or asthma. Finally, chest radiographs and computed tomography imaging (CT) are also used for assessing the diagnosis of emphysema. Radiological findings include hyperinflation and hyperlucency while CT images reveal a bullae pattern [13]. The destruction of the alveolar tissue is irreversible.

2.2.2. Lung neoplasm

Lung neoplasm is the fourth most common cause of cancer being the second that produces more deaths. It represents the 20% of cancers in men and the 12% of cancers in women with an estimated incidence of 1.6 million cases worldwide.

Lung neoplasm is characterized by abnormal cell growth (**Fig. 4**), losing the tissue architecture. Lung neoplasm is produced due to cellular function alterations that produce morphologic changes such as enlargement of the cells (hypertrophy), an increase in cell concentration due to much cell division (hyperplasia) or abnormal cell reprogramming to appear like different cell types (metaplasia). In addition of an excessive cell growth a reduction in the pressure of oxygen is produced thus secretion of angiogenic growth factors occur which leads to the proliferation of vascular structures into the neoplasm tissue for its nutrition and oxygenation [15].
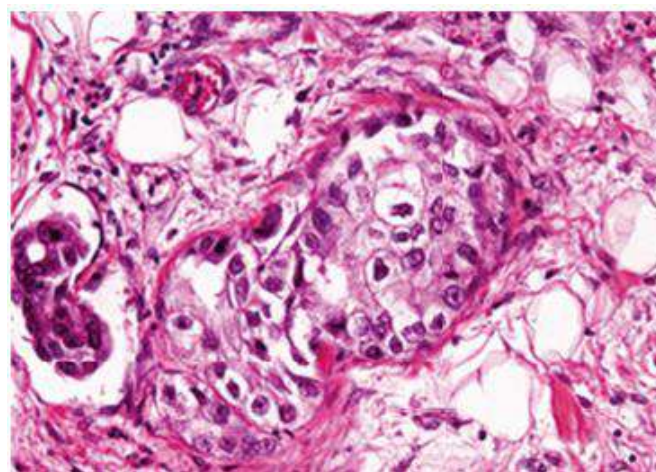

Figure 4. Tissue structure of lung neoplasm (Adenocarcinoma) [12].

There are different types of lung neoplasm which can be divided between non-small cell lung cancer (squamous cell carcinoma and adenocarcinoma) which represent the 85% of

lung neoplasms and small cell carcinoma. Squamous cell carcinomas are characterized for being more centrally located neoplasm while adenocarcinomas are commonly in the periphery of lungs although can occur more centrally. Adenocarcinomas can be found in association with fibrosis [13] and is the most frequent type of lung cancer. Small cell carcinomas are typically central and are characterized for being soft and necrotic with its cells having little cytoplasm.

The squamous cell carcinomas represent the 30% of the non-small cell lung cancers and are highly related to cigarette smoking. This type of lung neoplasm normally grows more quickly than the other non-small cell lung cancers. However, it tends to produce metastasis later. Necrosis is common in this type of lung neoplasm and it can be surrounded by consolidations that reflect obstructive pneumonia. Small cells lung carcinomas represent the 12% of lung neoplasms and also show necrosis [13].

The diagnosis is performed through an imaging test (radiography or CT) of the thorax and abdomen that determines if there is an opacity that needs to be investigated and its exact location. Moreover, a positron emission tomography (PET-CT) is performed to determine the activity of the suspicious mass. The diagnosis also requires sampling the abnormal tissue through a biopsy (explained in section 2.3.3) [12].

2.2.3. Fibrosis

Fibrosis is considered a rare disease with a median survival between 3 and 4 years. In Europe, there are approximately 40,000 new cases per year [16].

Fibrosis leads to different structural changes in lungs. In general terms, fibrosis is characterized by a thickened alveolar wall due to collagen deposition [13] and an increase tissue stiffness due to the accumulation of inflammatory cells as well as extracellular matrix collagen-rich. Contrary to emphysema, fibrosis leads to an increased lung elastic recoil and oxygen diffusion and gas exchange impairment.

Fibrosis can lead to the development of honeycomb cysts, visible in radiological images (**Fig. 5**) [15], which are characterized by the replacement of the alveolar architecture for cystic spaces surrounded by fibrous septa filled with mucous or air [13].
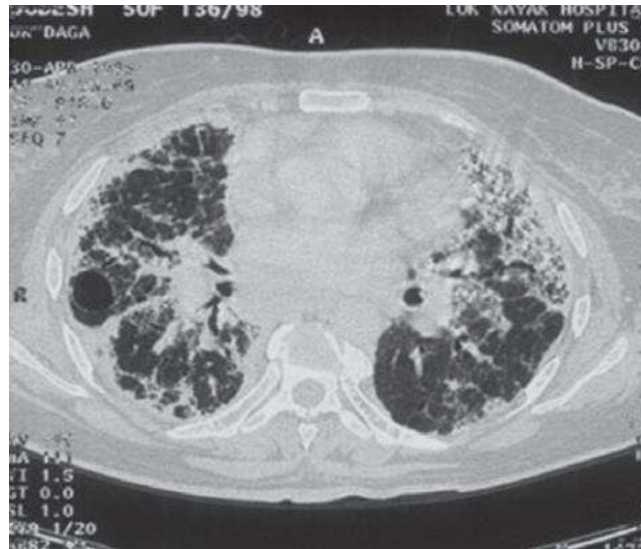
Figure 5. CT image of fibrosis [15].

Pulmonary function tests are used to evaluate the severity of the disease as well as its progression and response to treatment. CT images are taken for diagnosis to confirm abnormalities of the tissue. Often, it is necessary to perform a bronchoalveolar lavage through bronchoscopy for further studies of the pathologic tissue [12], [17].

2.2.4. Pneumonia

Pneumonia is a very common disease affecting 450 million people per year and causing 4 million death worldwide [14].

Pneumonia develops different patterns in lungs, depending on the pneumonia type. On one hand there are the pneumonias derived from infections, such as the mycoplasma pneumonia. This subtype of pneumonia is characterized by an infection and inflammation of the lung parenchyma in which fluid or pus (purulent material) fill the air sacs, appearing as dense consolidation (**Fig. 6**). The other group is characterized by the proliferation of fibroblastic tissue in the small airways and alveolar spaces [13] such as in the case of organized pneumonias. The major consequence of pneumonia is a decreased ventilation capacity of the affected areas [14].
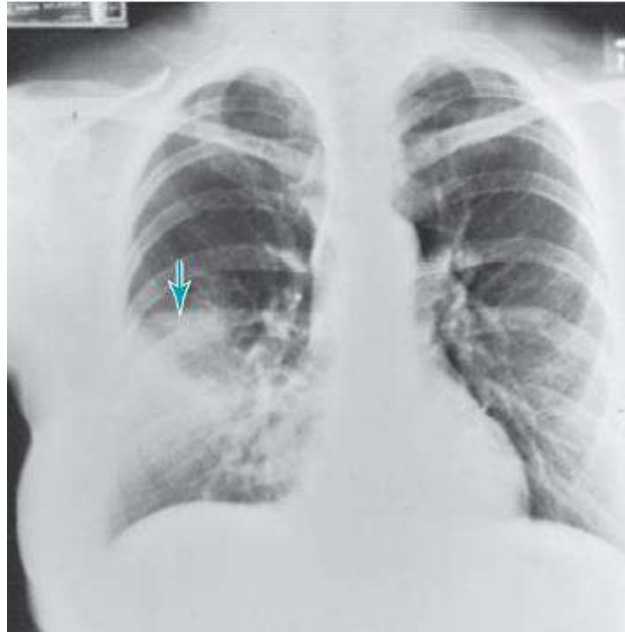
Figure 6. Radiological image of a pneumonia [14].

The most useful tool for the diagnosis of pneumonia is the chest radiography, which confirms the presence of the disease and shows its extent and severity. Radiological findings characteristics for pneumonia are air spaces consolidations. Moreover, microscopic examination of sputum (obtained through bronchoscopy) is also necessary to guide treatment [14].

2.3. Bronchoscopy

In complement to the different imaging techniques and pulmonary function tests, bronchoscopies (**Fig. 7**) enable the extraction of secretion, lung parenchyma and nodules for the characterization of disorders [12].

Bronchoscopy allows the visualization of the interior airways through the insertion of a flexible bronchoscope into the lungs with a camera at the tip of the bronchoscope that displays the images in a monitor screen [14]. The bioimpedance measurements obtained for this thesis have been acquired inserting a catheter trough the bronchoscope working channel.

The flexible bronchoscope consists on three main components: the control section, the insertion tube and the universal cord. The control section is the part that is hold by the left hand of the bronchoscopist. For the bronchoscope steering management, the clinician

controls with the thumb a lever that can be moved up and down to control the angle of the distal tip. The insertion tube consists on a flexible catheter that enters the patient together with another plastic catheter travelling from the middle of the insertion tube, known as working channel, that is used for passing accessories for fluid and tissue sampling. As there is no light in the respiratory airways, two fiber-optic bundles along the catheter carry light from an external light source. Finally, the universal cord provides information and light to and from the control body, the light source and the video processor [18].

Figure 7. Bronchoscopy procedure during the acquisition of the bioimpedance measurements in "Hospital de la Santa Creu i Sant Pau".

During bronchoscopy, patients are placed in a supine position. Topical lidocaine is used to anesthetize the upper airways. Moreover, intravenous sedation with benzodiazepine is administrated two to three minutes before the procedure to help the patient to relax [12]. Bronchoscopy is performed in patients with abnormal chest radiograph or CT image. Images determine the bronchoscopic tests needed as well as the sample location and the quantity of specimen needed [18]. There are different tests that can be done through a bronchoscopy.

2.3.1. Bronchial washing

Bronchial washing (BAS) is a technique that consists on the placement of the bronchoscope near the area to be sampled and the introduction of 5 to 50 mL of sterile

saline through the working channel of the bronchoscope for then aspirating the solution back to a specimen trap or syringe. Bronchial washing, although not enables cell differentiation, is useful for microbiological and cytological assessment when lesions are visible. Moreover, it is used for dislodging mucus plugs or clots. Bronchial washing should be performed prior to biopsies in order to avoid an excessive concentration of red blood cells in the specimen trap that sometimes difficults cytologic interpretation. In addition, bronchial washing increases the diagnostic yield if performed in conjunction of biopsies in endobronchial tumors from 93% biopsy alone to 96% [18]. It may be useful for the assessment of central airways secretions [19].

2.3.2. Bronchoalveolar lavage (BAL)

BAL is a technique used to obtain cellular samples from the most distal airways and alveolar spaces. BAL is performed through the flooding of the pathological area to move the cellular alveolar material and the aspiration and acquisition of the biological material. Aliquots of 50 mL of sterile saline are introduced to the region before being aspired and recollected into a syringe or a specimen trap. It allows the differentiation between cellular specimens and is particular useful in the study of diffuse interstitial lung diseases [19].

2.3.3. Biopsy

Biopsies are used to obtain samples of biological tissue, where clinicians pass through the working channel of the bronchoscope the forceps (**Fig. 8, left**). The process consists on arriving to the visual lesion, opening the forceps and close the forceps in order to take a piece of the damaged tissue. Biopsies are usually employed for the diagnosis of lung cancer and also for the detection of granulomas with a sensitivity between 72 % and 100 %. The most frequent complication when performing biopsies is the frequent minor bleeding of the tissue. For this reason, clinicians may take caution for vascularized lesions [19].

2.3.4. Bronchial brushing

Bronchial brushing is similar to biopsies. Instead of forceps, a brush (**Fig. 8, right**) is passed through the working channel of the bronchoscope. After moving the brush back and forth to move the abnormal mucosa the brush is removed from the bronchoscope.

Although the process is similar to biopsy, the bronchial brushing is used when the lesion is not visible [12]. For this reason, brushing is performed for the diagnosis of endobronchial lesions and peripheral lung abnormalities. As it happens with biopsies, in brushing there is also the complication of minor bleeding [19].

Figure 8. Biopsy forceps (left) and bronchial brush (right) [12].

2.3.5 Bronchoscopic techniques for diagnosis of lung neoplasm

As seen in previous sections, there are different procedures performed during a bronchoscopy, each of which with its specific utility. This section aims to explain the procedures performed for a case of lung neoplasm diagnosis. The section aims to show that multiple procedures are performed during the bronchoscopy for a correct diagnosis.

In bronchoscopy, there are two groups of lung neoplasm, the central nodules which are directly accessible through bronchoscope and the peripheral lung nodules which are not.

Historically, the histologic diagnosis of central lung nodules has been done by using a combination of bronchial washing, bronchial brushing and biopsies. History has proved that, although each of the techniques individually offers a good diagnosis yield, the sensitivity of the procedures is higher when a combination of the techniques is used [20].

The first of the techniques, bronchial washing, offers enough material for a good diagnosis in the 68 % of the cases. However, the implementation of this technique for the diagnosis of central lung nodules is under controversy because it does not increase the diagnostic yield when using biopsy and brush in some studies [20].

The diagnostic yield for bronchial brushing itself is 72 %. However, the diagnostic yield for nodule diagnosis is higher when performed in combination with biopsies [20].

Finally, endobronchial biopsies provide a diagnosis in the 80 % of the cases. The optimal number of biopsies is under discussion as some experts recommend a number of six biopsies although some studies recently have proven that it is enough with 3 to 4 samples [20].

For peripheral lung cancer, bronchoscopy provides diagnostic in 69 % of the cases. Bronchial washing provides diagnosis only in the 28 % of the cases. Other techniques, such as bronchial brushing, when performed under fluoroscopy, provides diagnosis in the 45 % of the cases. Finally, transbronchial biopsy, also performed under fluoroscopy guidance has a diagnosis sensitivity of the 52 % when 4 or less biopsies are collected. However, the diagnostic yield increases up to 70 % when more than four biopsies are obtained [20].

2.4. Bioimpedance

Lung sampling is vital for the correct characterization of a particular disorder through the multiple methods presented above. With endobronchial involvement lung sampling is relatively simple. However, in peripheral nodules other techniques such as electromagnetic navigation bronchoscopy is needed. However, its high cost does not allow the possibility to have these devices in all the interventional pulmonology units. In order to improve lung sampling, bioimpedance measurements aim to be implemented.

2.4.1. Fundamentals of bioimpedance

The electrical properties of biological tissue are complex. Biological tissue properties are categorized based on the source of the electricity (active or passive). Active properties originate in electrically active cells such as the ones originated in the heart or in the brain. Passive electrical properties should be excited with an external source of energy to be measured [21].

2.4.1.1. Duality conductor – dielectric

All the materials, biological or not, can be divided into two categories: conductors and dielectrics. In a conductive material, conductor charges move freely with the application of an electric field (which is the behavior of most of the biological tissues below the 100

kHz). On the contrary, charges in a dielectric material do not move and no net movement exist as charges are only reoriented. This reorientation of charges is a phenomenon known as polarization of the dielectric material. The process of polarization needs certain time to be produced, defined by the relaxation time (τ) [11], [22]. A dielectric material, as cell membranes behaves as, is capable of storing electrical energy.

Two parameters characterize the conductive and dielectric properties of the materials, the conductivity (σ) and the permittivity (ε). The conductivity describes the ability of the charges in a material to move with the application of an electric field. The second parameter, the permittivity, gives information about the ability of a material to store charges when an electric field is applied. The complex expression of permittivity is defined in **Equation 1** with its real part being the dielectric constant and its imaginary part being the dielectric loss. **Equation 2** relates the permittivity parameter with the conductivity.

$$\varepsilon^*(\omega) = \varepsilon'(\omega) - j\varepsilon''(\omega) \tag{1}$$

$$\sigma^*(\omega) = j\omega\varepsilon^*\varepsilon_0 \tag{2}$$

Biological tissues present both, conductive and dielectric properties. The conductivity is produced due to the hydrated ions that are present in the intracellular and extracellular medium. On the other hand, the dielectric properties are related to the electrical double layers around the surface of the cell membranes [23].

2.4.1.2. Duality relaxation – dispersion

As it has been already introduced, the polarization of the dielectric materials (thus, the cell membranes) is characterized by a relaxation time. **Equation 3** related this relaxation time with the permittivity parameter, where ε_∞ corresponds to the permittivity at high frequencies and ε_s corresponds to the value of the permittivity at low frequencies.

$$\varepsilon^* = \varepsilon_\infty + \frac{\varepsilon_s - \varepsilon_\infty}{1 + j\omega\tau} \tag{3}$$

The transition between low and high frequencies are called dispersions. In biological tissues there are three major dispersions (**Fig. 9**) [11], [24].
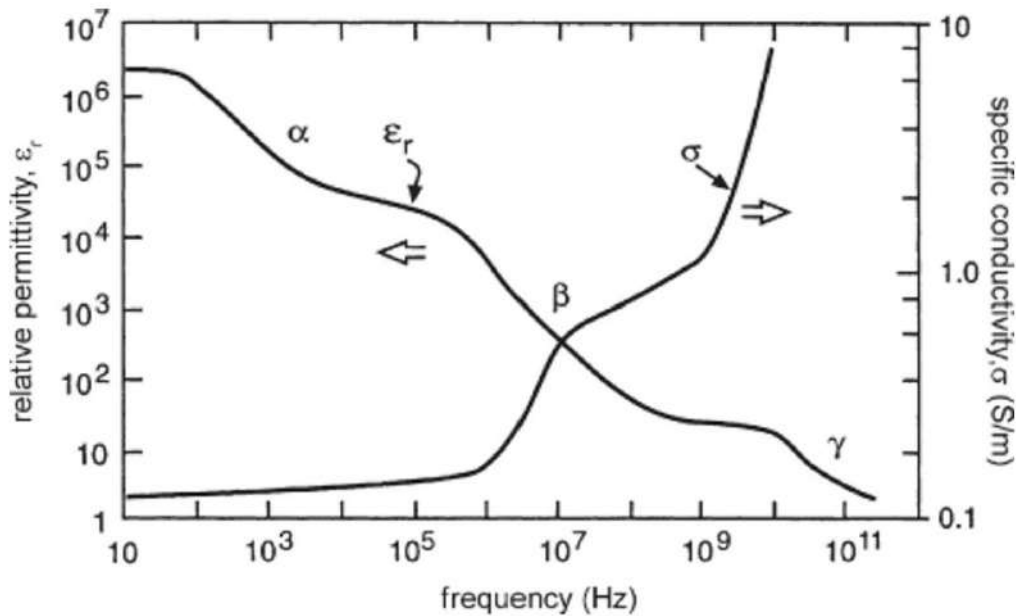
Figure 9. Dispersions of the biological tissue [25].

- Alpha dispersion: dispersion produced from millihertz to kilohertz frequencies caused by the sarcoplasmic reticulum, gap junctions and counterion relaxation.
- Beta dispersion: dispersion produced from the tens of kHz to the tens of MHz and produced mainly by the cellular structures of the tissues and its poor conductive membranes that separate the extracellular from the intracellular medium. Other tissue structures such as the relaxation effects produced by the proteins and organelles inside the cells also contribute to the beta dispersion slightly.
- Gamma dispersion: dispersion occurring above 1 GHz and produced by the polarization of the water molecules.

In biological tissues the most important dispersion is the beta-dispersion, as it characterizes the behavior of the cell membranes and is of vital importance in the concept of electrical impedance spectroscopy.

2.4.2. Electrical impedance spectroscopy

The dielectric properties of the biological tissue are frequency dependent. Therefore, for a complete characterization of the tissues the properties should be studied in a wide

frequency range, covering the band of the beta dispersion (polarization of the cell membranes).

2.4.3.1. Bioimpedance

The general definition of bioimpedance is stated as the ability of the biological tissue to oppose when electric current is applied [26]. The physical basis of bioimpedance is that biological tissue can be represented by an electric circuit model composed by a resistance (representing the extracellular medium) in parallel with a capacitor and resistance in series (representing the intracellular medium and the cell membrane) (**Fig. 10**).
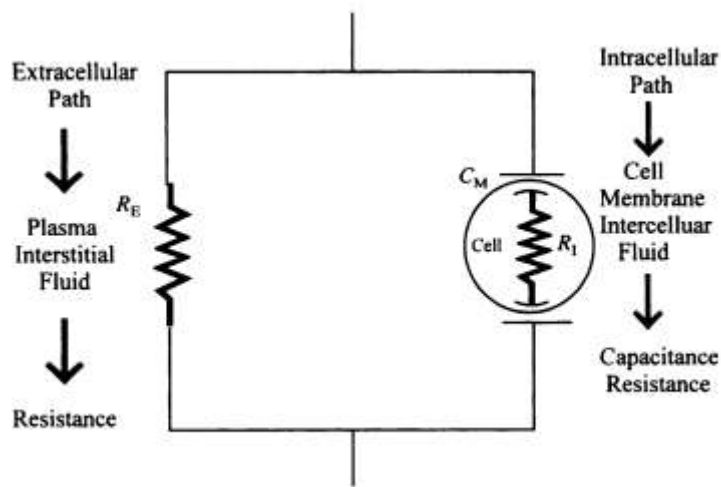
Figure 10. Circuit model of biological tissue [26].

When direct current is applied to the biological tissue the bioimpedance becomes purely resistive (R). However, the application of alternating current to the biological tissue makes the bioimpedance frequency dependent, thus the term is called Z [27]. The term Z is represented using complex numbers (**Equation 4**). The real part describes the resistive term (R) and denotes the behavior of both the extracellular and intracellular medium. The imaginary part is defined by the reactance (Xc) which describes the capacitive behavior of the cell membranes and is the term frequency dependent (**Equation 5**), where $\omega=2\pi f$.

$$Z = R + JX_C \qquad\qquad (4)$$

$$X_c = -\frac{j}{\omega C} \qquad\qquad (5)$$

From the combination of R and Xc the bioimpedance module (|Z|) defined as $|Z| = \sqrt{R^2 + Xc^2}$ and the phase angle (φ) defined as $\varphi = \tan^{-1}(\frac{X_C}{R})$ are derived. The phase angle is produced due to the lag of the current behind the voltage [26].

The Xc is produced due to the polarization of the cell membranes. This polarization can be endogenic, when is produced by the body, or exogenic due to an external agent. In bioimpedance measurements this polarization of the cell membranes is exogenic as energy is applied to polarize the biological tissue from outside the body [11].

2.4.3.2. Electrical impedance spectroscopy (EIS)

EIS consists on the impedance measurement on a wide range of frequencies. In the study of the structure of biological tissues, this range goes from few kHz to MHz.

Biological tissue and organs are very heterogeneous. Multiple types of cells can be part of the same type of tissue. The difference between the conductivity of blood from the blood vessels and the conductivity from the connective cells for mechanical stress endurance is large. Then, from an electrical point of view the biological tissue is considered an heterogeneous material [11]. The basic principle of EIS in biological tissue is that at low frequencies the current flow only through the extracellular medium due to the high impedance of the cell membranes. The intracellular medium contributes to the current flow but to a small degree. At high frequencies the current is able to penetrate the cell membranes and current circulates through the intracellular and extracellular mediums, disappearing the membrane effects (**Fig. 11**).
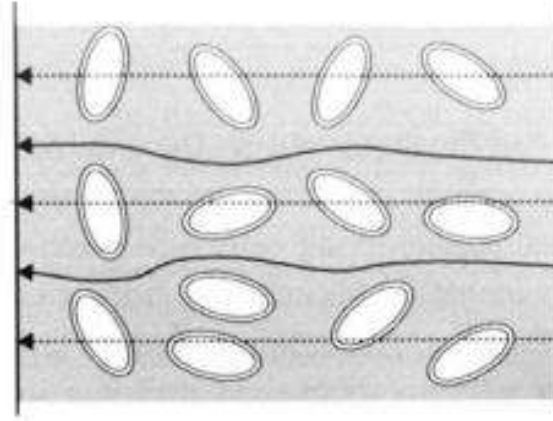
Figure 11. Current flow at low frequencies (continuous line) and at high frequency (continuous and dashed lines) [28].

The impedance spectrum will thus depend on the ratio between the intra and extracellular volumes, and the cell size and homogeneity. This behaviour was modelled by Cole brothers [29].

According to this model, the variation in Z in the biological tissues in function of frequency can be represented following the Cole function (**Equation 6**), where R_0 is the value of R at DC frequency, R_∞ is the value of R at infinite frequency, τ is the relaxation time previously mentioned and α is the distribution of the time constant [26].

$$Z = R_\infty + \frac{R_0 - R_\infty}{1 + (j\omega\tau)^{1-\alpha}} \tag{6}$$

2.4.3. Previous studies

2.4.3.1. Previous clinical studies using EIS

The use of the electrical impedance spectroscopy in biomedical applications is currently under research. Several authors are studying it in different medical fields with the aim of improving the tissue characterization as well as the efficiency of diagnostic trying to solve the drawbacks of the currently used methods. For years, researchers have been studying the use of the technique in different fields of the medicine, from a more general vision or study of the tissue characteristics to a more specific applications in the field of oncology

or cardiology. In this section a review of the existing research lines about the use of the technique is presented, with emphasis in lung applications.

In the study of the tissue characteristics, Dean et al. [30] studied the properties of the electric impedance from 0.01 Hz to 1 MHz in different tissues in ex-vivo rats including the pulmonary tissue. They observe the changes in the impedance for both, the real and the imaginary parts, as a function of the frequency. They arrived to the conclusion that the data obtained and the changes in the impedance were consistent according to the basic principles of the bioimpedance (they showed a decrease in impedance module with the increase of frequency). Also, in rats, Heroux and Bordages [31] studied the evolution of the impedance from 200 Hz to 13 MHz in different tissues and organs such as the kidney, the heart and also the muscular tissue validating its implementation in biological research. In contrast to the previous commented study, measures were made in-vivo.

Other studies such as da Silva et al. [32] investigated the possible use of the technique for the distinction of different types of tissue in 64 patients with a breast surgery prescribed. Specially, they focus on breast tissue to differentiate between cancerous (carcinoma, fibro-adenoma and mastopathy) and healthy tissue (connective tissue, adipose tissue and glandular tissue). They obtained 12 impedance measurements between the 488 Hz and 1 MHz with an initial dataset of 120 impedance spectra collected. They used different indicators obtained from the impedance measures using the Cole-Cole plots and with the use of linear discriminant analysis they perfomed classification among the different tissues. They obtained an overall accuracy of 92% for breast tissue classification. Specially, they discriminate carcinoma with an accuracy higher than 86%. However, they concluded it could not be possible to distinguish between the other pathological breast tissues by using impedance parameters. Nonetheless they concluded that Electrical Impedance Spectroscopy could be clinically applied for breast cancer detection.

Yoon et al. [33] used electrical impedance spectroscopy (101 frequencies between 0.1 kHz to 10 MHz) to analyze the frequency response of normal and abnormal tissues of tendinitis in 26 rabbits by recording the resistance and the reactance of the left (pathological) and right (healthy) patellar tendons (both longitudinally and transversally) obtaining significant differences both in resistance and reactance between both measurement sites in the longitudinal direction.

E.Gersing [34] investigated the ischemia-induced phenomena both in heart and in liver in dogs and pigs. Impedance was measured between 0.1 Hz and 10 MHz. They studied the evolution in the impedance spectrum through the 100h duration of the experiment. Impedance measurements were taken between 5 and 20min during all the time duration.

In the same research line, Mellert et al. [35] evaluated the bioimpedance response (at 1 kHz, 10 kHz and 1 MHz) in resistance and phase angle in induced myocardial ischemia in six patients undergoing on-pump open heart surgery. Lately, Kun et al. [36] implemented an algorithm (an artificial neural network) for estimation of skeletal muscle ischemia in real time using parameters extracted from the electrical impedance spectra in the beta dispersion region (27 frequencies between 100 Hz and 1 MHz) in data from in vivo animal models (25 animals used with 102 ischemia episodes). They proved that the use of the electrical impedance spectroscopy for skeletal muscle ischemia estimation showed results comparable to the pH measurement technique, a technique clinically used despite its low precision.

Previous studies regarding the use of EIS in the clinical practice can be found in oncology.

Skourou et al. [37] evaluated the capacity of the impedance spectroscopy for its use in the detection of tumors (adenocarcinoma) in initial stage implanted intramuscularly in the center of the biceps femoris muscle in 8 mature male rats. A decrease in the area under the curve of the permittivity-resistivity plot of the adenocarcinoma respect to the control measurement was shown. They evaluated the sensibility of the impedance measures in front of the increase of tumor's size and their morphology. They concluded that the technique allowed the detection of tumors that were not possible to detect with other conventional techniques such as computed tomography due to the reduced size.

In prostate cancer, Halter et al. [38] studied the possibility of differentiation between carcinogenic tissue (adenocarcinoma) and healthy tissue using electrical impedance spectroscopy measurements (20 frequencies between 10 kHz and 1 MHz) in five patients with a total of 50 impedance spectra recorded. The analysis was performed through the use of electric properties such as the permittivity and the conductivity and through statistical tests. Statistically significant results showed an increase with the signal frequency in the difference between normal tissue and tumor. In contrast, permittivity differences between normal tissue and tumor were larger at lower frequencies.

Teixeira et al. [39] used electrical impedance spectroscopy measurements between 1 MHz and 100 MHz in cell suspensions to evaluate the possibility to differentiate between two types of prostate cancer cells, one metastatic and the other non-metastatic, PC-3 y DU-145 respectively. The study found higher differences between both types of cells at higher cell numbers. Metastatic cells (PC-3) showed lower impedance magnitude values than non-metastatic cells (DU-145) at the same concentration.

In uterine cancer, Homola et al. [40] studied the viability to implement electrical impedance spectroscopy in the gynecological setting in 143 women with a colposcopy prescribed by determining the diagnostic usefulness of the technique in complement to colposcopies to diagnose high-grade squamous intraepithelial lesions in those women with abnormal cytology findings. In addition, Tidy et al. [41] performed a similar study to evaluate the implantation of electrical impedance spectroscopy (14 frequencies between 76.3 kHz and 625 kHz) in complement to colposcopy in those women with abnormal cervical cytology to increase the accuracy of the diagnostic. Both studies concluded that the impedance spectroscopy, used together with a colposcopy, allowed the detection of more uterine cancer cases, increasing the accuracy of the diagnostic, than when only using the second technique mentioned.

As far as it seems, the research in cancer for the use of the electrical impedance spectroscopy is focused on a faster detection of tumors and the differentiation between healthy and carcinogenic tissue.

Hillary et al. [42] analyzed the spectrum of the impedance obtained (using 14 frequencies between 76 Hz and 625 kHz) in 56 patients of different soft tissues located at the neck among which were adipose, parathyroid, thyroid, and muscle tissue in those patients with a thyroid and/or parathyroid surgery prescribed. The purpose of the study was the correct identification of the parathyroid tissue in order to preserve it to facilitate surgery of the parathyroid glands and reduce post-surgery hypoparathyroidism. Comparisons were made between the spectra of the different tissues in both in-vivo and ex-vivo. The study found significant differences in ratios of electrical impedance at low (152 Hz) to high (312 kHz) frequencies among thyroid, muscle and normal parathyroid tissue, concluding that changes in impedance over the frequencies appear to be different depending on the tissue.

In pneumology, Desai et al. [43] studied the ability of the EIS for the differentiation between carcinogenic and healthy cells. To perform the study, they extracted different cancer cells types and through pattern recognition techniques they evaluate the capacity of differentiation between both types of cells. They studied multiple cancer types among which was lung cancer. Gabriel et al. [44] proposed a model to predict dielectric data based on the data present in literature. They applied the model to different tissues and organs among which inflated lung was present in the study evaluating the permittivity and conductivity from 10 Hz to 100 GHz frequency range for all of the different tissues and organs.

Regarding the specific studies of lung bioimpedance measurements, Toso et al. [45] applied bioelectric impedance vector analysis using an impedance plethysmograph emitting 50 kHz alternating current to evaluate difference in the R-Xc plane of impedance vectors between healthy subjects and subjects suffering from lung cancer (stages IIIb and IV). The study reported different impedance vector distribution in patients with lung cancer as compared with healthy patients. A reduced Xc and a smaller PA were found while R was preserved in patients with lung cancer. Nierman et al. [46] performed transthoracic bioelectrical impedance analysis to quantify extravascular lung water in a porcine endotoxemic model of acute lung injury. Finally, Orschulik et al. [47] used non-invasive bioimpedance spectroscopy (256 frequencies between 4 kHz and 1 MHz) for the diagnosis of acute respiratory distress syndrome in an animal model.

2.4.3.2. Thesis background

Before exploring the idea of performing tissue differentiation in lungs, the research group had been applying electrical impedance spectroscopy in porcine hearts, in the Cardiology Department of "Hospital de la Santa Creu i Sant Pau" of Barcelona. Jorge *et al*. [48] characterized the systolic and diastolic changes in myocardial resistivity in healthy and ischemic heart tissue by defining three phases for the cardiac cycle: preejection, ejection and relaxation and finding changes in resistivity according to tissue state and depending on the cycle phase. Amorós et al. [49] continue with the prior study by analyzing phasic changes of myocardial resistivity in pigs with 1 month of healed myocardial infarction. In this study, they analyze changes in resistivity according to the quantity of fibrotic tissue

in the infarct scar. Finally, Amorós et al. [50] study the viability of electrical impedance spectroscopy measurements to differentiate healthy heart tissue from infarct scar in one month old cardiac infarction. Results from the study showed a decrease in impedance magnitude of 37% and a decrease in phase angle of 21% in scar tissue compared to healthy tissue.

To the extent of our knowledge, the only literature found related to bioimpedance measures in lungs through electrical impedance spectroscopy are the previous studies developed by our research group.

First, Sanchez *et al.* [51] described, characterized, calibrated and experimentally validated an EIS instrument for performing minimally-invasive bioimpedance measurements through bronchoscopy. Coll *et al.* [28] performed tissue differentiation between healthy lung tissue, bronchi and pathological lung tissue obtaining statistical differences among the different groups. However, in that first study, pathologies were not differentiated from each other and all pathological tissues were put into the same group. Riu *et. al* [52] presented a preliminary artificial intelligence predictive algorithm that was able to discriminate between healthy lung tissue and pathological lung tissue automatically.

2.5. Machine learning

The use of machine learning, a branch for data analysis of artificial intelligence, in the clinical field is raising importance in recent years, especially for patient monitoring, for the development of new diagnostics and for improving prognostics [53].

2.5.1. The learning problem

Machine learning algorithms can be classified into two main categories, unsupervised and supervised algorithms. The first ones are used for clustering problems, which consists on finding multiple groups in the data. The second groups are used for developing two tasks, classification and regression. The main difference between these two subgroups is that the output of the classification algorithm is a class (such as neoplasm, fibrosis or pneumonia) and the output of the regression algorithms are predicted numbers. The big differences between the unsupervised and the supervised algorithms is that in

unsupervised algorithms data is not labelled while in the supervised algorithms data is labelled and defined [54], [55].

In general terms, the principle of machine learning algorithms is the following: data is distributed in a way defined by a function (h) so the algorithm aims to find an approximate function (h') such as the error between h and h' is minimized. The process of finding h' is called as training. The process of evaluation of the error is called testing. The process of training and testing is performed on the same dataset. For this reason, data is split into two sub-datasets, the training dataset and the testing dataset. By convention, normally training data is the 80% of the dataset while 20% is used for testing [54], [55].

The main problem of these algorithms is what is called overfitting. Overfitting is the condition in which the algorithm performs really well on the training data (training error low and accuracy high) but not in the test set (test error high and accuracy low), thus not being able to generalize.

To avoid overfitting of the data, the optimization of the parameters that define the algorithms is important (Hyperparameter tuning) in order to detect the parameters with whom the classification accuracy is higher both, in the training and in the testing set.

There are multiple machine learning algorithms, such as k-means for clustering, support vector machines (SVM) or logistic regression for binary classification and decision trees for multiple class classification. The selection of the algorithm will depend on the data characteristics and the learning problem [54], [55].

In this project, the multi-class classification algorithms that have been applied to the bioimpedance data have been: Decision Tree, Random Forest, K-Nearest neighbors (KNN), Naïve Bayes and Gradient Boosting. In the following sections, the methodology of learning and classification of the algorithms is explained.

2.5.2. Decision Tree, Random Forest and Gradient Boosting

The three algorithms (Decision Tree, Random Forest and Gradient Boosting) have been joined in the same section as their basic principle is the same.

The principle of decision trees (**Fig. 12(a)**) consists on learning a hierarchy of if/else questions leading to a final decision. For this algorithm, all data starts in the same group

and a hierarchy is constructed until each data point is in different groups. The algorithm is widely used due to its simplicity and easy interpretation of the results. However, the algorithm is really prone to overfitting [54], [55].

To avoid overfitting, the hyperparameter "Maximum depth" can be controlled and indicates the maximum partitions that the algorithm will produce in the data when learning.

Random Forest (**Fig. 12(b)**), which is accepted to be one of the best classification algorithms available, solves the overfitting problem of decision trees. Basically, random forest is an algorithm that consists on building multiple decision trees under the assumption that each tree is different from each other. A final decision is made based on the principle of "Majority voting" which consists on deciding the class based on the most repeated class in the multiple trees created [54], [55]. The parameter to optimize in the Random Forest algorithms is the number of trees to create.

(a)   (b)
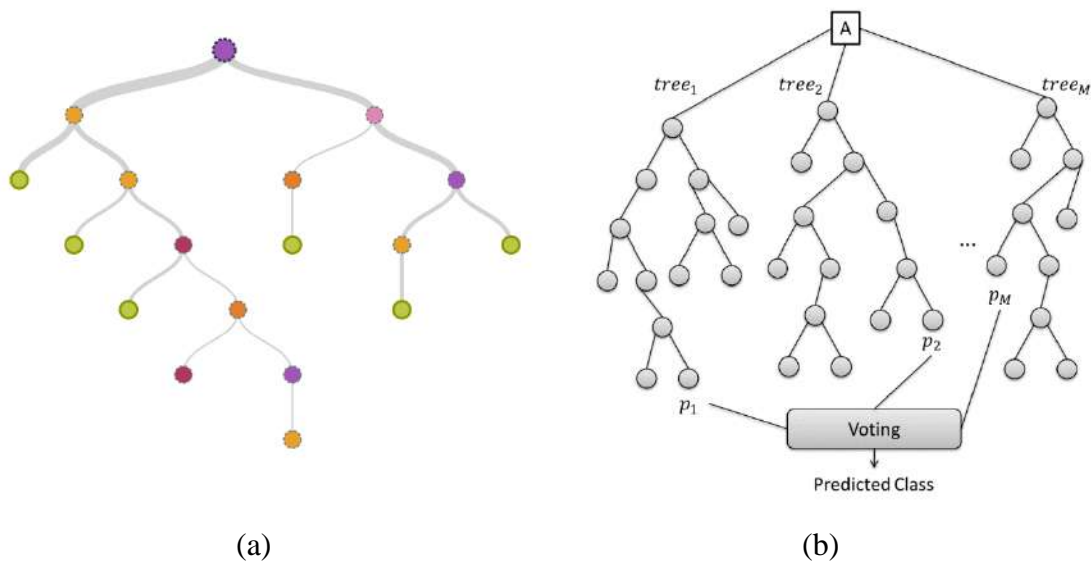
Figure 12. (a) Scheme of decision tree method algorithm and (b) scheme of random forest algorithm [56].

The last method, Gradient Boosting works similarly to Random Forest. However, in this algorithm, each tree tries to correct the errors produced by the previous tree. One parameter needed to be controlled is the learning rate, which is the strength to which each tree corrects the errors from the previous one. The other two parameters that can be

studied are, from the previous two algorithms, the maximum depth of each tree and the number of trees to be created [54].

2.5.3. KNN

KNN algorithm makes predictions of each new data point based on the information of each K number of neighbors nearer to it. The parameter to select is the number of neighbors under which the classification of a new data point is made, which is the first step of the algorithm. Then, the algorithm selects the K nearest neighbors based on the calculation of the Euclidean distance between the new data point and the points of the dataset. After that, the algorithm, under the majority voting principle, assigns a class to the new point based on the classes of the K nearest neighbors calculated.
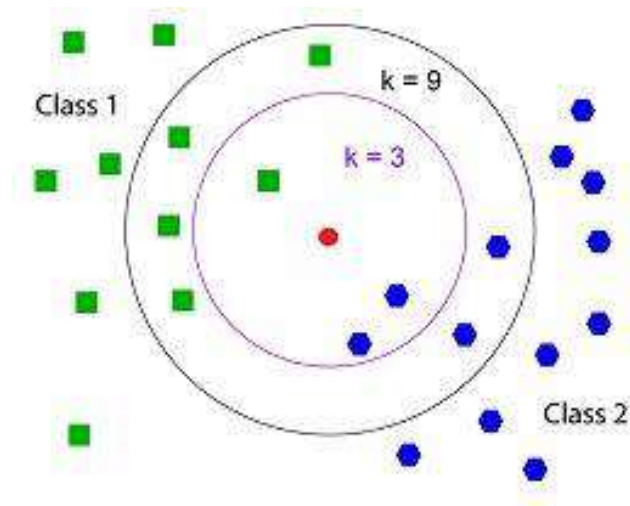
Figure 13. Scheme of KNN algorithm [57].

An example of the KNN algorithm principle can be seen in **Fig. 13**. The new data point (red) has two "Class 2" nearest neighbors and 1 "Class one" when 3 neighbors are selected so the new data point will belong to the "Class 2". On the contrary, if 9 nearest neighbors are selected, the new data point will belong to the "Class 1".

With the example of **Fig. 13** it is demonstrated the importance of the optimum numbers of neighbors to be selected.

2.5.4. Naïve Bayes

Naïve Bayes classifier is promoted to be a highly efficient algorithm. It works by learning looking individually at each of the features and make statistics of each of the classes. The are three types of classifiers: Gaussian, Bernoulli and Multinomial. The first type can be applied to any continuous data while the second type works for binary data and the last type assumes each feature to be count data. The statistics that Gaussian Naïve Bayes takes are the mean and the standard deviation while the Multinomial Naïve Bayes takes only into account the mean values. Differently, the Bernoulli Naïve Bayes, counts how often each feature of each class is positive (or not zero) [54].

To make a prediction of a new data point, the point is compared to the statistics of each of the classes [54].

As it will be seen in the future chapters, the total number of patients measured is 102 which is a relatively low value for the application of Machine Learning algorithms. For this reason, the main core of the thesis (Chapter 2, Chapter 3 and Chapter 4) has been done using classical statistical methods. In Chapter 5, preliminary results regarding the application of Machine Learning classification algorithms are presented. The following chapters show the three articles published as result of the thesis.

CHAPTER 2: Minimally Invasive Lung Tissue Differentiation Using Electrical Impedance Spectroscopy: A Comparison of the 3- and 4-Electrode Methods

Title: Minimally invasive lung tissue differentiation using electrical impedance spectroscopy: a comparison of the 3- and 4-electrode methods

Authors: Georgina Company-Se, Lexa Nescolarde, Virginia Pajares, Alfons Torrego, Pere J. Riu, Javier Rosell and Ramon Bragós

Journal: IEEEAccess

Year: 2022

Volume: 10

Number of Pages: 7354-7367

Quartile: Q2 (105/276)

Minimally Invasive Lung Tissue Differentiation Using Electrical Impedance Spectroscopy: A Comparison of the 3- and 4-Electrode Methods

GEORGINA COMPANY-SE[ID]1, **LEXA NESCOLARDE**[ID]1, **VIRGINIA PAJARES**2, **ALFONS TORREGO**2, **PERE J. RIU**[ID]1, (Senior Member, IEEE), **JAVIER ROSELL**[ID]1, (Senior Member, IEEE), **AND RAMON BRAGÓS**[ID]1

1Department of Electronic Engineering, Universitat Politècnica de Catalunya, 08034 Barcelona, Spain
2Department of Respiratory Medicine, Hospital de la Santa Creu i Sant Pau, 08041 Barcelona, Spain

Corresponding author: Lexa Nescolarde (lexa.nescolarde@upc.edu)

ABSTRACT Multiple imaging techniques are used for the diagnosis of lung diseases. The choice of a technique depends on the suspected diagnosis. Computed tomography (CT) of the thorax and positron emission tomography (PET) are imaging techniques used for the detection, characterization, staging and follow-up of lung cancer, and these techniques use ionizing radiation and are radiologist-dependent. Electrical impedance spectroscopy (EIS) performed through a bronchoscopic process could serve as a minimally invasive non-ionizing method complementary to CT and PET to characterize lung tissue. The aim of this study was to analyse the feasibility and ability of minimally invasive EIS bioimpedance measures to differentiate among healthy lung, bronchial and neoplastic lung tissues through bronchoscopy using the 3- and 4-electrode methods. Tissue differentiation was performed in 13 patients using the 4-electrode method (13 healthy lung, 12 bronchial and 3 neoplastic lung tissues) and the 3-electrode method (9 healthy lung, 10 bronchial and 2 neoplastic lung tissues). One-way analysis of variance (ANOVA) showed a statistically significant difference ($P < 0.001$) between bronchial and healthy lung tissues for both the 3- and 4-electrode methods. The 3-electrode method seemed to differentiate cancer types through changes in the cellular structures of the tissues by both the reactance (Xc) and the resistance (R). Minimally invasive measurements obtained using the 3-electrode method seem to be most suitable for differentiating between healthy and bronchial lung tissues. In the future, EIS using the 3-electrode method could be a method complementary to PET/CT and biopsy in lung pathology diagnosis.

INDEX TERMS Bronchi, bronchoscopy, electrical impedance spectroscopy (EIS), electrode methods, lung.

I. INTRODUCTION

Respiratory diseases are among the most prevalent illnesses worldwide, along with heart complications. Moreover, each year, an estimated 3 million people die due to respiratory disease complications, making respiratory diseases the third leading cause of death worldwide [1]. Lung cancer is the leading cause of cancer-related death in men and the

The associate editor coordinating the review of this manuscript and approving it for publication was Zhen Ren[ID].

second-leading cause in women [2]. However, diagnosis in early-stage disease is associated with substantially improved overall survival.

There are different ways to proceed to diagnoses of lung diseases. Computed tomography (CT) allows the detailed representation of interstitial, pleural, mediastinal and vascular structures [4]. Positron emission tomography (PET) provides information about cellular metabolism. Integrated CT with PET (PET/CT) [5] combines the anatomical information from CT with the metabolic information from

PET, which makes it possible to obtain a more accurate diagnosis.

Flexible bronchoscopy, the least invasive bronchoscopic procedure, is of limited value for obtaining tissue from lesions in the peripheral segments of the lung.

The selection of the biopsy site is relatively simple when the patient has endobronchial involvement. However, in peripheral tumours without endobronchial involvement, additional techniques are necessary to help to confirm that the location of the biopsy is correct. The increasing need to efficiently and safely sample lung lesions has led to the development of virtual bronchoscopy (VB), radial endobronchial ultrasound (r-EBUS), electromagnetic navigation (EMN) and ultrathin bronchoscopes. The diagnostic yield using these bronchoscopic techniques remains suboptimal [6], [7], and their high economic cost makes them unavailable in most centres. To complement the current methods of diagnosing lung diseases, we aim to use electrical impedance spectroscopy (EIS). EIS could allow the differentiation of healthy tissue from tumour tissue and help in the choice of the specific sampling location.

Impedance analysis techniques (such as EIS) consist of the application of electrical current to biological tissues to observe changes in their passive electrical properties [8]. Impedance is the general term used to define the opposition of a conductor to a current flow [9]. When a current is injected into biological tissue, the opposition that biological tissues produce to the current is called bioimpedance. Bioimpedance is composed of two components, resistance (R) and reactance (Xc). On the one hand, the opposition that the physiological fluid, both intracellular and extracellular, presents to a given current flow produces the resistive component. On the other hand, reactance is given by the polarization of the cellular membranes and the tissue interfaces, producing a delay between the current flow and the voltage. This delay defines the parameter called the phase angle (PA) [10], [11]. Both components of bioimpedance (R and Xc) are positively correlated. The current flow applied to the tissues can be either direct current or alternating current. When direct current is applied, the reactive effect disappears, making the bioimpedance completely resistive. This means that when direct current is applied, the current flow circulates only through the physiological fluid. However, when alternating current is applied to tissues, the current is able to flow for both physiological fluid and capacitive elements. This phenomenon makes bioimpedance a frequency-dependent measure [10]. At low frequencies, the current is not able to penetrate the cellular membranes, so there is no conduction within the cells, which is due to the high impedance of the cellular membranes and the tissue interfaces. Therefore, we define the bioimpedance (Z) as a vector as a function of R and Xc [9] and the PA as the arctangent of the ratio between Xc and R.

The impedance modulus (|Z|) is highly correlated with the resistive component, with |Z| being slightly higher than R because of the reactive component [10].

Bioimpedance measures can be obtained using single or multiple frequencies. When the measures are obtained using a single frequency, the most common frequency is 50 kHz due to its high signal-to-noise ratio [10]. Regarding non-invasive single frequency (50 kHz), Toso et al. [11] observed a decrease in the Xc parameter and, as a consequence, a decrease in the PA, preserving the R component in patients with lung neoplasms.

Different studies can be found regarding the applicability of EIS for tissue differentiation and characterization [12]–[21]. Dean et al. [12] and Héroux and Bordages [13] studied the properties of the electrical impedance of biological tissue. They observed changes in impedance as a function of frequency, arriving at the conclusion that the data obtained and the changes in impedance were consistent according to the basic principles of the bioimpedance already introduced. Other studies, such as da Silva et al. [14] and Yoon et al. [15], investigated the possible use of the technique for the distinction of different types of tissue. The first study was focused on breast tissue and the differentiation between cancerous and healthy tissue. The second study focused on the evaluation of the frequency response of bioimpedance measures in rabbits' tendons through two different types of measures, one longitudinal and other transverse in relation to the tendon fibbers to detect pathological changes in tendons to find the exact location of a tendinitis lesion. Skourou et al. [16] and Desai et al. [17] evaluated the ability of impedance spectroscopy to detect tumours in their initial stages. The first concluded that the technique allowed the detection of tumours that were not possible to detect with other conventional techniques, such as CT, due to their reduced size. Hillary et al. [18] analysed the spectrum of the impedance values obtained for different soft tissues located in the neck, including adipose, parathyroid, thyroid, and muscle tissues. The purpose of the study was to correctly identify the parathyroid tissue to preserve it to facilitate surgery on the parathyroid glands and reduce the occurrence of post-surgery hypoparathyroidism. A bioimpedance method to detect cancer, using a custom-designed catheter with 4-electrodes placed on the front face of a catheter, was tested for Barret's Esophagus [19] and for cervical neoplasia [20].

Regarding the use of EIS to measure lung bioimpedance, Gabriel et al. [21] proposed a model to predict dielectric data based on the data present in the literature for different tissues, among which they analysed the inflated lung. Desai et al. [17] studied the ability of the technique to differentiate between carcinogenic and healthy cells by extracting different cancer cell types and through pattern recognition techniques evaluating the ability to differentiate between the two types of cells. They studied multiple cancer types, including lung cancer.

Sanchez et al. [22], in a previous report, validated the use of minimally invasive EIS with the 4-electrode method for lung bioimpedance measures through a bronchoscopic process. Later, Riu et al. [23] published a preliminary report using a single frequency response with a 4-electrode method

to differentiate among healthy lung tissue, bronchi and multiple parenchymal pathologies. They found a statistically significant difference with respect to the PA at 33 kHz between healthy lung tissue and bronchial tissue and between bronchial tissue and multiple parenchymal pathologies.

Later more references will be added in the discussion section, to highlight their relationship with our findings. The use of 4 electrodes in the tip of the catheter produces a local estimation of the tissues in contact with the electrodes and reduces the contribution of electrode-tissue impedances to the measurements; however, we hypothesize that the use of 4 electrodes is more prone to artefacts due to the difficulties in obtaining good contact between all four electrodes and the surrounding tissue. Using the 3-electrode method (typical in electrochemical EIS but not so typical in biomedical measurements), only one contact must be established between the catheter and the surrounding tissues. Additionally, the catheter could be simpler, reducing its cost and size. However, there are no previous studies regarding the use of EIS for minimally invasive lung measures for tissue differentiation using the 3- and 4-electrode methods.

The aim of this study was to analyse the capability of minimally invasive EIS, using 3 and 4-electrode methods, to differentiate healthy lung tissue and bronchial and neoplasm lung tissue

II. MATERIALS AND METHODS

A. PARTICIPANTS

Minimally invasive EIS was performed in 13 patients (69 ± 12 yr; 70.1 ± 15.1 kg; 25.7 ± 4.7 kgm^{-2}) for whom bronchoscopy was indicated during July 2020 at the "Hospital de la Santa Creu i Sant Pau". The bioimpedance measures were obtained via the 4-electrode method (13 healthy lung, 12 bronchial and 3 neoplastic lung tissues) and 3-electrode method (9 healthy lung, 10 bronchial and 2 neoplastic lung tissues).

Ethics approval was obtained from the Hospital de la Santa Creu i Sant Pau (CEIC-73/2010) according to principles of the Declaration of Helsinki for experiments with human beings. All patients provided signed informed consent.

B. MEASUREMENT SYSTEM

To acquire the bioimpedance measures, a tetrapolar catheter, 115 cm long with a diameter of 1.65 mm (5 F), was used (Medtronic 5F RF Marinr steerable catheter with electrode separation 2/5/2 mm) (**Fig. 2**). To convert the 4-electrode measurement system of the catheter to the 3-electrode system, a switch was introduced so that the same catheter could be used for the measures obtained with both three and four electrode methods (**Fig. 1**). Moreover, for the measures obtained with 3 electrodes, two skin electrodes placed on the right side of the patients at the level of the ribs were used (**Fig. 2**).

The measurement system consists of 3 devices (**Fig. 1**): an insulated front end, which is an optically insulated battery-powered patient interface, including the impedance front end;

a rugged PC platform based on a PXI system from National Instruments; and an analog–optical interface front end to connect the PXI with the insulated front end. The system includes an arbitrary waveform generator that generates a multisine excitation signal, which is a broadband signal composed of 26 frequencies between 1 kHz and 1 MHz. The front-end includes an AC-coupled current source which ensures a current lower than the maximum allowable patient auxiliary current stablished in the IEC 60601-1:2005 (<1 mA rms measured with the circuit proposed in the IEC 60601-1:2005). The voltage ($V(t)$) and current ($I(t)$) are simultaneously acquired. The excitation is converted into an optical signal with the optical–analog interface connected to the PXI. This optical signal is then reconverted into an electrical signal inside the front end. The voltage and current signals, which are optically transmitted from the front end to the optical–electrical interface, are filtered (cut-off frequency 10 MHz) and acquired with the digitizer card. A schematic representation of the bioimpedance acquisition system is shown in **Fig. 1**.

Bioimpedance measures were obtained using the 4-electrode method and the 3-electrode method through bronchoscopy. With the 4-electrodes method, the 4 electrodes located in the distal part of the catheter were placed in the desired area. The external electrodes injected electrical current (high current (HC) and low current (LC)), while the internal electrodes measured the voltage differences generated (high potential (HP) and low potential (LP)). When measuring with three electrodes, the electrode placed at the tip of the catheter was used to inject the current (HC) and to detect the potential (HP), and the LC and LP electrodes were the two skin electrodes placed on the right side of the patient at rib level. A schematic representation of both methods is shown in **Fig. 2**.

C. MEASUREMENT PROTOCOL

To obtain the bioimpedance measures, bronchoscopy, a medical procedure used to inspect the airways, was performed. Prior to bronchoscopy, a radiological imaging technique (CT or PET/CT) was performed as part of the diagnostic process. In addition, the catheter was inserted through a port of the bronchoscope.

During the process, patients were placed in a supine position. The upper airway was anaesthetized with topical 2% lidocaine; intravenous sedation was provided throughout the procedure with midazolam, fentanyl and propofol. All samples were harvested through a flexible bronchoscope during procedures that included endoscopic exploration and other diagnostic tests as required.

Once at the region of interest, measures were taken first with 4 electrodes and then with 3 electrodes after closing the switch (**Fig. 1**). The process was always the same. First, bronchial measures were taken, followed by healthy lung tissue measures and then pathological lung tissue (if any) measures. Once the bronchoscope arrived at the region of interest, we had to ensure that the patient was
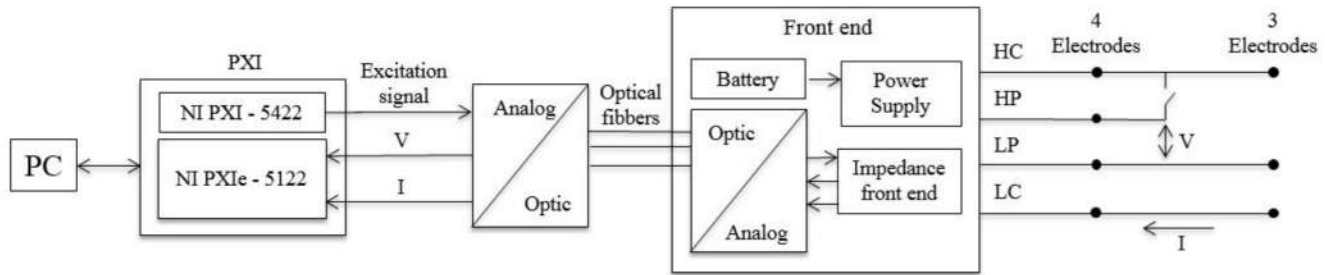
FIGURE 1. Schematic representation of the bioimpedance acquisition system. For better understanding of the electrodes' connection in each case, please also see Figure 2.
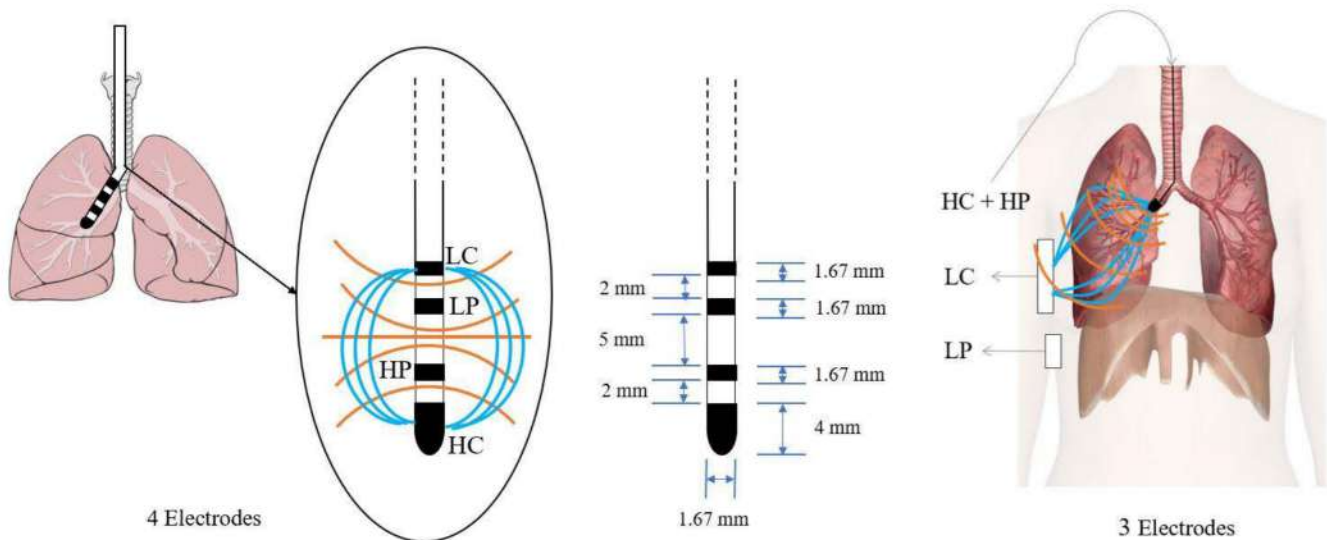

FIGURE 2. Schematic representation of the 4- (left image) and 3- (right image) electrode methods. Blue lines represent the current lines, and orange lines represent the voltage lines. In 4-electrode method, the four electrode are inside the lung, while 3-electrode method, LC and LP are on the skin using skin surface electrode. In the central figure, the dimensions of the electrodes are represented.

not moving during the 15 seconds of recording for each location.

D. EIS MEASUREMENTS

Bioimpedance measurements were obtained at the same location with both 4 and 3 electrodes, with approximately 15 seconds of difference between the measurements. EIS consisted on the application of a multisine current signal (26 frequencies from 1 kHz to 1 MHz) and the acquisition of the voltage and current signals. The fast Fourier transform (FFT) was calculated for both the acquired voltage and current signals. The bioimpedance was calculated by obtaining the ratio between the voltage and current coefficients of the FFT corresponding to each injected frequency. 50 spectra per second were acquired along 15 s for each measurement and were averaged to reduce the effect of the modulation induced by ventilation and perfusion.

The 4 electrode configuration measurements were calibrated with 3 saline solutions which covered the measurement impedance range and following the method described in [24]. In the configuration with 3 electrodes, and being two of them in the body surface, this set-up could not be used and

was substituted by a measurement over a known resistor (100 Ohms) connected to the catheter tip and to the external electrode connectors.

E. DATA ANALYSIS

In this study, the averaged spectra of the bioimpedance measurements, obtained using the 3 and 4-electrode methods, throughout the acquisition time were used for the tissue differentiation analysis among healthy lung, bronchial and neoplastic lung tissues. The frequency range chosen to visualize the data was 5 kHz – 209 kHz. The values from the frequencies higher and lower than this range were discarded due to electrode and capacitive errors. The interval of 11 kHz – 95 kHz showed a better discriminatory response for tissue differentiation.

For mono-frequency analysis, a central frequency of 33 kHz was chosen (as done in Riu *et al.* [23]) to develop the statistical analysis of $|Z|$, PA, R and Xc for tissue differentiation between healthy lung tissue and bronchial tissue.

The normality of the distribution of the variables was determined by the Shapiro-Wilk test. Normally distributed variables are shown as the mean $\pm$ standard error of the
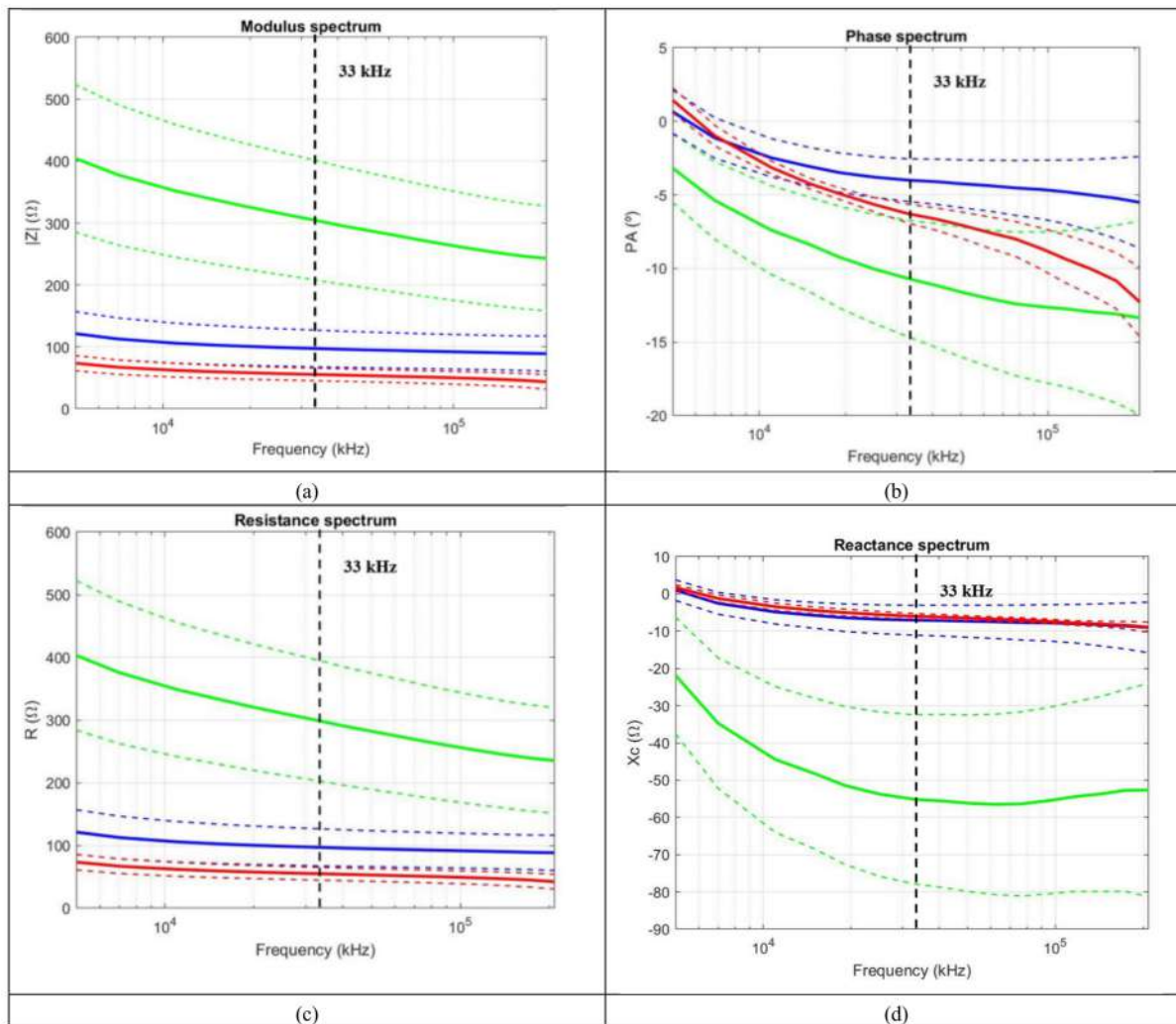
FIGURE 3. The mean (continuous line) and SD (dashed line) values from the bioimpedance signal along the different frequencies analysed obtained with 4-electrode method. The (a) modulus, (b) phase angle, (c) resistance and (d) capacitive reactance. Green: healthy lung tissues; blue: bronchial tissues; red: neoplastic lung tissues.

mean (SEM) and 95% confidence interval for the mean (lower limit and upper limit). One-way analysis of variance (ANOVA) was used to determine statistically significant differences in the |Z|, PA, R and Xc values between healthy lung tissue and bronchial tissue for both the 3- and 4-electrode methods.

In the case of the measurements in neoplasic lung tissue, due to the small sample size, the descriptive analysis (for both the 3- and 4-electrode methods) was performed using the mean impedance spectra.

The statistical software IBM®SPSS®version 26.0 (IBM Corp, Armonk, NY, United States) was used for data analysis. The level of statistical significance was set at $P < 0.05$.

III. RESULTS
A. MULTI-FREQUENCY RESPONSE FOR MINIMALLY INVASIVE LUNG EIS MEASURES

Fig. 3 and **Fig. 4** show the mean (continuous line) and SD (dashed line) values of |Z|, PA, R and Xc plotted along the

frequency range (5 kHz - 209 kHz) used for the measures obtained with 4 and 3-electrode method, respectively. The green line represents healthy lung tissue, the blue line represents bronchial tissue, and the red line represent tissues from three different types of lung neoplasms. The vertical dashed black lines represent the frequency (33 kHz) at which the data were analysed for tissue differentiation.

Table 1 and **Table 2** show the values of |Z|, PA, R and Xc at a frequency of 33 kHz according to measurement location (healthy lung tissue and bronchial tissue) obtained with 4 and 3 electrodes, respectively, in the sample of patients.

B. TISSUE DIFFERENTIATION

Table 3 lists the descriptive parameters, specified as the mean ± SEM, 95% confidence interval for the mean (lower limit and upper limit), of |Z|, PA, R and Xc and the results of the one-way ANOVA including the Fisher coefficient (F) for the 4-electrode method (healthy tissues: n = 13; bronchial tissues: n = 12) and the 3-electrode method (healthy tissues: n = 9; bronchial tissues: n = 10).
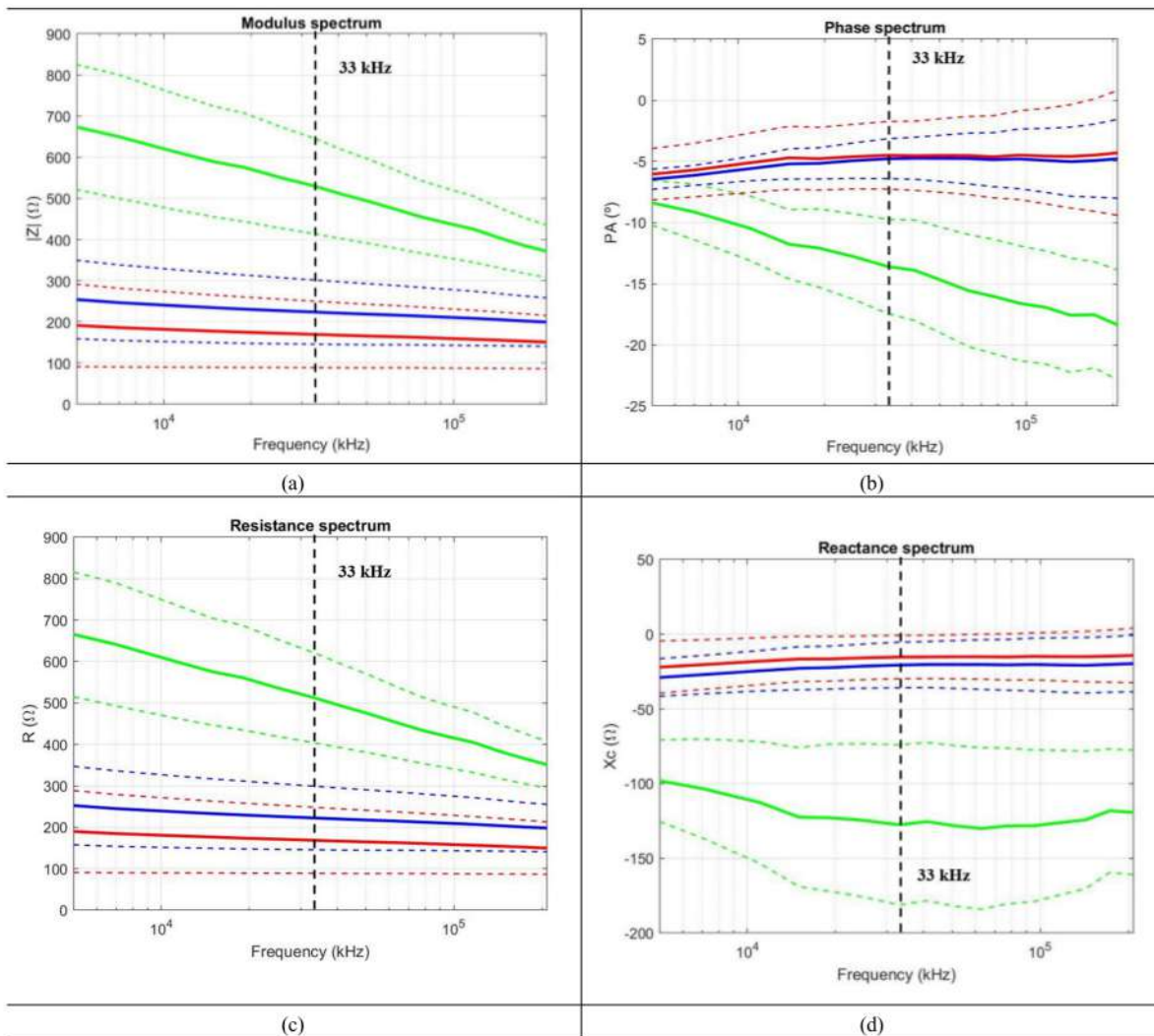
FIGURE 4. The mean (continuous line) and SD (dashed line) values from the bioimpedance signal along the different frequencies analysed obtained with 3-electrode method. The (a) modulus, (b) phase angle, (c) resistance and (d) capacitive reactance. Green: healthy lung tissues; blue: bronchial tissues; red: neoplastic lung tissues.

With the use of four electrodes, a statistically significant difference ($P < 0.001$) between healthy tissue and bronchial tissue was observed, with higher Fisher coefficient in Xc ($F = 52.103$; $P < 0.001$), $|Z|$ ($F = 50.719$; $P < 0.001$) and R ($F = 48.648$; $P < 0.001$) and lower Fisher coefficient in PA ($F = 30.471$; $P < 0.001$). With the use of 3 electrodes, a statistically significant difference ($P < 0.001$) between healthy tissue and bronchial tissue was also observed, with higher F in $|Z|$ ($F = 46.417$; $P < 0.001$), R ($F = 46.002$; $P < 0.001$) and PA ($F = 43.796$; $P < 0.001$) and lower in Xc ($F = 36.784$; $P < 0.001$).

C. LUNG NEOPLASM MEASURES

Fig. 5 and **Fig. 6** show the mean impedance spectra of the values of $|Z|$, PA, R and Xc plotted along the frequency range (5 kHz - 209 kHz) for the measures obtained from lung neoplasms with 4 and 3 electrodes, respectively; these values could be used to differentiate the different neoplasm types evaluated. The vertical dashed black lines

represent the frequency (33 kHz) at which the data were analysed. Each of the colours of the graphs represents a different neoplasm sample. Histologically, lung squamous carcinoma (infiltrating: black and non-infiltrating: red) and lung adenocarcinoma (cyan) were identified. In **Fig. 6**, the values obtained from the lung adenocarcinoma (cyan) were discarded due to poor electrode contact because patient coughed.

Table 4 shows the values of $|Z|$, PA, R and Xc obtained at a frequency of 33 kHz from lung neoplasms with both the 4- and 3-electrode methods. In addition, the type of cancer is specified in **Table 4**.

The different cancer types could also be distinguished using only bioimpedance measures, as the measures obtained from different neoplasm types were different from each other, as shown in **Fig. 5** and **Fig. 6**.

Fig. 7 shows the PET/CT images and CT images of each of the lung neoplasm types according to the histological diagnosis.

TABLE 1. Individual values of |Z|, PA, R and Xc at 33 kHz extracted from the bioimpedance measurements obtained with 4 electrodes.

	Healthy lung tissues					Bronchial tissues			
ID-H	|Z| (Ω)	PA (°)	R (Ω)	Xc (Ω)	ID-B	|Z| (Ω)	PA (°)	R (Ω)	Xc (Ω)
1H-4	215.42	-4.70	214.70	-17.63	1B-4	133.77	-3.78	133.48	-8.80
2H-4	257.72	-7.73	255.37	-34.65	2B-4	65.92	-4.73	65.70	-5.44
3H-4	359.49	-5.81	357.63	-36.44	3B-4	48.61	-2.41	48.57	-2.04
4H-4	249.47	-16.80	238.82	-72.11	4B-4	75.03	-2.27	74.97	-2.98
5H-4	421.58	-5.35	419.75	-39.24	6B-4	130.09	-7.05	129.11	-15.97
6H-4	507.17	-11.02	497.81	-97.00	7B-4	85.32	-5.12	84.98	-7.61
7H-4	135.70	-10.79	133.30	-25.39	8B-4	72.06	-4.68	71.82	-5.88
8H-4	258.49	-14.80	249.91	-66.05	9B-4	106.02	-3.44	105.83	-6.37
9H-4	344.34	-11.06	337.91	-66.12	10B-4	134.78	-5.61	134.13	-13.18
10H-4	283.05	-11.12	277.72	-54.63	11B-4	102.12	-3.02	101.98	-5.38
11H-4	380.71	-10.33	374.50	-68.05	12B-4	84.69	-3.01	84.57	-4.45
12H-4	250.91	-15.96	241.24	-68.93	13B-4	129.74	-2.90	129.58	-6.56
13H-4	301.37	-13.60	292.92	-70.84					

TABLE 2. Individual values of |Z|. PA. R and Xc at 33 kHz extracted from the bioimpedance measurements obtained with 3 electrodes.

	Healthy lung tissues					Bronchial tissues			
ID-H	|Z| (Ω)	PA (°)	R (Ω)	Xc (Ω)	ID-B	|Z| (Ω)	PA (°)	R (Ω)	Xc (Ω)
1H-3	429.83	-5.86	427.58	-43.86	1B-3	217.89	-4.34	217.26	-16.44
2H-3	607.15	-10.92	596.14	-115.07	3B-3	132.55	-3.52	132.29	-8.15
3H-3	585.55	-13.99	568.18	-141.53	4B-3	159.61	-3.26	159.35	-9.06
7H-3	372.84	-14.15	361.52	-91.18	7B-3	323.93	-7.72	320.99	-43.54
8H-3	634.40	-16.78	607.39	-183.13	8B-3	173.34	-3.94	172.93	-11.91
9H-3	668.97	-18.96	632.65	-217.41	9B-3	218.43	-4.56	217.73	-17.32
10H-3	629.11	-14.15	610.00	-153.83	10B-3	392.00	-7.85	388.32	-53.55
12H-3	400.23	-11.30	392.47	-78.41	11B-3	198.67	-4.40	198.09	-15.23
13H-3	443.99	-16.15	426.45	-123.53	12B-3	196.00	-3.97	195.53	-13.57
					13B-3	226.28	-4.26	225.66	-16.82

IV. DISCUSSION

This project, developed by the Universitat Politècnica de Catalunya (UPC) Biomedical Engineering Instrumentation Group and the Interventional Pulmonology Unit of the Respiratory Medicine Department of the Hospital de la Santa Creu i Sant Pau, evaluates the ability of EIS to differentiate lung tissue according to disease state and anatomical location using 3 and 4 electrodes to obtain the measures. The lungs are the organs of the respiratory system, whose most basic function is to facilitate gas exchange [25]. Other structures of the respiratory system are trachea, bronchi, bronchioles. Each of these structures has anatomical and histological characteristics. Therefore, differences in bioimpedance measurement can be expected based on the type of tissue and its state.

This work reports the use of minimally invasive EIS in lungs through a bronchoscopic process using the 4- and 3-electrode methods to differentiate among healthy lung tissue, bronchi and lung neoplasms. A previous study regarding the validation of minimally invasive EIS for lung bioimpedance measures through a bronchoscopic process [22] obtained the measures using the 4-electrode configuration, while the 3-electrode strategy has been used in heart applications [26].

TABLE 3. Descriptive parameters of |Z|, PA, R and Xc extracted from the bioimpedance measurements obtained with 4 and 3 electrodes and one-way ANOVA test results.

	4 Electrodes			
	Mean ± SEM 95% CI (lower limit – upper limit)			
	Healthy tissues (n=13)	Bronchial tissues (n=12)	F	P
|Z| (Ω)	305.34 ± 29.17 (241.14 - 369.53)	97.35 ± 8.60 (78.43 - 116.26)	50.719	0.000
PA (°)	-10.46 ± 1.16 (-13.02 – (-7.89))	-4.00 ± 0.42 (-4.92 – (-3.08))	30.471	0.000
R (Ω)	299.89 ± 29.00 (236.05 - 363.72)	97.06 ± 8.55 (78.24 - 115.88)	48.648	0.000
Xc (Ω)	-53.85 ± 6.70 (-68.61 – (-39.10))	-7.06 ± 1.16 (-9.60 – (-4.51))	52.103	0.000
	3 Electrodes			
	Mean ± SEM 95% CI (lower limit – upper limit)			
	Healthy tissues (n=9)	Bronchial tissues (n=10)	F	P
|Z| (Ω)	530.23 ± 38.74 (440.90 - 619.56)	223.60 ± 27.58 (160.00 - 287.21)	46.417	0.000
PA (°)	-13.58 ± 1.28 (-16.54 – (-10.63))	-4.84 ± 0.57 (-6.16 – (-3.52))	43.796	0.000
R (Ω)	513.60 ± 36.30 (429.90 - 597.30)	222.50 ± 27.17 (159.84 - 285.15)	46.002	0.000
Xc (Ω)	-127.55 ± 17.86 (-168.73 – (-86.37))	-20.97 ± 5.38 (-33.37 – (-8.58))	36.784	0.000

TABLE 4. Individual values of lung neoplasm measurements of |Z|, PA, R and Xc extracted from the bioimpedance measurements obtained with 4 and 3 electrodes and the corresponding lung neoplasm type.

	Lung neoplasm									
	4 Electrodes				3 Electrodes					Cancer type
ID-NL	|Z| (Ω)	PA (°)	R (Ω)	Xc (Ω)	ID-NL	|Z| (Ω)	PA (°)	R (Ω)	Xc (Ω)	
1NL-4	45.00	-6.57	44.70	-5.16	1NL-3	112.55	-2.54	112.44	-5.00	Lung squamous carcinoma (infiltrating)
4NL-4	65.38	-5.56	65.07	-6.33	4NL-3	226.71	-6.45	225.27	-25.48	Lung squamous carcinoma (non-infiltrating)
5NL-4	55.60	-6.74	55.22	-6.52						Lung adenocarcinoma

The measured bioimpedance used in this work is proportional to the intrinsic properties of the tissues (conductivity and permittivity) multiplied by a factor, the so called "cell constant" that depends on geometric factors of electrode arrangement and tissue distribution. In order to know the feasibility to differentiate different tissues we used the measured impedance because the application of a cell constant will not modify the comparative results, and also because the cell constant will be unknown for in vivo measurements.

Measures obtained with 4 electrodes reduce the effect of the impedance of the electrode-tissue interfaces. The electrodes are all placed in the distal part of a catheter and are sensitive to the region in contact with the electrodes. In the 3-electrode method, only one electrode is used in the distal tip of the catheter, while the other two electrodes are placed on the skin surface of the thorax [26]. There is an effect on the measured impedance related to the effective area of contact of the electrodes in the catheter against the lung tissue to be investigated. Reducing the contact area will increase the measured impedance due to the increase of current density in the tissue. In the tubular structure of the bronchi and bronchioles the measured impedance will increase if the diameter of the catheter and the diameter of the tubular structure are similar but will decrease as the diameter of the bronchi is bigger and the electrode is losing contact
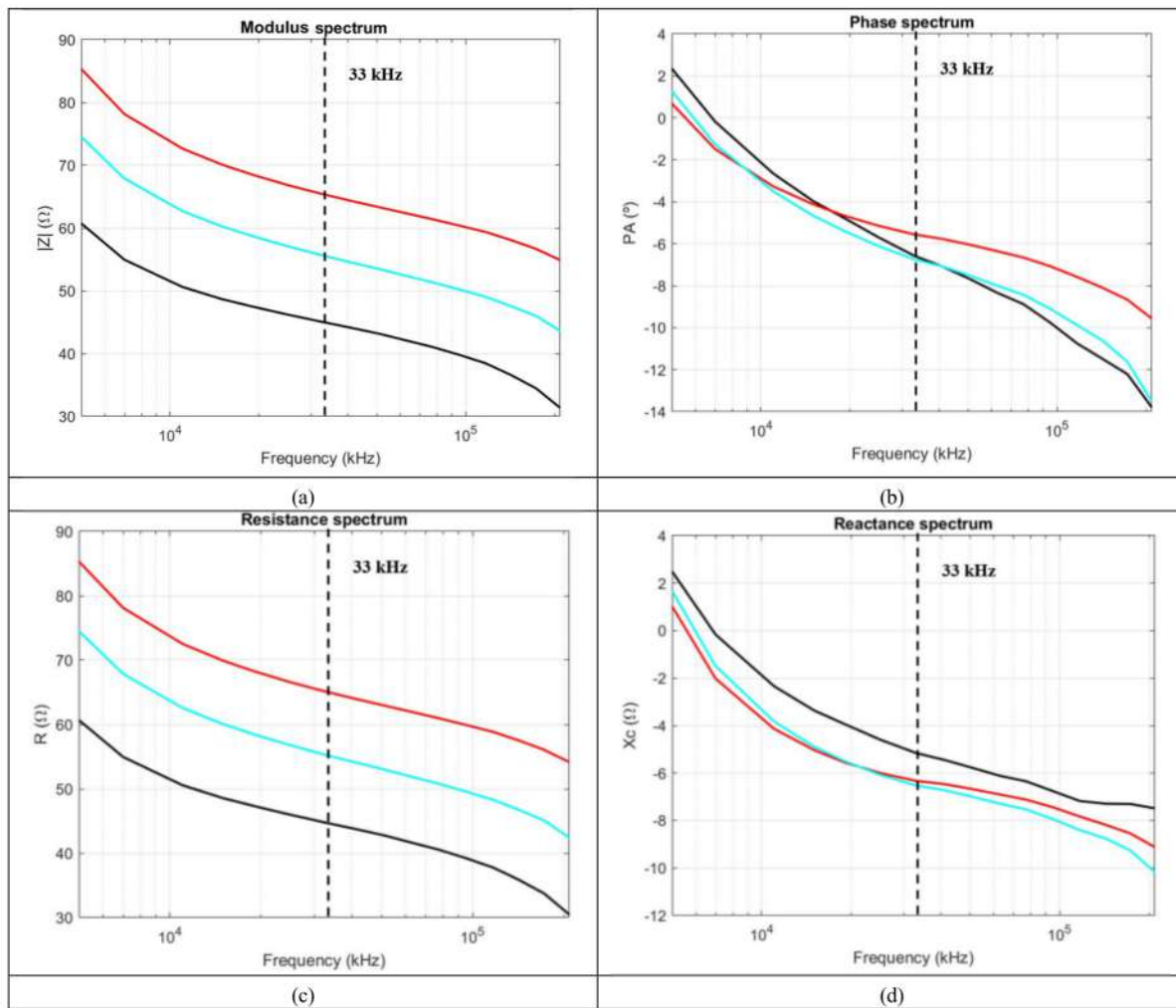
FIGURE 5. Results of the parameters extracted from the bioimpedance signal along the different frequencies analysed obtained with 4 electrodes from lung neoplasms. The a) modulus, b) phase angle, c) resistance and d) reactance of the bioimpedance of all the different measures obtained. Black: lung squamous carcinoma (infiltrating); red: lung squamous carcinoma (non-infiltrating); and cyan: lung adenocarcinoma.

with the tissue surface. Another factor that will modify the measured impedance is the mucosa content (or other liquids for example in the case of carcinoma) in the bronchi or bronchiole. This effect will be higher for healthy tissue because the impedance of the liquid is lower than the impedance of healthy tissue.

The simplest method, the two-electrode method using the tip of the catheter and an external skin electrode, was discarded because the impedance of the skin electrode is also measured and it has high interpatient variability (that is not related to the characteristics of the lung tissue) and depends on skin hydration and sweat regulation.

Other authors [19] [20] have proposed electrode arrangements based on 4 electrodes on the front face of a catheter, either intended to be introduced through an endoscope [19] or to be used as a pencil-like probe [20]. However, these implementations are very thick (3.2 mm and 5.5 mm in

diameter) for many in-vivo applications. Reference [27] acknowledged these limitations and developed a probe which is 2 mm in diameter. One of the main problems with all these probes is the very small electrode area ($0.5\ mm^2$, $0.8\ mm^2$ and $0.2\ mm^2$ respectively) which increases electrode impedance at low frequencies, up to a point where it is not possible to make measurements due to instrumentation limitations. These limitations are clearly shown in in-vivo measurements [28], where usable data is only at frequencies over 500 kHz, much above the frequency range where we found significant differences in lung tissues. In addition, these probes need to make a perpendicular contact with the tissue, which is not granted in lung tissue at the level of bronchioles.

In contrast, our catheter has only a diameter of 1.67 mm (5F) while keeping electrode areas of about $10\ mm^2$. Contact can be difficult in the bronchi, but it is granted at the alveolar level. At that level, it would be impossible to make contact
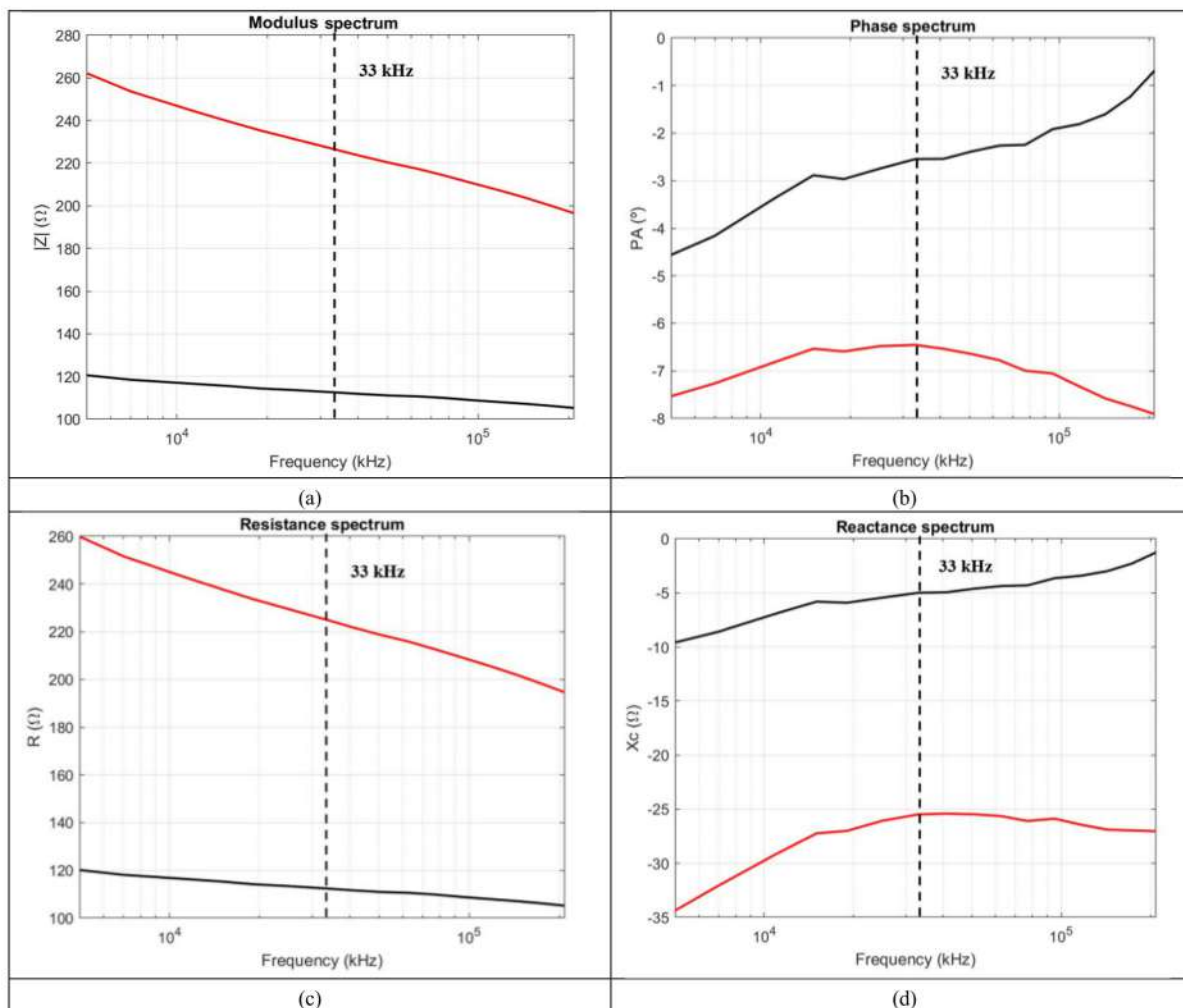
FIGURE 6. Results of the parameters extracted from the bioimpedance signal along the different frequencies analysed obtained with 3 electrodes from lung neoplasms. The a) modulus, b) phase angle, c) resistance and d) reactance of the bioimpedance of all the different measures obtained. Black: lung squamous carcinoma (infiltrating) and red: lung squamous carcinoma (non-infiltrating).
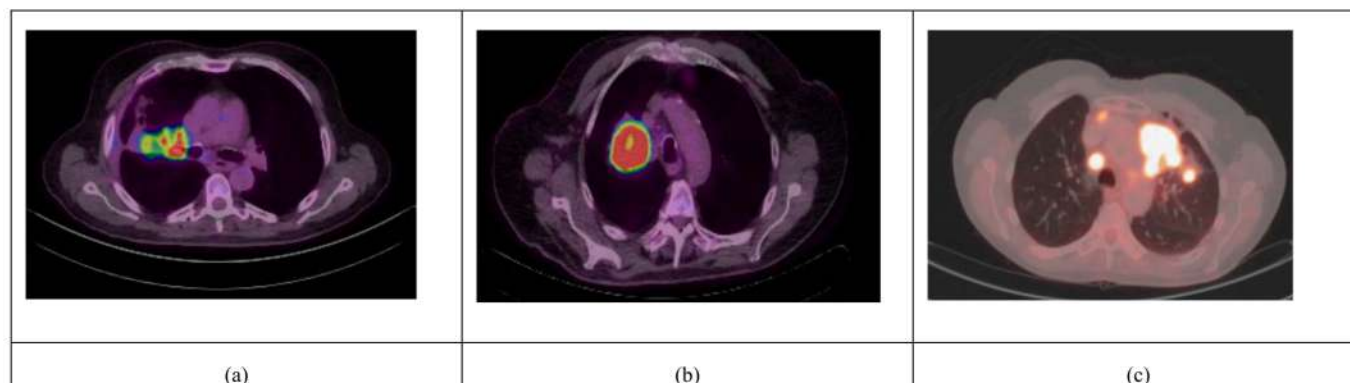

FIGURE 7. PET/TC and CT images of the lung neoplasms. The histological diagnoses were a) lung squamous carcinoma (infiltrating), b) lung squamous carcinoma (non-infiltrating) and c) lung adenocarcinoma.

with a frontal electrode arrangement without risking breaking the walls of the alveoli.

Other authors, like [29], have proposed more sophisticated arrangements to make measurements in lung tissue in-vivo. However, there are no experimental results with this proposed probe, and to our knowledge, it can also risk damaging the tissue.

Following this description, and due to the trabecular structure of the lung, the placement of the electrodes with the 3-electrode method is easier to perform than with the

4-electrode method (**Fig. 1** and **Fig. 2**) since the 4 electrodes are internal and need to be in contact with the lung tissue. During the bronchoscopy process (used to obtain the bioimpedance measurements of the lungs), patients may cough, despite sedation, and contact between the electrode and the tissue of interest may be lost, resulting in a loss of data.

In this preliminary study the same patient was measured first with 4 electrodes and then with 3 electrodes, increasing the measurements time. Despite sedation, some of them did not tolerate long time without coughing. For this reason, some measurements made with the 3-electrode method had to be removed.

Another aspect taken into account was the possible loss of contact in the two skin surface electrodes in the case of the 3-electrode method (**Fig. 2**). However, this problem did not occur.

In addition, ensuring the contact of the four electrodes in a 4-electrode lateral configuration is not easy and the loss of contact of one of the electrodes may be difficult to detect. Using the described 3-electrode configuration, the loss of contact of one of the electrodes is clearly detected.

The multi-frequency range from 11 kHz to 95 kHz shows a better discriminatory response for tissue differentiation. Healthy lung tissue is clearly differentiable from bronchial and neoplastic lung tissues in both the 4- and 3-electrode methods, while bronchial and neoplastic lung tissues show a similar frequency response.

|Z| and R were higher in healthy lung tissue than in bronchi, while PA and Xc were lower in these locations. Additionally, |Z| and R values obtained with 3 electrodes were higher than those obtained with 4 electrodes. A decrease in the mean PA and Xc values obtained using the 3-electrode method compared with the 4-electrode method was observed. This could be explained because with the 4-electrode method, the voltage drop is sensed at the probe where the current is injected, meaning there are no surrounding tissues that could influence the measure. In contrast, with the 3-electrode method, the voltage drop includes the tissue-electrode impedance of the HC electrode (the distal electrode of the catheter) and the tissues between the catheter and the skin electrodes placed on the right side of the patient (LP) at the level of the ribs, producing an increase in the values of |Z| *and R*. The main contribution to this increment of impedance is due to the tissue-electrode interface because the 3-electrode method shows more sensitivity at the catheter tip due to the decay of sensitivity with the distance to the current injection point [30].

As expected, the |Z| and R values obtained are similar, showing a higher influence of R than Xc on |Z|.

Emphasizing the importance of the analysis of R and Xc according to the theory of Lukaski *et al.* [9], [10], [31], [32], we selected the frequency (33 kHz) that allowed us to differentiate among tissues with the 3-electrode method as well as

the 4-electrode method, following the preliminary report of Riu *et al.* [23]. According to the results obtained (**Fig. 3** and **Fig. 4**), the optimal frequency could be different from the one analyzed in this work (33 kHz). In the bioimpedance equation ($Z = R + jX_c$), the variable R describes the behaviour of the medium through which the injected current flows, while $X_c = -\frac{1}{wC}$ describes the capacitive component of the cellular membranes [9], [10]. The values of modulus Z and PA ($|Z| = \sqrt{(R^2 + Xc^2)}$ and $\Phi = \tan^{-1}\left(\frac{Xc}{R}\right)$, respectively) are dependent on the values of R and Xc. Regarding tissue differentiation at 33 kHz, in both the 4- and the 3-electrode methods, one-way ANOVA reported significant results ($P < 0.001$) for all variables (|Z|, PA, R and Xc). The Fisher coefficient represents the relationship between the inter-group variance and the intra-group variance. Therefore, a higher F coefficient indicates a greater inter-group variance than intra-group variance [33]. For the 4-electrode method, the Fisher coefficient (F) is higher for Xc, while for the 3-electrode method, F is higher for R.

The small number of cancer sample allows only an observational analysis of the medical images obtained by PET/CT, for which the strongest point of CT is the detailed representation of interstitial structures [6]; the confirmation of biopsy sample findings; and the mean impedance spectra of Z|, PA, R and Xc.

The types of cancer analysed (lung squamous carcinoma and lung adenocarcinoma) are included among the non-small-cell lung cancers [34].

The sample sizes of the different cancer types analysed did not allow us to perform a comparative analysis of the cancer histological observations; and the bioimpedance values (|Z|, PA, R and Xc) obtained. Moreover, the small sample size did not allow us to perform a statistical analysis of the measurements obtained with a single frequency at 33 kHz. However, all results seem to indicate that the 3-electrode method seems to differentiate the cancer types in terms of changes in the cellular structures of the tissue (by Xc) as well as in terms of changes in the extracellular fluid-related parameters (R), whereas with the 4-electrode method, only R is able to differentiate between the cancer types. To be able to differentiate using both parameters (R and Xc) with the 4-electrode method, we should increase the frequency at which the bioimpedance samples are analysed; this frequency should be between 70 kHz and 80 kHz.

The mean impedance spectra of the bioimpedance data of the measures obtained with the 4-electrode method and the 3-electrode method show a higher differentiation between cancer samples (black: lung infiltrating squamous carcinoma and red: lung non-infiltrating squamous carcinoma) in the 3-electrode method (|Z| ∼ 114.16 Ω, PA ∼ −3.91°, R ∼ 112.83 Ω and Xc ∼ −20.48 Ω) than in the 4-electrode method (|Z| ∼ 20.38 Ω, PA ∼ 1.01°, R ∼ 20.37 Ω

and Xc ~ −1.17 Ω), which also seems to indicate that the 3-electrode method is a suitable method to differentiate among cancer types. Although the number of samples in this study is very small, these preliminary observations in neoplastic lung tissue are encouraging for the design of future studies to evaluate the ability of EIS to aid in the selection of biopsy location and thereby the histological characterization of lung diseases.

V. CONCLUSION

In conclusion, the 3- and 4-electrode methods showed a statistically significant difference (P < 0.001) to differentiate between bronchial and healthy lung tissues. However. minimally invasive EIS with the 3-electrode method could be more suitable than that with the 4-electrode method because: 1) the 3-electrode method is easier for clinicians to perform because the positioning of the catheter against the tissue is easier; 2) there are fewer motion artefacts in the 3-electrode method; 3) the catheter design could be simpler (only at the distal electrode); and 4) the use of a single electrode in the catheter allows the use of catheters with smaller diameters and increases the extension of the bronchial tree that could be explored.

Regarding to neoplastic tissue, minimally invasive bioimpedance might be able to give information on neoplastic types. These preliminary observations in neoplastic lung tissue are encouraging for the design of future studies to evaluate the ability of EIS to aid in the selection of biopsy location and thereby the histological characterization of lung diseases.

AUTHOR CONTRIBUTIONS

REFERENCES

[1] *The Global Impact of Respiratory Disease*, Forum of International Respiratory Societies, Lausanne, Switzerland, 2017.

[2] F. Bray, J. Ferlay, I. Soerjomataram, R. L. Siegel, L. A. Torre, and A. Jemal, "Global cancer statistics 2018: GLOBOCAN estimates of incidence and mortality worldwide for 36 cancers in 185 countries," *CA, Cancer J. Clinicians*, vol. 68, no. 6, pp. 394–424, Nov. 2018, doi: 10.3322/caac.21492.

[3] C. H. Park, K. Han, J. Hur, S. M. Lee, J. W. Lee, S. H. Hwang, J. S. Seo, K. H. Lee, W. Kwon, T. H. Kim, and B. W. Choi, "Comparative effectiveness and safety of preoperative lung localization for pulmonary nodules," *Chest*, vol. 151, no. 2, pp. 316–328, Feb. 2017, doi: 10.1016/j.chest.2016.09.017.

[4] T. Welte, "Imaging in the diagnosis of lung disease," *Deutsches Ärzteblatt Int.*, vol. 111, no. 11, pp. 179–180, Mar. 2014, doi: 10.3238/arztebl.2014.0179.

[5] R. Fonti, M. Conson, and S. D. Vecchio, "PET/CT in radiation oncology," *Seminars Oncol.*, vol. 46, no. 3, pp. 202–209, Jun. 2019, doi: 10.1053/j.seminoncol.2019.07.001.

[6] D. E. Ost, A. Ernst, X. Lei, K. L. Kovitz, S. Benzaquen, J. Diaz-Mendoza, S. Greenhill, J. Toth, D. Feller-Kopman, J. Puchalski, and D. Baram, "Diagnostic yield and complications of bronchoscopy for peripheral lung lesions. Results of the AQuIRE registry," *Amer. J. Respiratory Crit. Care Med.*, vol. 193, no. 1, pp. 68–77, Jan. 2016, doi: 10.1164/rccm.201507-1332OC.

[7] J. S. Wang Memoli, P. J. Nietert, and G. A. Silvestri, "Meta-analysis of guided bronchoscopy for the evaluation of the pulmonary nodule," *Chest*, vol. 142, no. 2, pp. 385–393, Aug. 2012, doi: 10.1378/chest.11-1764.

[8] S. Khalil, M. Mohktar, and F. Ibrahim, "The theory and fundamentals of bioimpedance analysis in clinical status monitoring and diagnosis of diseases," *Sensors*, vol. 14, no. 6, pp. 10895–10928, Jun. 2014, doi: 10.3390/s140610895.

[9] H. C. Lukaski, "Biological indexes considered in the derivation of the bioelectrical impedance analysis," *Amer. J. Clin. Nutr.*, vol. 64, no. 3, pp. 397S–404S, Sep. 1996, doi: 10.1093/ajcn/64.3.397S.

[10] H. C. Lukaski, N. V. Diaz, A. Talluri, and L. Nescolarde, "Classification of hydration in clinical conditions: Indirect and direct approaches using bioimpedance," *Nutrients*, vol. 11, no. 4, p. 809, Apr. 2019, doi: 10.3390/nu11040809.

[11] S. Toso, A. Piccoli, M. Gusella, D. Menon, A. Bononi, G. Crepaldi, and E. Ferrazzi, "Altered tissue electric properties in lung cancer patients as detected by bioelectric impedance vector analysis," *Nutrition*, vol. 16, no. 2, pp. 120–124, Feb. 2000, doi: 10.1016/s0899-9007(99)00230-0.

[12] D. A. Dean, T. Ramanathan, D. Machado, and R. Sundararajan, "Electrical impedance spectroscopy study of biological tissues," *J. Electrostatics*, vol. 66, nos. 3–4, pp. 165–177, Mar. 2008, doi: 10.1016/j.elstat.2007.11.005.

[13] P. Héroux and M. Bourdages, "Monitoring living tissues by electrical impedance spectroscopy," *Ann. Biomed. Eng.*, vol. 22, no. 3, pp. 328–337, May/Jun. 1994, doi: 10.1007/BF02368239.

[14] J. E. da Silva, J. P. M. de Sá, and J. Jossinet, "Classification of breast tissue by electrical impedance spectroscopy," *Med. Biol. Eng. Comput.*, vol. 38, no. 1, pp. 26–30, Jan. 2000, doi: 10.1007/BF02344684.

[15] K. Yoon, K. W. Lee, S. B. Kim, T. R. Han, D. K. Jung, M. S. Roh, and J. H. Lee, "Electrical impedance spectroscopy and diagnosis of tendinitis," *Physiolog. Meas.*, vol. 31, no. 2, pp. 171–182, Feb. 2010, doi: 10.1088/0967-3334/31/2/004.

[16] C. Skourou, P. J. Hoopes, R. R. Strawbridge, and K. D. Paulsen, "Feasibility studies of electrical impedance spectroscopy for early tumor detection in rats," *Physiolog. Meas.*, vol. 25, no. 1, pp. 335–346, Feb. 2004, doi: 10.1088/0967-3334/25/1/037.

[17] S. P. Desai, A. Coston, and A. Berlin, "Micro-electrical impedance spectroscopy and identification of patient-derived, dissociated tumor cells," *IEEE Trans. Nanobiosci.*, vol. 18, no. 3, pp. 369–372, Jul. 2019, doi: 10.1109/TNB.2019.2920743.

[18] S. L. Hillary, B. H. Brown, N. J. Brown, and S. P. Balasubramanian, "Use of electrical impedance spectroscopy for intraoperative tissue differentiation during thyroid and parathyroid surgery," *World J. Surg.*, vol. 44, no. 2, pp. 479–485, Feb. 2020, doi: 10.1007/s00268-019-05169-7.

[19] C. A. Gonzalez-Correa, B. H. Brown, R. H. Smallwood, N. Kalia, C. J. Stoddard, T. J. Stephenson, S. J. Haggie, D. N. Slatter, and K. D. Bardhan, "Virtual biopsies in Barrett's esophagus using an impedance probe," *Ann. New York Acad. Sci.*, vol. 873, no. 1, pp. 313–321, Apr. 1999, doi: 10.1111/j.1749-6632.1999.tb09479.x.

[20] B. H. Brown, J. A. Tidy, K. Boston, A. D. Blackett, R. H. Smallwood, and F. Sharp, "Relation between tissue structure and imposed electrical current flow in cervical neoplasia," *Lancet*, vol. 355, no. 9207, pp. 892–895, Mar. 2000, doi: 10.1016/S0140-6736(99)09095-9.

[21] C. Gabriel, S. Gabriel, and E. Corthout, "The dielectric properties of biological tissues: III. Parametric models for the dielectric spectrum of tissues," *Phys. Med. Biol.*, vol. 41, no. 11, pp. 2271–2294, 2000. [Online]. Available: http://iopscience.iop.org/article/10.1088/0031-9155/41/11/003/pdf

[22] B. Sanchez, G. Vandersteen, I. Martin, D. Castillo, A. Torrego, P. J. Riu, J. Schoukens, and R. Bragos, "*in vivo* electrical bioimpedance characterization of human lung tissue during the bronchoscopy procedure. A feasibility study," *Med. Eng. Phys.*, vol. 35, no. 7, pp. 949–957, Jul. 2013, doi: 10.1016/j.medengphy.2012.09.004.

[23] P. J. Riu, G. Company, R. Bragos, J. Rosell, V. Pajares, and A. Torrego, "Minimally invasive real-time electrical impedance spectroscopy diagnostic tool for lung parenchyma pathologies," in *Proc. 42nd Annu. Int. Conf. IEEE Eng. Med. Biol. Soc. (EMBC)*, Jul. 2020, pp. 5077–5080, doi: 10.1109/EMBC44109.2020.9175860.

[24] J.-Z. Bao, C. C. Davis, and R. E. Schmukler, "Impedance spectroscopy of human erythrocytes: System calibration, and nonlinear modeling," *IEEE Trans. Biomed. Eng.*, vol. 40, no. 4, pp. 364–378, Apr. 1993, doi: 10.1109/10.222329.

[25] J. F. Murray, "The structure and function of the lung," *Int. J. Tuberc. lung Dis. Off. J. Int. Union Against Tuberc. Lung Dis.*, vol. 14, no. 4, pp. 391–396, Apr. 2010.

[26] G. Amorós-Figueras, E. Jorge, C. Alonso-Martin, D. Traver, M. Ballesta, R. Bragós, J. Rosell-Ferrer, and J. Cinca, "Endocardial infarct scar recognition by myocardial electrical impedance is not influenced by changes in cardiac activation sequence," *Heart Rhythm*, vol. 15, no. 4, pp. 589–596, Apr. 2018, doi: 10.1016/j.hrthm.2017.11.031.

[27] A. Keshtkar, "Design and construction of small sized pencil probe to measure bio-impedance," *Med. Eng. Phys.*, vol. 29, no. 9, pp. 1043–1048, Nov. 2007, doi: 10.1016/j.medengphy.2006.10.010.

[28] A. Keshtkar, Z. Salehnia, M. H. Somi, and A. T. Eftekharsadat, "Some early results related to electrical impedance of normal and abnormal gastric tissue," *Phys. Medica*, vol. 28, no. 1, pp. 19–24, Jan. 2012, doi: 10.1016/j.ejmp.2011.01.002.

[29] R. Baghbani, "Small-sized probe for local measuring electrical properties of the tissues inside of human body: Design, modelling and simulation," *IET Nanobiotechnol.*, vol. 13, no. 9, pp. 946–951, Dec. 2019, doi: 10.1049/iet-nbt.2019.0040.

[30] M. B. Garcia, *Evaluation of New Methods to Assess Infarcted Myocardial Tissue by measuring electrical Impedance*. Barcelona, Spain: Polytechnic Univ. Catalonia (UPC), 2017.

[31] A. Piccoli, B. Rossi, L. Pillon, and G. Bucciante, "A new method for monitoring body fluid variation by bioimpedance analysis: The RXc graph," *Kidney Int.*, vol. 46, no. 2, pp. 534–539, Aug. 1994, doi: 10.1038/ki.1994.305.

[32] K. R. Foster and H. C. Lukaski, "Whole-body impedance-what does it measure," *Amer. J. Clin. Nutr.*, vol. 64, no. 3, pp. 388S–396S, Sep. 1996, doi: 10.1093/ajcn/64.3.388S.

[33] D. F. Morrison, *Multivariate statistical Methods*. New York, NY, USA: McGraw-Hill, 1967.

[34] V. Ambrosini, S. Nicolini, P. Caroli, C. Nanni, A. Massaro, M. C. Marzola, D. Rubello, and S. Fanti, "PET/CT imaging in different types of lung cancer: An overview," *Eur. J. Radiol.*, vol. 81, no. 5, pp. 988–1001, May 2012, doi: 10.1016/j.ejrad.2011.03.020.

GEORGINA COMPANY-SE received the B.S. degree in biomedical engineering from the Universitat Politècnica de Catalunya (UPC), Barcelona, Spain, in 2018, and the M.S. degree in computational biomedical engineering from Universitat Pompeu Fabra (UPF), Barcelona, in 2019. She is currently pursuing the Ph.D. degree in biomedical engineering with UPC. Her research interests include bioimpedance measures and analysis, signal processing, and data science. She is interested in machine learning and data science.

LEXA NESCOLARDE received the Ph.D. degree in biomedical engineering from the Universitat Politècnica de Catalunya (UPC), Barcelona, Spain, in 2006, under the supervision of Professor Javier Rosell. Since January 2001, she has been a member of the Electronic and Biomedical Instrumentation Group (IEB) and the Centre for Research in Biomedical Engineering (CREB-UPC). She is currently an Associate Professor with UPC. Since 2002, she has been participating in 22 research projects and has led three research and technology transfer contracts of special relevance and two of which are still valid. Her current research interests include use of non-invasive localized bioimpedance measurement (L-BIA) for muscle assessment in high-performance athletes, body composition analysis, and data analysis.

VIRGINIA PAJARES was born in Girona in 1979. She received the Ph.D. degree in medicine and surgery from the Universitat Autònoma de Barcelona, in 2015. She has been a Medical Doctor and a Respiratory Specialist, since 2008. Moreover, she is a Consultant with the Respiratory Department, Hospital Santa Creu i Sant Pau of Barcelona. She is part of the Bronchosocopy Unit Staff, and also works as a Respiratory Residents' Mentor. As of 2021, she is an author of 20 scientific articles in PubMed. Her research interests include interventional pulmonology, lung cancer, and pleural diseases.

ALFONS TORREGO was born in Barcelona, Spain, in 1971. He has been a Medical Doctor and a Respiratory Specialist, since 2000, and a Consultant with the Respiratory Department, Hospital Santa Creu i Sant Pau of Barcelona, Spain. He is also the Bronchosocopy Unit Coordinator at the Hospital Santa Creu i Sant Pau of Barcelona. Moreover, he is an Associate Professor of medicine at the Universitat Autònoma de Barcelona and a Former Chairperson of the Spanish Respiratory Society Scientific Committee. As of 2021, he is an author of more than 60 scientific articles in PubMed. His research interests include interventional pulmonology, lung cancer, and severe asthma.

PERE J. RIU (Senior Member, IEEE) received the M.Sc. degree in telecommunication engineering and the Ph.D. degree in electronic engineering from the Universitat Politecnica de Catalunya (UPC), Barcelona, Spain, in 1986 and 1991, respectively. He was a Visiting Associate Professor with the Department of Bioengineering, University of Pennsylvania, Philadelphia, PA, USA, in 1997. He is currently a Full Professor of electronics with the Department of Electronic Engineering, UPC. His research interests include electromagnetic compatibility, computational electromagnetics, the interaction of electromagnetic fields with biological tissues, and biomedical instrumentation design with emphasis on electrical bioimpedance techniques, including electrical impedance tomography (EIT). These activities are performed within the Centre for Research on Biomedical Engineering (CREB, UPC) and the Institut de Recerca Sant Joan de Déu (IRSJD). He is a member of the Committee on Man and Radiation (COMAR) (IEEE-BMES) and the Vice President of the International Society for Electrical Bio-Impedance.

RAMON BRAGÓS received the degree in electrical engineering (major in telecommunications engineering) and the Ph.D. degree in electronic engineering from the Technical University of Catalonia (UPC), in 1991 and 1997, respectively. Since 1998, he has been an Associate Professor with the Electronic Engineering Department, UPC. He belongs to the Electronic and Biomedical Instrumentation Research Group and the Centre for Research in Biomedical Engineering (CREB). His research interests include design of methods and systems for the characterization of biological materials and systems using minimally invasive methods, mainly electrical impedance spectroscopy.

· · ·

JAVIER ROSELL (Senior Member, IEEE) was born in Barcelona, Spain, in June 1959. He received the Ingeniero de Telecomunicación and Doctor Ingeniero de Telecomunicación degrees from the Polytechnic University of Catalunya (UPC), Barcelona, in 1983 and 1989, respectively. He is currently a Full Professor with the Department of Electronic Engineering, UPC, and the Head of the Research Group, Centre for Research in Biomedical Engineering (CREB-UPC). His current research interests include non-invasive and non-obtrusive measurement methods in sports and medical and biological fields, particularly based on bioelectrical impedance spectroscopy and magnetic induction spectroscopy.

CHAPTER 3: Effect of Calibration for Tissue Differentiation Between Healthy and Neoplasm Lung Using Minimally Invasive Electrical Impedance Spectroscopy

Title: Effect of calibration for tissue differentiation between healthy and neoplasm lung using minimally invasive electrical impedance spectroscopy

Authors: Georgina Company-Se, Lexa Nescolarde, Virginia Pajares, Alfons Torrego, Pere J. Riu, Javier Rosell and Ramon Bragós

Journal: IEEEAccess

Year: 2022

Volume: 10

Number of Pages: 103150-103163

Quartile: Q2 (105/276)

RESEARCH ARTICLE

Effect of Calibration for Tissue Differentiation Between Healthy and Neoplasm Lung Using Minimally Invasive Electrical Impedance Spectroscopy

GEORGINA COMPANY-SE[1], **LEXA NESCOLARDE**[1], **VIRGINIA PAJARES**[2], **ALFONS TORREGO**[2], **PERE J. RIU**[1], **(Senior Member, IEEE), JAVIER ROSELL**[1], **(Senior Member, IEEE), AND RAMON BRAGÓS**[1]

[1]Department of Electronic Engineering, Universitat Politècnica de Catalunya, 08034 Barcelona, Spain
[2]Department of Respiratory Medicine, Hospital de la Santa Creu i Sant Pau, 08041 Barcelona, Spain

Corresponding author: Lexa Nescolarde (lexa.nescolarde@upc.edu)

ABSTRACT This study proposes a calibration method and analyses the effect of this calibration in lung measures, using minimally invasive electrical impedance spectroscopy with the 3-electrode method, for tissue differentiation between healthy and neoplasm lung tissue. Tissue measurements were performed in 99 patients [54 healthy tissue and 15 neoplastic tissue samples obtained] with an indicated bronchoscopy. Statistically significant difference ($P < 0.001$) were found between healthy lung tissue and neoplasm lung tissue in bioimpedance parameters. The calibration of the bioimpedance measures with respect to a measure performed in bronchi reduces the inter-patient dispersion, increasing the sensitivity, decreasing the specificity and increasing the area below the ROC curve for three out of four impedance-derived estimators. Results also show that there are no significant differences between healthy lung tissue among smoker, non-smoker and ex-smoker samples, which was initially stated as a possible cause of EIS measurement dispersion in lungs.

I. INTRODUCTION

Respiratory disorders have a big impact in the population worldwide. According to the European Respiratory Society, chronic obstructive pulmonary disease (COPD) is the third global cause of death in more developed countries. Moreover,

The associate editor coordinating the review of this manuscript and approving it for publication was Norbert Herencsar.

lung cancer is the leading cause of cancer death in the world. Both are smoking-related conditions [1].

In lung cancer, late detection in advance stages is common and is related to poor prognosis [2]. Diagnostic of lung peripheral and central nodules is increasing because of number of patients with indeterminate nodules are discovered in CT screening and verified with other diagnostic options such as minimally invasive bronchoscopic procedures to establish final histological type. However, the diagnostic yield using

virtual bronchoscopy (VB), radial endobronchial ultrasound (r-EBUS), electromagnetic navigation (EMN) and ultrathin bronchoscopes remains suboptimal [3], [4], and their high economic cost makes them unavailable in most centers.

We aim to use Electrical Impedance Spectroscopy (EIS) to complement the actual methods of diagnosis of lung diseases as it could allow the differentiation between healthy lung tissue and neoplasm lung tissue and help in the choice of the specific sample location.

EIS technique is one of the existing methods of impedance analysis. Impedance is defined as the opposition to the flow of an alternating electrical current which is dependent on the frequency of this current [5]. When the impedance is measured in biological tissue is named as bioimpedance (Z). It measures the passive electrical properties of the tissue after the introduction of a low amplitude alternating current to the organism [5], [6]. The bioimpedance is a complex number with a real part (the resistance, R) and an imaginary part (the reactance, Xc), both parts are dependent of the geometry of the measured region, the location of electrodes and the tissue electrical passive properties [5]. The physiological fluids have low resistance and dominates the measured resistance, while cell membranes act as capacitors, having high impedance at low frequencies and low impedance at high frequencies and contributes mainly to the reactive part. Due to these behaviors, the electrical current introduced in the biological tissue divides into resistive and capacitive pathways and it changes with the frequency [6]. An alternative representation of the Bioimpedance, as a complex number, is the use of the modulus (Z) and the phase angle (PA). The PA represents the relative time lag between the injected current and the generated voltage [7]. Bioimpedance data can be obtained using single or multiple frequencies. When the bioimpedance data is obtained using a broad band of frequencies is known as bioimpedance spectroscopy [6]. The advantage of the EIS method, to measure and analyze bioimpedance data, is based on the fact that current at low frequency (lower than 10 kHz) flows through the extracellular medium while current at high frequencies (over 100 kHz) flows through both, intracellular and extracellular medium, giving more information about the structure of the tissue.

There are previous studies about lung bioimpedance measurements. Toso *et al.* [8], through an impedance plethysmograph emitting 50 kHz alternating current, reported different impedance vector distribution in patients with lung cancer as compared with healthy patients. A reduced Xc and a smaller PA were found while R was preserved in patients with lung cancer. Nierman *et al.* [9] performed transthoracic bioelectrical impedance analysis to quantify extravascular lung water in animal models. Orschulik *et al.* [10] used non-invasive bioimpedance spectroscopy for the diagnosis of acute respiratory distress syndrome in an animal model.

Some previous studies have been carried out by our research group. Sanchez *et al.* [11] performed minimally invasive lung bioimpedance measurements to study the characteristics of lung bioimpedance (calibration and linearity)

and the differences between inflated and deflated lung. Later Coll *et al.* [12] and Riu *et al.* [13] present studies demonstrating the potential for tissue differentiation through minimally invasive electrical impedance spectroscopy in lung using the 4-electrode method.

This manuscript (2nd phase) is the continuation of the previous study (1st phase) entitled ''Minimally invasive lung tissue differentiation using electrical impedance spectroscopy: a comparison of the 3- and 4- electrode methods'' performed by Company-Se *et al.* [14]. It compared the capacity of tissue differentiation of the minimally invasive electrical impedance spectroscopy in lungs using the 4-electrode method and the 3-electrode method. The results showed that both methods were adequate for tissue differentiation but 3-electrode method was more feasible for its clinical use because of its lower complexity, both in the catheter configuration (single electrode) and in the measurement system architecture. This previous study proposed for future works to increase the sample size for the differentiation between healthy lung tissue and neoplasm lung tissue using the 3-electrode method.

In this 2nd phase the measures performed in healthy lung tissue and in neoplasm lung tissue showed high inter-patient variability. This variability could hinder the tissue differentiation in lungs. There are several causes for this variability: 1) The measured absolute values of the R and Xc spectra are influenced by the tissue properties (the variable under measurement) but also by the geometry of the measurement (body shape of the patient and electrode positions). Geometrical factors such as body mass index (BMI) has been reported as one significant factor for changes in lung metrics [15]; 2) The breathing produces also impedance changes due to the considerable air volume change from inspiration to expiration and the influence of the non-conductive air contents in the lung tissue. This phenomenon could increase the inter-patient variability as depending on the patient, the breathing cycle will be different; 3) In the 3-electrode method, the electrode impedance of the catheter tip is measured and could increase the intra- and inter-patient variability due to poor contact of the catheter tip against the lung tissue and the liquids accumulation in the airways; 4) Another potential cause for inter-patient variability is cigarette consumption. It could contribute to the increase of the inter-patient dispersion. Smoking-induced epithelial abnormalities can serve both as targets for abnormal inflammatory responses and as initiators of deregulated inflammation. Cytokines, chemokines, and growth factors released by alveolar macrophages, lymphocytes, neutrophils, endothelial cells, and fibroblasts may act to promote epithelial dysfunction and malignant progression [16], [17].

While the ventilation-induced impedance modulation effect can be reduced using averaging, the other potential causes of variability need a calibration method capable to reduce this variability in order to perform tissue differentiation with success. For example, electrical impedance measures using the 3-electrode method in cardiology uses a floating measure within the heart (catheter completely
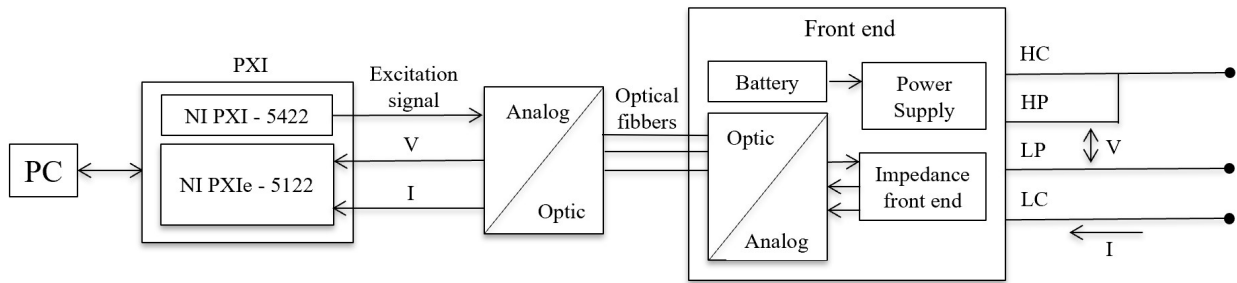
FIGURE 1. Schematic representation of the bioimpedance acquisition system.

surrounded by blood) to calibrate the geometrical factors in the bioimpedance measures obtained in contact with the myocardial walls [18], and also, partially, the electrode impedance effect. In lungs, a floating measure completely surrounded by air to calibrate is not viable due to the non-conductive property of the air and it is not feasible to locate the catheter in a place where the tip electrode will be surrounded by a well-known tissue and which will be affected by geometrical factors similar to the ones that will affect the tissue impedance measurements for each patient. For this reason, we proposed to acquire a bioimpedance measure in principal bronchus and use it to calibrate the lung tissue bioimpedance measures.

The aim of this study, by using minimally invasive electrical impedance spectroscopy with the 3-electrode method, is to propose a calibration method and to analyze the effect of this calibration in measures performed in the bronchi for tissue differentiation in different groups: healthy lung tissue (no radiological abnormalities in CT Thorax) and neoplasm lung tissue. Also, the possible differences in the impedance measurements in healthy tissue in smokers, non-smokers and ex-smokers will be verified to check if this factor would affect the ability to differentiate between healthy lung tissue and lung neoplasm.

II. MATERIALS AND METHODS
A. PARTICIPANTS
Minimally invasive EIS measures were taken in 99 patients (Age: 65 ± 16 yr; Weight: 76.8 ± 15.6 kg; BMI: 27.7 ± 5.5 kgm^{-2}) with a bronchoscopy indicated during the period between November 2021 and February 2022 at the "Hospital de la Santa Creu i Sant Pau". All of them underwent bioimpedance measurement. However, 30 of them had other characteristics than healthy lung tissue or neoplasm lung tissue such as emphysema or fibrosis. For this reason, out of the 99 patients measured by bioimpedance, only 69 were considered for analysis (healthy: 54 and neoplastic: 15).

The number of bioimpedance samples obtained in healthy lung tissue were 54 [(non-smokers: n = 22, Age: 59 ± 19 yr; Weight: 70.8 ± 16.6 kg; BMI: 26.7 ± 5.8 kgm^{-2}); smokers: n = 9, Age: 66 ± 7 yr; Weight: 83.5 ± 11.9 kg; BMI:

31.0 ± 4.3 kgm^{-2}); (ex-smokers: n = 23, Age: 71 ± 12 yr; Weight: 79.3 ± 13.8 kg; BMI: 27.5 ± 4.8 kgm^{-2}; years without smoking $= 22 \pm 11$ yr)] while the number of samples obtained from neoplasm lung tissue were 15 (Age: 70 ± 9 yr; Weight: 75.3 ± 11.2 kg; BMI: 26.3 ± 4.1 kgm^{-2}).

Ethics approval was obtained from the Hospital de la Santa Creu i Sant Pau (CEIC-73/2020) according to principles of the Declaration of Helsinki for experiments with human beings. All patients proved signed informed consent.

B. MEASUREMENT SYSTEM
The acquisition of bioimpedance measures were performed using a tetrapolar catheter (Medtronic 5F RF Marinr), 115 cm long with a diameter of 1.65 mm (5 F) and two skin electrodes (Ambu BlueSensor VLC ref: VLC-00-s/10 and 3M Company ref: 9160F) placed on the right side of the patients at the level of the ribs. Only the catheter tip electrode will be used in the measurements.

The measurement system is made up of 3 devices (Fig. 1): 1) an optically insulated battery-powered patient interface insulated front end (that includes the impedance front end); 2) a rugged PC platform based on a PXI system from National Instruments; and 3) an analog-optical interface front-end to connect the PXI with the insulated front end. An arbitrary waveform generator generates a multisine excitation signal that is composed of 26 frequencies between 1 kHz and 1 MHz. To ensure a current lower than the maximum allowable patient auxiliary current stablished in the IEC 60601-1:2005 (<1mA rms measured with the circuit proposed in the IEC 60601-1:2005) the front end includes an AC-coupled current source that attenuates the low-frequency components accordingly with the current limit pattern specified by this standard. The system was verified including the 26 frequency components (1 kHz – 1MHz) simultaneously.

The voltage (V(t)) and current (I(t)) are simultaneously acquired. Then, with the optical-analog interface connected to the PXI, the excitation is converted into an optical signal. The optical signal is then converted back into an electrical signal inside the front end. The voltage and current signals, optically transmitted from the front end to the optical-electrical interface, are acquired with the digitizer card. The acquisition
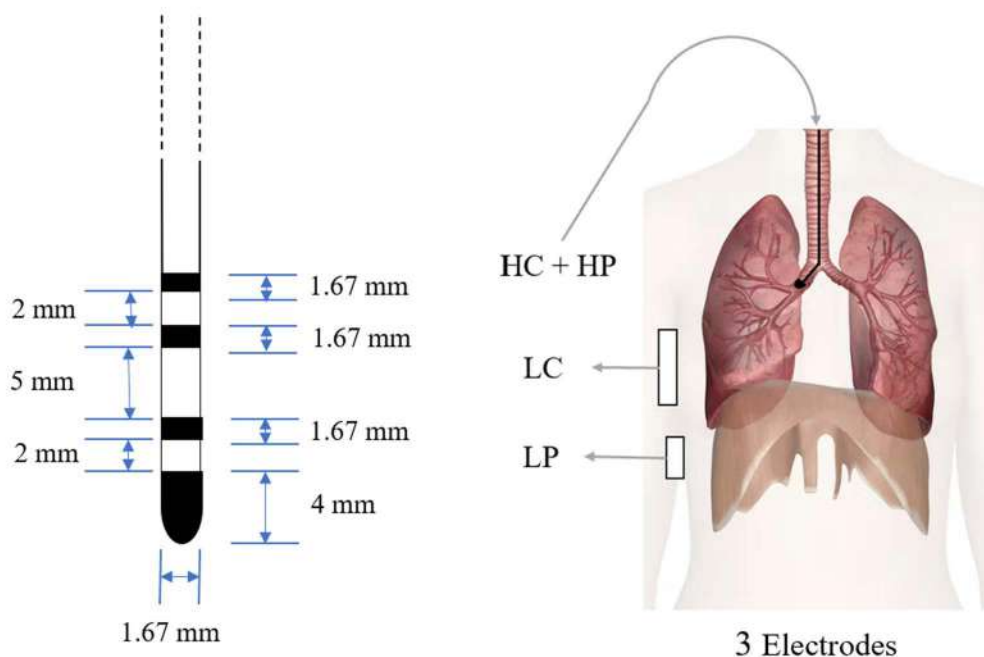
FIGURE 2. Right figure: Schematic representation of the 3-electrode method. In the 3-electrode method the LC and LP electrodes are placed on the skin using skin surface electrodes. Left figure: dimensions of the catheter. Only the tip electrode of the catheter is used to perform the measurements.

system takes simultaneous samples of voltage and current at 20 MSamples/s. From the acquired signals, 60 impedance spectra per second are obtained.

Bioimpedance measures were obtained using the 3-electrode method. To inject the current (HC) and detect the potential (HP) the electrode located at the tip of the catheter is used. The two skin electrodes are used as low current (LC) and loc potential (LP) electrodes (Fig. 2).

C. MEASUREMENT PROTOCOL

Bronchoscopy, a procedure used to inspect the airways, was performed to obtain the bioimpedance measures. As part of the diagnostic process, radiological imaging technique (CT or PET/CT) were performed in each patient before bronchoscopy procedure. To obtain the bioimpedance measures, the catheter was inserted through a port of the bronchoscope. During the bronchoscopy, patients are placed in a supine position with the upper airways anaesthetized with topical 2% lidocaine. Moreover, intravenous sedation is provided with midazolam, fentanyl and propofol. During the process, measures in bronchial tissue, healthy lung tissue and neoplasm lung tissue, if applicable, were taken. The acquisition of the measures had a duration of 12 seconds.

D. EIS MEASUREMENTS

To obtain the EIS measurements the system applies a multisine current signal and acquires the voltage and current signals. The Fast Fourier Transform (FFT) is used to obtain the ratio between the voltage and current coefficients of the FFT corresponding to each injected frequency.

The acquisition takes 12 s at 60 spectra per second. The 3-electrode measurements were calibrated with a measurement over a known resistor (600 Ohms) connected to the catheter tip and to the external electrode connectors.

E. CALIBRATION USING BRONCHUS

To remove the geometrical factors of the patients a multiplicative factor calibration of the bioimpedance of the lung measures is proposed. The proposed method aims to calibrate the lung measures with respect to a measure performed in the bronchial tissue (principal bronchus) for each respective patient. A measurement in the bronchi is of no interest in clinical practice, therefore, impedance measurement in bronchial tissue offers the advantage of calibration while not losing relevant clinical information. Moreover, because of its low cell content, bronchial tissue should have a flat impedance spectrum, thus being suitable as calibration reference [14]. The obtained impedance modulus ($|Z|$) of the lung is divided by the mean value (mean value of impedance at each frequency, during a time interval) of $|Z|$ of the bronchial tissue and then multiplied by a factor of 100 Ω, which is the expected impedance magnitude value obtained in the bronchi [12] (1). The PA calibrated of the lung measure is obtained by subtracting the original value of the PA of the lung measure minus the mean value of the PA obtained in the bronchi tissue

sample (2).

$$|Z(f,t)|_{calibrated}$$
$$= 100 * |Z(f,t)|_{lung}/mean(|Z(f,t)|_{bronchi}) \qquad (1)$$
$$PA_{calibrated}(f,t)$$
$$= PA_{lung}(f,t) - mean(PA_{bronchi}(f,t)) \qquad (2)$$

F. DATA ANALYSIS

For tissue differentiation analysis among non-smoker, smoker and ex-smoker samples in healthy lung tissue samples as well as for tissue differentiation analysis between healthy lung tissue and neoplasm lung tissue the averaged spectra of the bioimpedance measurements, obtained using the 3-electrode method, throughout the acquisition time was used.

The frequency range chosen to visualize and analyze the data was 15 kHz – 307 kHz. The values from frequencies higher and lower than this range were discarded due to electrode effects at low frequency and capacitive coupling errors at high frequency. For tissue differentiation analysis the frequency of 15 kHz for |Z| and R and the frequency of 307 kHz for PA and Xc were chosen. These frequencies were chosen based on the higher distance between the means of the groups used to perform the tissue differentiation.

The normality of the distribution of the variables was determined by the Kolmogorv-Smirnov (healthy lung tissue samples) test and Shapiro-Wilk test (neoplasm lung tissue samples). The variables normally distributed are shown as the mean ± standard deviation (SD) and 95% confidence interval (CI) for the mean (lower bound and upper bound). Non-normally distributed variables are shown as statistic median (interquartile range, IQR) and minimum - maximum. One-way analysis of variance (ANOVA) was used to determine statistically significant differences in the |Z|, PA, R and Xc values among smokers, non-smokers and ex-smoker samples in healthy lung tissue. Repeated measures t-test was used to determine statistically significant differences in the |Z|, PA, R and Xc values between non-calibrated data and calibrated data among smokers, non-smokers and ex-smoker healthy lung samples. One-way analysis of variance (ANOVA, parametric data) and Mann–Whitney U test (non-parametric data) was used to determine statistically significant differences in the |Z|, PA, R and Xc values between healthy lung tissue and neoplasm lung tissue. In addition, the area under the Receiver Operating Characteristic (ROC) curve was used to measure the discriminative capacity of the non-calibrated and calibrated measure of |Z|, PA, R and Xc according to tissue classification (1: healthy lung tissue; 2: neoplasm lung tissue) by biopsy. Following the ROC analysis area under curve (AUC) above 0.9 is considered a very good model and AUC above 0.97 it is considered as excellent. A value less than 0.5 indicates the model is no better than random prediction.

The statistical software IBM® SPSS® version 28.0 (IBM Corp, Armonk, NY, United States) was used for data analysis. The level of statistical significance was set at P < 0.05.

III. RESULTS

A. MULTI-FREQUENCY RESPONSE FOR MINIMALLY INVASIVE HEALTHY LUNG TISSUE MEASUREMENTS

Fig. 3 shows the mean (continuous line) and SD (dashed lines) values of |Z|, PA, R and Xc plotted along the frequency range (15 kHz – 307 kHz) used for the measures obtained in healthy lung tissue divided in smoker patients (red), non-smokers patients (green) and ex-smoker patients (blue) for non-calibrated (left) bioimpedance measures and calibrated bioimpedance measures (right) showing an inter-sample reduction of the dispersion and increasing data homogeneity.

B. TISSUE DIFFERENTIATION AMONG NON-SMOKERS, SMOKERS AND EX-SMOKERS PATIENTS IN CALIBRATED AND NON-CALIBRATED DATA

Table 1 lists the descriptive parameters, specified as the mean ± SD, 95% confidence interval for mean (lower bound and upper bound) of |Z|, PA, R and Xc and the results of the one-way ANOVA including the Fisher coefficient (F) for the minimally-invasive bioimpedance measures performed in healthy lung tissue (non-smokers: n = 22; smokers: n = 9; ex-smokers: n = 23) for the measures calibrated and non-calibrated. No statistically significant differences (P > 0.05) related to the smoking condition are found among the three groups analyzed for both calibrated and non-calibrated data.

C. MULTI-FREQUENCY RESPONSE FOR MINIMALLY INVASIVE HEALTHY LUNG TISSUE AND NEOPLASM LUNG TISSUE MEASUREMENTS

Fig. 4 shows the mean (continuous line) and SD (dashed lines) values of |Z|, PA, R and Xc plotted along the frequency range (15 kHz – 307 kHz) used for the measures obtained in healthy lung tissue (green) and neoplasm lung tissue (black) before (left) and after (right) calibration respectively. Results show an increase in the separation between tissues in |Z|, R and Xc, especially the first two.

D. TISSUE DIFFERENTIATION BETWEEN HEALTHY LUNG TISSUE AND NEOPLASM LUNG TISSUE

Table 2 lists the descriptive parameters, specified as the mean ± SD, 95% confidence interval for mean (lower bound and upper bound) for normally distributed variables and specified as statistic median (interquartile range, IQR) and minimum – maximum for non-normally distributed variables of |Z|, PA, R and Xc and the results of the one-way ANOVA including the Fisher coefficient (F) and the Mann–Whitney U test results including the U statistic (U) for the minimally invasive bioimpedance measures performed in healthy lung tissue (n = 54) and in neoplasm lung tissue (n = 15) for the measures calibrated and non-calibrated. Statistically significant differences (P < 0.001) are found between
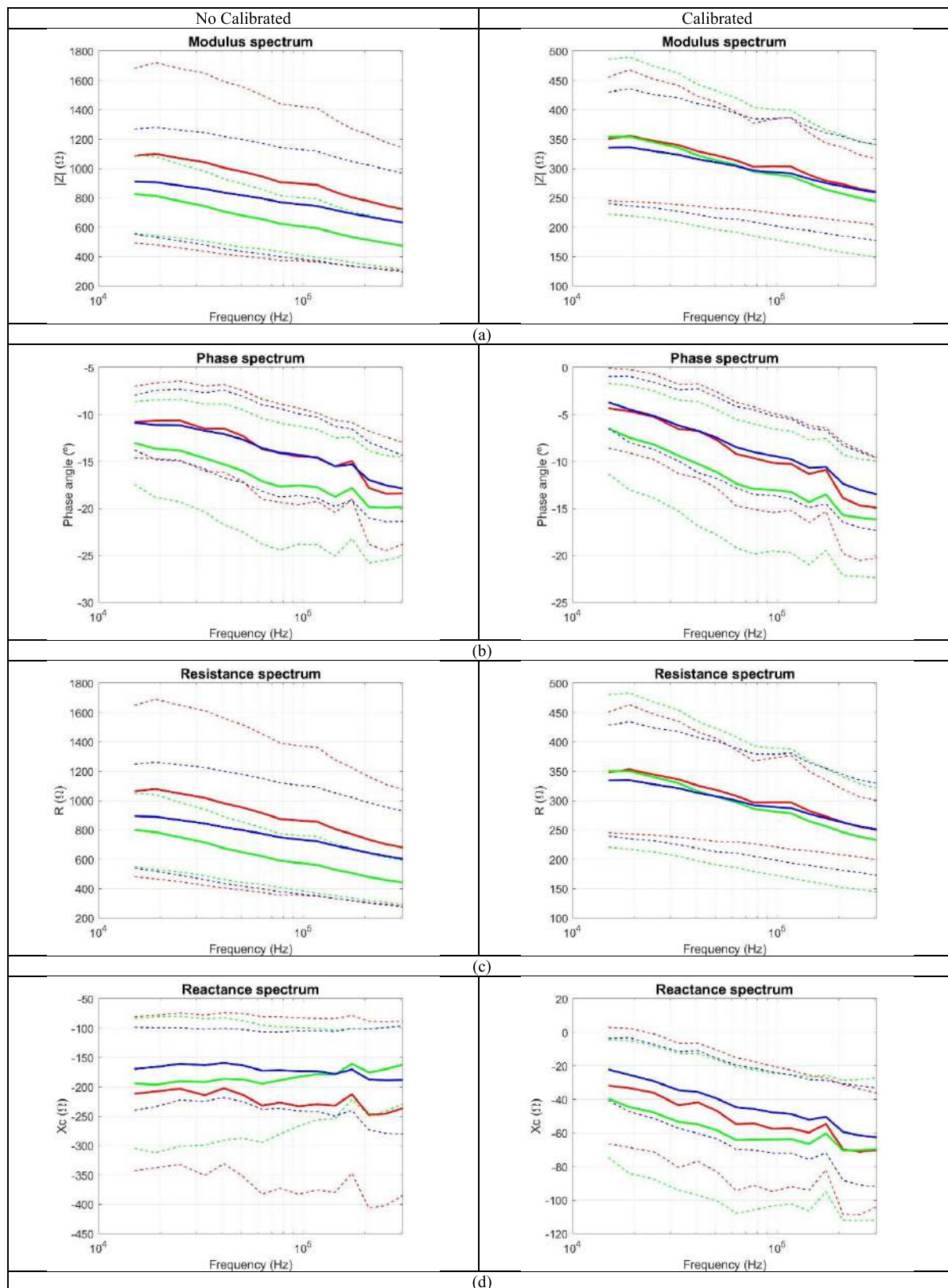
FIGURE 3. Results of the non-calibrated (left) and calibrated (right) mean (continuous line) and SD (dashed lines) parameters extracted from the bioimpedance signal along the different frequencies analyzed (15 kHz – 307 kHz). In order, (a) Modulus, (b) Phase angle, (c) Resistance and (d) Reactance of the bioimpedance of all the different measures taken in healthy lung tissue classified according to cigarette consumption. Green: non-smoker; blue: ex-smokers; red: smokers.

TABLE 1. Descriptions of bioimpedance measurements performed in healthy lung tissue for non-smokers, smokers and ex-smokers. The variables normally distributed are shown as mean ± SD, 95% confidence interval for mean (lower bound and upper bound). In addition, the Fisher (F) coefficient for variance analysis and the statistical significance (P) are also shown.

	No calibrated data				
	Mean ± SD 95% CI (lower bound – upper bound)				
	Non-smokers (n = 22)	Smokers (n = 9)	Ex-smokers (n = 23)	F	P
|Z| (Ω)	670.99 ± 308.96 (433.51 - 908.48)	1086.97 ± 594.40 (630.07 - 1543.86)	1016.66 ± 492.09 (638.40 - 1394.92)	1.523	0.228
PA (°)	-17.47 ± 6.77 (-22.68 – (-12.27))	-18.40 ± 5.41 (-22.56 – (-14.24))	-17.56 ± 4.08 (-20.70 – (-14.42))	1.000	0.375
R (Ω)	649.35 ± 289.72 (426.65 - 872.05)	1064.34 ± 583.33 (615.95 - 1512.72)	997.28 ± 487.75 (622.36 - 1372.20)	1.646	0.203
Xc (Ω)	-116.62 ± 64.24 (-166.00 – (-67.24))	-236.36 ± 147.90 (-350.05 – (-122.68))	-203.36 ± 115.60 (-292.22 – (-114.50))	1.929	0.156
	Calibrated data				
	Mean ± SD 95% CI (lower bound – upper bound)				
	Non-smokers (n = 22)	Smokers (n = 9)	Ex-smokers (n = 23)	F	P
|Z| (Ω)	298.72 ± 107.35 (216.21 - 381.24)	350.61 ± 105.20 (269.74 - 431.47)	304.16 ± 86.61 (237.58 - 370.74)	0.156	0.856
PA (°)	-14.88 ± 8.01 (-21.04 – (-8.72))	-14.91 ± 5.34 (-19.01 – (-10.81))	-12.53 ± 5.02 (-16.38 – (-8.67))	1.422	0.881
R (Ω)	296.07 ± 105.24 (215.18 - 376.96)	348.24 ± 102.79 (269.23 - 427.25)	302.71 ± 85.53 (236.96 - 368.46)	0.127	0.881
Xc (Ω)	-50.69 ± 30.68 (-74.27 – (-27.11))	-70.10 ± 33.83 (-96.11 – (-44.10))	-50.20 ± 22.79 (-67.72 – (-32.69))	0.255	0.776

healthy and neoplasm lung tissue for both calibrated and non-calibrated data.

E. EFFECTS OF CALIBRATION IN DATA VARIABILITY IN HEALTHY LUNG TISSUE AND IN NEOPLASM LUNG TISSUE

Fig. 5 shows the effect of calibration in bioimpedance data variability for healthy lung tissue and neoplasm lung tissue respectively for |Z| and R at 15 kHz and for PA and Xc at 307 kHz. Results show a decrease in data dispersion within the same tissue group, especially in |Z| and R parameters, after the calibration of the bioimpedance data. Fig. 6 shows the receiver operating characteristic (ROC) curves for |Z|, PA, R and Xc before and after calibration for healthy lung tissue and neoplasm lung tissue groups. Results show an increase of the area under curve (AUC) after the calibration of the bioimpedance data in |Z|, R and Xc (AUC > 0.96) and a decrease of the AUC in PA (AUC < 0.95).

IV. DISCUSSION

This project evaluates the need of the calibration of the minimally invasive EIS bioimpedance measures performed in lung tissue using a measure performed in bronchial tissue. Moreover, it evaluates the influence of cigarette smoking in healthy lung tissue bioimpedance measures as a possible cause of dispersion. Finally, it differentiates between healthy and neoplasm lung tissue and assesses the possible improvement of this differentiation using the calibration.

Lungs are organs that belong to the respiratory system whose principal function is to produce gas exchange. Structures from the respiratory system include trachea, bronchi and terminal bronchioles. Each of these structures has its own anatomical and histological characteristics [19]. Therefore, differences in bioimpedance measurements can be expected based not only on the type of tissue but also on its state.

This work reports the use of minimally invasive EIS in lungs through a bronchoscopy process using the 3-electrode method to differentiate among smoker, non-smokers and ex-smoker healthy lung tissue samples, in order to analyze its potential role in the measurements variability and to differentiate between healthy lung tissue and neoplasm lung tissue. Both tissue differentiations are used to evaluate the inter-patient variability in the mentioned groups and to evaluate the utility of calibration using a bioimpedance measure performed in a principal bronchus. This strategy of taking a measure to calibrate the other measures has been previously used in heart applications [18].

The inflammatory response due to cigarette consumption is not differentiable through bioimpedance EIS measures neither with the non-calibrated measurements nor with the calibrated measures. Therefore, the initial hypothesis that the smoking condition could be a cause of dispersion in the EIS-derived estimators can be discarded. According to **Fig. 3** the |Z| and R show a decrease in their values when calibrating with respect to a bronchi measurement while PA and Xc increase their values (nearer to 0 than the non-calibrated
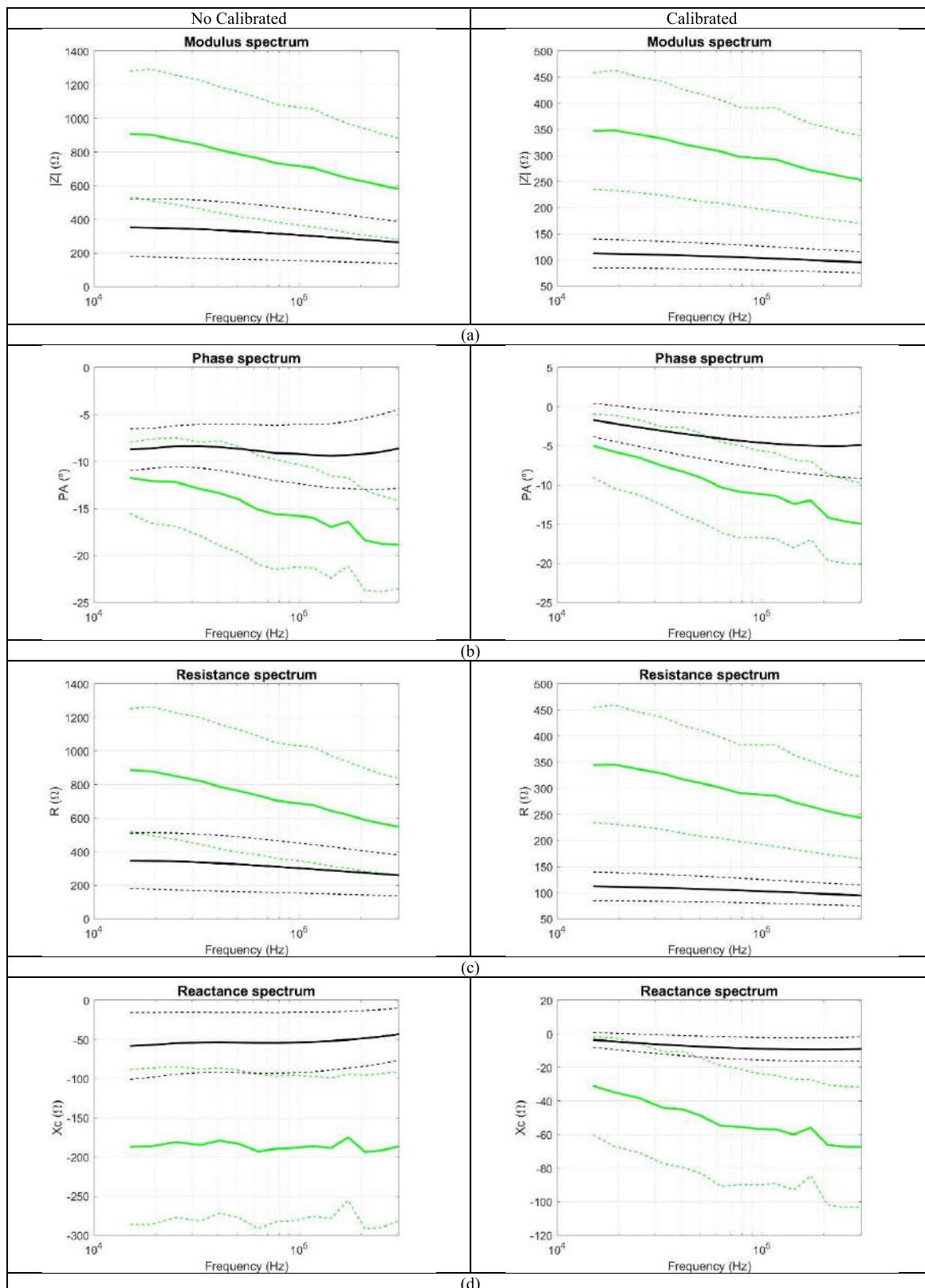
FIGURE 4. The mean (continuous line) and SD (dashed lines) values from the bioimpedance signal along the different frequencies analyzed before and after calibration. The (a) modulus, (b) phase angle, (c) resistance and (d) capacitive reactance. Green: healthy lung tissue; black: neoplasm lung tissue.

TABLE 2. Descriptions of minimally-invasive bioimpedance measurements for healthy lung tissue and neo-plasm lung tissue. The variables normally distributed are shown as mean ± SD, 95% confidence interval for mean (lower bound and upper bound) while that non-normally distributed data are shown as statistic median (interquartile range, IQR) and minimum-maximum. In addition, the statistic of the Mann Whitney U test (U), the Fisher (F) coefficient for variance analysis and the statistical significance (P) are also shown.

	No calibrated data				Calibrated data			
	Healthy (n = 54)	Neoplasm (n = 15)	U	P	Healthy (n = 54)	Neoplasm (n = 15)	F	P
|Z| (Ω)	751.97 (759.66) (305.85 - 1823.16)	284.95 (308.09) (134.68 - 668.53)	44	<0.001	283.26 ± 80.68 (238.58 - 327.94)	112.38 ± 27.56 (97.12 - 127.65)	64.735	<0.001
PA (°)	-15.98 ± 5.60 (-19.08 – (-12.88))	-8.61 ± 4.21 (-10.94 – (-6.28))	36	<0.001	-11.61 ± 5.21 (-14.49 – (-8.72))	-4.90 ± 4.24 (-7.25 – (-2.55))	47.597	<0.001
R (Ω)	741.72 (731.03) (303.32 - 1799.63)	283.41 (302.44) (133.39 - 650.79)	44	<0.001	281.77 ± 79.71 (237.63 - 325.91)	112.26 ± 27.51 (97.02 - 127.49)	65.099	<0.001
Xc (Ω)	-146.04 (139.73) (-405.34 – (-21.95))	-43.17 ± 33.05 (-61.48 – (-24.87))	39	<0.001	-44.46 ± 22.51 (-56.92 – (-31.99))	-8.97 ± 7.18 (-12.94 – (-4.99))	39.142	<0.001

data). The non-calibrated |Z| and R as well as the PA show slightly although non-significative higher values in those samples in which cigarette consumption is present. However, Xc present lower values in smoker samples. When we calibrate the bioimpedance measurements we show an intra-sample variability reduction. This variability reduction specially affects |Z| and R due to the geometrical dependence of R and the high correlation between |Z| and R [5], [6].

Emphasizing the importance of the analysis of R and Xc according to the theory of Lukaski *et al.* [6], [7], Piccoli *et al.* [20], and Lukaski *et al.* [21] we selected the frequencies (15 kHz and 307 kHz) to check the hypothetical differentiation among non-smokers, smokers and ex-smokers healthy lung tissue samples following the calculation of the maximum distance between means of the three groups. From the bioimpedance parameters, R describes the behavior of the medium through which the current flows while Xc describes the capacitive component of the cell membranes. The values of |Z| and PA are dependent of R and Xc [6], [7].

The significance of the test was determined with the p-value which is the probability of obtaining test results at least as extreme as the result observed, assuming that the null hypothesis is correct. Therefore, considering the level of significance set, results will be statistically significant if a P < 0.05 is obtained in the test. Regarding tissue differentiation among non-smokers, smokers and ex-smokers healthy lung tissue samples, one-way ANOVA reported non-significant results (P > 0.05) for all variables (|Z|, PA, R and Xc) for both, the non-calibrated and the calibrated measures. No post-hoc test has been done as no significant results have been found. The Fisher coefficient parameter (F) represents the relationship between the inter-group variance and the intra-group variance. Therefore, a higher F coefficient indicates a higher inter-group variance than intra-group variance [22]. According to the results obtained in **Table 1**, the F coefficient obtained in the non-calibrated data is higher in |Z|, R and Xc than in the calibrated data. In contrast, F coefficient in PA obtained in the calibrated data is higher than in the non-calibrated data. Therefore, the statistical results obtained show that the effect of cigarette consumption should not be considered to perform tissue differentiation

through bioimpedance analysis. Moreover, results show an intra-sample dispersion reduction with the effect of calibration, especially in |Z| and R, which depend on the geometrical factors.

Regarding tissue differentiation between healthy lung tissue and neoplasm lung tissue we have taken all the healthy lung tissue samples without considering the tabaco habits as it has been demonstrated that this factor is not significant (P > 0.05). Lung cancer is a highly complex neoplasm and comprise several histological types. The groups most frequently are the non-small cell lung cancer (NSCLC) such as adenocarcinoma and squamous carcinoma, followed by small cell lung cancer (SCLC) [23]. Lung cancer are the results of the accumulation of genetic and epigenetic changes, including abnormalities of the inactivation of tumour-suppression genes and the activation of oncogenes [24]. For the tissue differentiation between healthy lung tissue and neoplasm lung tissue all cancer types have been included in the same group so we assume that the remaining dispersion in neoplasm lung tissue might be due to the differences within lung cancer types. We have selected the frequencies (15 kHz and 307 kHz) that offered us a better discriminatory response between healthy lung tissue and neoplasm by taking the frequency with the maximum difference between the mean of the healthy lung tissue and the mean of the neoplasm lung tissue. We have also visualized the mean impedance spectrum and SD of the healthy lung tissue samples and the neoplasm lung tissue samples between the frequency range analyzed (15 kHz – 307 kHz) with the data non-calibrated and calibrated to show the effects of the calibration. According to the results obtained in **Fig. 4** the calibration of the bioimpedance measures with respect to a measure performed in bronchi reduces the intra-group variability and, in consequence, increases the inter-patient distance in both, the healthy lung tissue and the neoplasm lung tissue, especially in |Z| and R, which are the two parameters that are dependent on geometrical factors (**Fig. 5**). Results obtained show a higher |Z| and R and a lower PA and Xc in healthy lung tissue than in neoplasm lung tissue. Moreover, |Z| and R show higher difference between the lower frequencies and the higher frequencies in healthy lung tissue than in neoplasm lung tissue.
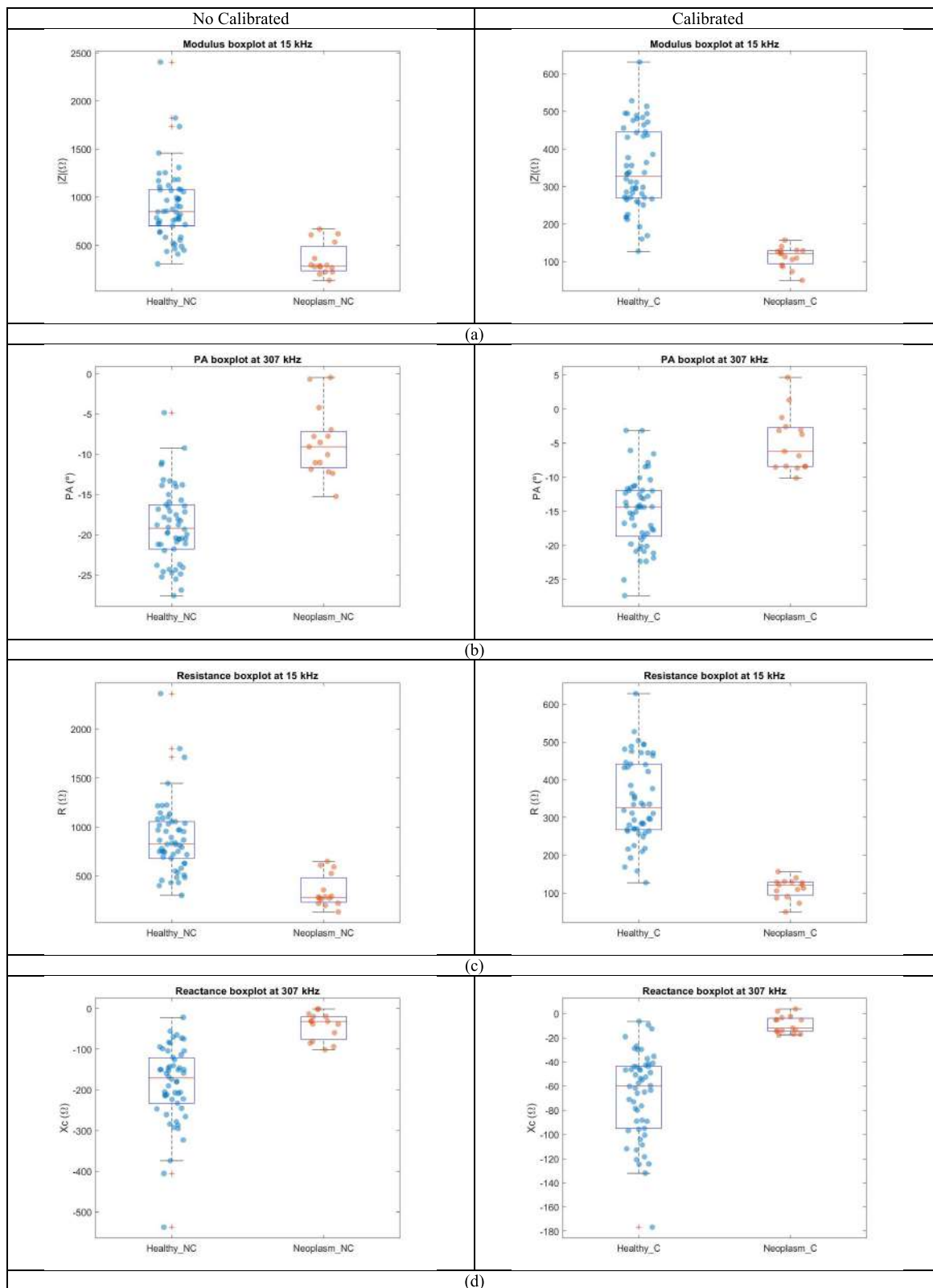
FIGURE 5. Boxplot of bioimpedance calibrated (C) and non-calibrated (NC) data of healthy lung tissue and neoplasm lung tissue for (a) |Z| and (c) R at 15 kHz and for (b) PA and (d) Xc at 307 kHz. The central mark of each box indicates the median, and the bottom and top edges of the box indicate the 25th and 75th percentiles, respectively. The whiskers extend to the most extreme data points that are not considered outliers. In addition, the bioimpedance data values for the calibrated (blue) and non-calibrated (orange) measures. Vertical axis are different for the calibrated and non-calibrated data for better data visualization.
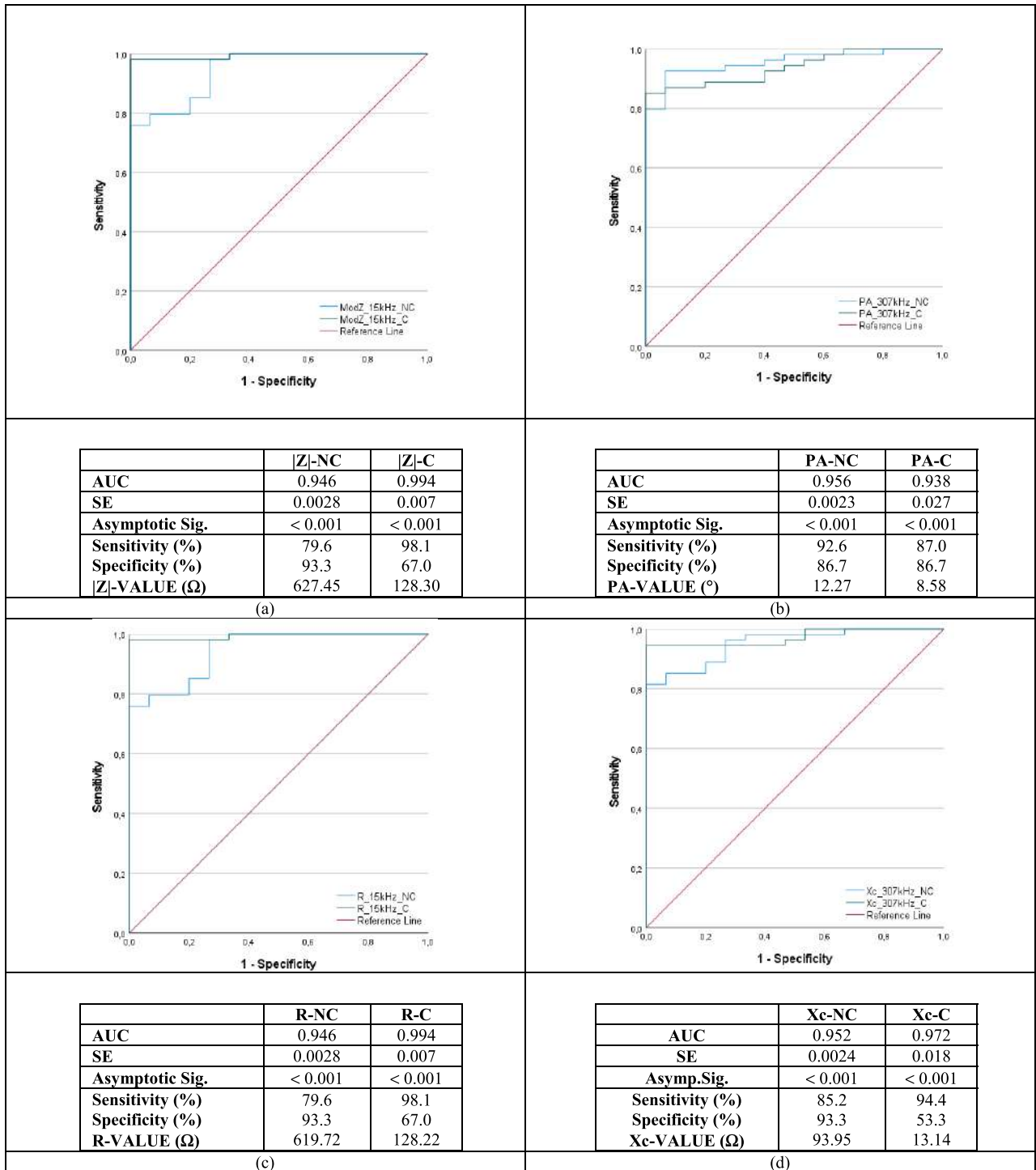
	|Z|-NC	|Z|-C
AUC	0.946	0.994
SE	0.0028	0.007
Asymptotic Sig.	< 0.001	< 0.001
Sensitivity (%)	79.6	98.1
Specificity (%)	93.3	67.0
|Z|-VALUE (Ω)	627.45	128.30

(a)

	PA-NC	PA-C
AUC	0.956	0.938
SE	0.0023	0.027
Asymptotic Sig.	< 0.001	< 0.001
Sensitivity (%)	92.6	87.0
Specificity (%)	86.7	86.7
PA-VALUE (°)	12.27	8.58

(b)

	R-NC	R-C
AUC	0.946	0.994
SE	0.0028	0.007
Asymptotic Sig.	< 0.001	< 0.001
Sensitivity (%)	79.6	98.1
Specificity (%)	93.3	67.0
R-VALUE (Ω)	619.72	128.22

(c)

	Xc-NC	Xc-C
AUC	0.952	0.972
SE	0.0024	0.018
Asymp.Sig.	< 0.001	< 0.001
Sensitivity (%)	85.2	94.4
Specificity (%)	93.3	53.3
Xc-VALUE (Ω)	93.95	13.14

(d)

FIGURE 6. Receiver operating characteristic (ROC) curves to assess the predictive ability of the different electrical impedance parameters before and after calibration between healthy and neoplasm lung tissue. In (a) the results of the \|Z\| before calibration (NC) and after calibration (C) at 15 kHz. In (b) the results of the PA before calibration (NC) and after calibration (C) at 307 kHz. In (c) the results of the R before (NC) and after (C) calibration at 15 kHz. In (d) the results of the Xc before (NC) and after (C) calibration at 307 kHz.

EIS assumes that current at low frequency flows through the extracellular space while current at high frequencies flows through both, intracellular and extracellular space. Moreover, healthy lung tissue is composed of alveolar epithelial and endothelial cells separated by a thin basement membrane and interstitial space. Interstitial space is a non-conductive medium, than the neoplasm lung tissue. These two main characteristics produce a higher \|Z\| and R in healthy lung tissue than in neoplasm lung tissue. Lung cancer produce multiples histological changes of the normal bronchial mucosa. Proliferation of epithelial cells with abundant cytoplasm and vesicular nuclei, intercellular bridging, thickening of alveolar

septa and others pathological changes [25]. The morphologic features in neoplasm lung tissue seem to contribute to lose their capacitive behavior which is translated into a PA and Xc flat mean impedance spectrum, as compared to the healthy lung tissue mean impedance spectrum (**Fig. 4**). Regarding tissue differentiation between healthy lung tissue and neoplasm lung tissue, one-way ANOVA for the calibrated data and Mann–Whitney U test for the non-calibrated data (**Table 2**) show statistically significant differences between the two groups (healthy and neoplasm lung tissue, P < 0.001). These statistical differences are probably due to the histological differences between both groups by minimally-invasive EIS measurements. Focusing only in the calibrated data results in **Table 2** show higher significance in |Z| and R than in PA and Xc as the F coefficient is higher in the first two parameters.

The study has shown that there is an effect on the measurement when calibrating, reducing the dispersion of the measurements (**Fig. 5**). Calibration doesn't change the outcome of the hypothesis test, showing a statistically significant difference in both cases, but the higher-F coefficient (Fisher coefficient from one-way ANOVA test, used for comparing the factors of the total deviation) than U (statistic from Mann–Whitney U test, used to assess whether two sampled groups are likely to derive from the same population) suggests stronger separation between the groups (**Table 2**), which is highly significant (P < 0.01) for both calibrated and non-calibrated measures. On the other hand, according to the ROC curve analysis, (**Fig. 6**) we have observed that the area under the curve (AUC) is equally excellent in all the variables (AUC > 0.9) both calibrating and not calibrating, although higher AUC values are observed when calibrating. After calibrating, the AUC is greater than 0.96 for all cases except in PA. The |Z|, R and Xc increase the sensitivity (true positive fraction) and decrease the specificity (false positive fraction) after calibration. Only PA showed a decrease in sensitivity maintaining its specificity (**Fig. 6**). Considering that PA has a trigonometric relationship between R and Xc and that these improve with calibration, the authors recommend performing the calibration of the measurements with respect to the bronchi.

In the previous study performed by Company-Se *et al.* [14] we performed tissue differentiation between healthy lung tissue and bronchi tissue. We proposed continuing with the study by including neoplasm lung tissue for lung tissue differentiation. Results obtained in **Table 2** show that minimally invasive electrical impedance spectroscopy using the 3-electrode method is able to discriminate with both, calibrated data (not considering geometrical factors) and with non-calibrated data. In future studies we aim to include other lung pathologies with other histological characteristics.

V. CONCLUSION
In conclusion, results of the healthy lung tissue bioimpedance measurements show that there are no significant differences

between healthy lung tissue among smoker, non-smoker and ex-smoker measures, which was initially stated as a possible cause of EIS measurement dispersion in lungs. Then, to perform tissue differentiation between healthy lung tissue and neoplasm lung tissue the effect of tobacco habit will not be considered. Also, this effect will not be considered in our future studies.

On the other hand, we found that there is a statistically significant difference in both calibrated and non-calibrated measurements at 15 kHz (|Z| and R) and 307 kHz (Xc and PA) between healthy and neoplasm lung tissue. This shows that minimally invasive electrical impedance spectroscopy measurements using the 3-electrode method are able to discriminate between healthy lung and neoplasm both with and without calibration.

Calibration has, however, been demonstrated to reduce data variability and increase the tissue state separation capability, which will be useful in future studies when including other pathologies with similar pathological mechanisms.

Moreover, significant differences are found between calibrated and non-calibrated paired samples of smoker, non-smoker ex-smoker and neoplasm lung tissue showing that calibration is beneficial to reduce intra-sample variability.

The authors recommend calibrating the measures obtained with respect to the bronchi given that it is demonstrated that it increases the sensitivity of the 3-electrode minimally invasive electrical impedance spectroscopy for tissue differentiation.

AUTHOR CONTRIBUTIONS
Ramon Bragós, Virginia Pajares, Pere J. Riu, Javier Rosell, Georgina Company-Se, Alfons Torrego, and Lexa Nescolarde designed the experiments; Georgina Company-Se, Virginia Pajares, and Alfons Torrego performed the experiments; Lexa Nescolarde and Georgina Company-Se performed the data processing; Lexa Nescolarde, Georgina Company-Se, and Ramon Bragós analyzed the data; Georgina Company-Se and Lexa Nescolarde drafted the manuscript and prepared the tables and figures; and Ramon Bragós, Virginia Pajares, Pere J. Riu, Javier Rosell, Georgina Company-Se, Alfons Torrego, and Lexa Nescolarde revised the paper and approved the final version of the manuscript.

REFERENCES
[1] I. Annesi-Maesano and G. Viegi, Eds., *Respiratory Epidemiology*. Lausanne, Switzerland: European Respiratory Society, 2014.

[2] H. J. de Koning, "Reduced lung-cancer mortality with volume CT screening in a randomized trial," *New England J. Med.*, vol. 382, no. 6, pp. 503–513, Feb. 2020, doi: 10.1056/NEJMoa1911793.

[3] D. E. Ost, "Diagnostic yield and complications of bronchoscopy for peripheral lung Lesions. Results of the AQuIRE registry," *Amer. J. Respiratory Crit. Care Med.*, vol. 193, no. 1, pp. 68–77, Jan. 2016, doi: 10.1164/rccm.201507-1332OC.

[4] J. S. Wang Memoli, P. J. Nietert, and G. A. Silvestri, "Meta-analysis of guided bronchoscopy for the evaluation of the pulmonary nodule," *Chest*, vol. 142, no. 2, pp. 385–393, Aug. 2012, doi: 10.1378/chest.11-1764.

[5] S. Khalil, M. Mohktar, and F. Ibrahim, "The theory and fundamentals of bioimpedance analysis in clinical status monitoring and diagnosis of diseases," *Sensors*, vol. 14, no. 6, pp. 10895–10928, Jun. 2014, doi: 10.3390/s140610895.

[6] H. C. Lukaski, N. V. Diaz, A. Talluri, and L. Nescolarde, "Classification of hydration in clinical conditions: Indirect and direct approaches using bioimpedance," *Nutrients*, vol. 11, no. 4, p. 809, Apr. 2019, doi: 10.3390/nu11040809.

[7] H. C. Lukaski, "Biological indexes considered in the derivation of the bioelectrical impedance analysis," *Amer. J. Clin. Nutrition*, vol. 64, no. 3, pp. 397S–404S, Sep. 1996, doi: 10.1093/ajcn/64.3.397S.

[8] S. Toso, "Altered tissue electric properties in lung cancer patients as detected by bioelectric impedance vector analysis," *Nutrition*, vol. 16, no. 2, pp. 120–124, Feb. 2000, doi: 10.1016/s0899-9007(99)00230-0.

[9] D. M. Nierman, D. I. Eisen, E. D. Fein, E. Hannon, J. I. Mechanick, and E. Benjamin, "Transthoracic bioimpedance can measure extravascular lung water in acute lung injury," *J. Surgical Res.*, vol. 65, no. 2, pp. 101–108, Oct. 1996, doi: 10.1006/jsre.1996.0350.

[10] J. Orschulik, N. Hochhausen, S. A. Santos, M. Czaplik, S. Leonhardt, and M. Walter, "Detection of acute respiratory distress syndrome using sectoral bioimpedance spectroscopy—A pilot study," in *Proc. 11th Int. Conf. Bioelectromagn.*, Aachen, Germany, May 2018, pp. 1–10. [Online]. Available: http://publications.rwthaachen.de/record/723538/files/723538.pdf

[11] B. Sanchez, G. Vandersteen, I. Martin, D. Castillo, A. Torrego, P. J. Riu, J. Schoukens, and R. Bragos, "*in vivo* electrical bioimpedance characterization of human lung tissue during the bronchoscopy procedure. A feasibility study," *Med. Eng. Phys.*, vol. 35, no. 7, pp. 949–957, Jul. 2013, doi: 10.1016/j.medengphy.2012.09.004.

[12] N. Coll, R. Bragós, A. M. Muñoz, V. Pajares, A. Torrego, and P. J. Riu. (2016). *Espectrometría de Impedancia Eléctrica en Tejido Pulmonar*. [Online]. Available: https://upcommons.upc.edu/handle/2117/100980

[13] P. J. Riu, G. Company, R. Bragos, J. Rosell, V. Pajares, and A. Torrego, "Minimally invasive real-time electrical impedance spectroscopy diagnostic tool for lung parenchyma pathologies," in *Proc. 42nd Annu. Int. Conf. IEEE Eng. Med. Biol. Soc. (EMBC)*, Jul. 2020, pp. 5077–5080, doi: 10.1109/EMBC44109.2020.9175860.

[14] G. Company-Se, L. Nescolarde, V. Pajares, A. Torrego, P. J. Riu, J. Rosell, and R. Bragos, "Minimally invasive lung tissue differentiation using electrical impedance spectroscopy: A comparison of the 3- and 4-electrode methods," *IEEE Access*, vol. 10, pp. 7354–7367, 2022, doi: 10.1109/ACCESS.2021.3139223.

[15] K. Subramaniam, A. R. Clark, E. A. Hoffman, and M. H. Tawhai, "Metrics of lung tissue heterogeneity depend on BMI but not age," *J. Appl. Physiol.*, vol. 125, no. 2, pp. 328–339, Aug. 2018, doi: 10.1152/japplphysiol.00510.2016.

[16] S. Weitzman and L. Gordon, "Inflammation and cancer: Role of phagocyte-generated oxidants in carcinogenesis," *Blood*, vol. 76, no. 4, pp. 655–663, Aug. 1990.

[17] R. O'Donnell, "Inflammatory cells in the airways in COPD," *Thorax*, vol. 61, no. 5, pp. 448–454, May 2006, doi: 10.1136/thx.2004.024463.

[18] G. Amorós-Figueras, E. Jorge, C. Alonso-Martin, D. Traver, M. Ballesta, R. Bragós, J. Rosell-Ferrer, and J. Cinca, "Endocardial infarct scar recognition by myocardial electrical impedance is not influenced by changes in cardiac activation sequence," *Heart Rhythm*, vol. 15, no. 4, pp. 589–596, Apr. 2018, doi: 10.1016/j.hrthm.2017.11.031.

[19] J. F. Murray, "The structure and function of the lung," *Int. J. Tuberculosis Lung Diseases, Off. J. Int. Union Tuberculosis Lung Diseases*, vol. 14, no. 4, pp. 391–396, Apr. 2010.

[20] A. Piccoli, B. Rossi, L. Pillon, and G. Bucciante, "A new method for monitoring body fluid variation by bioimpedance analysis: The RXc graph," *Kidney Int.*, vol. 46, no. 2, pp. 534–539, Aug. 1994, doi: 10.1038/ki.1994.305.

[21] K. R. Foster and H. C. Lukaski, "Whole body impedance what does it measure?" *Amer. J. Clin. Nutrition*, vol. 64, no. 3, pp. 388S–396S, Sep. 1996, doi: 10.1093/ajcn/64.3.388S.

[22] D. F. Morrison, *Multivariate Statistical Methods*. Boca Raton, FL, USA: CRC Press, 1967.

[23] M. Zheng, "Classification and pathology of lung cancer," *Surgical Oncol. Clinics North Amer.*, vol. 25, no. 3, pp. 447–468, Jul. 2016, doi: 10.1016/j.soc.2016.02.003.

[24] E. A. Engels, "Inflammation in the development of lung cancer: Epidemiological evidence," *Expert Rev. Anticancer Therapy*, vol. 8, no. 4, pp. 605–615, Apr. 2008, doi: 10.1586/14737140.8.4.605.

[25] W. D. Travis, "International association for the study of lung cancer/american thoracic society/European respiratory society international multidisciplinary classification of lung adenocarcinoma," *J. Thoracic Oncol.*, vol. 6, no. 2, pp. 244–285, Feb. 2011, doi: 10.1097/JTO.0b013e318206a221.

GEORGINA COMPANY-SE received the B.S. degree in biomedical engineering from the Universitat Politècnica de Catalunya (UPC), Barcelona, Spain, in 2018, and the M.S. degree in computational biomedical engineering from Universitat Pompeu Fabra (UPF), Barcelona, in 2019. She is currently pursuing the Ph.D. degree in biomedical engineering with UPC. Her research interests include bioimpedance measures and analysis, signal processing, and data science. She is interested in machine learning and data science.

LEXA NESCOLARDE was born in Baracoa, Cuba, in 1970. She received the Ph.D. degree in biomedical engineering from the Universitat Politècnica de Catalunya (UPC), Barcelona, Spain, in 2006, under supervision of Professor Javier Rosell. Since January 2001, she has been a member of the Electronic and Biomedical Instrumentation Group (IEB) as well as the Biomedical Research Center (CREB-UPC). She is currently an Associate Professor at UPC. Since 2002, she has been participating in 22 research projects and has led three research and technology transfer contracts of special relevance and two of which are still valid. Her current research interests include use of non-invasive localized bioimpedance measurement (L-BIA) for muscle assessment in high performance athletes, body composition analysis, and data analysis.

VIRGINIA PAJARES was born in Girona, in 1979. She received the Ph.D. degree in medicine and surgery from the Universitat Autónoma de Barcelona, in 2015. She has been a Medical Doctor and a Respiratory Specialist, since 2008. Moreover, she is a Consultant with the Department of Respiratory, Hospital de la Santa Creu i Sant Pau, Barcelona. She is part of the Bronchosocopy Unit Staff and also she works as a Respiratory Residents' Mentor. On 2021, she is author of 20 scientific articles in PubMed. Her main research interests include interventional pulmonology, lung cancer, and pleural diseases.

ALFONS TORREGO was born in Barcelona, Spain, in 1971. He has been a Medical Doctor and a Respiratory Specialist, since 2000, and a Consultant with the Department of Respiratory, Hospital de la Santa Creu i Sant Pau, Barcelona. He is also the Bronchosocopy Unit Coordinator at the Hospital de la Santa Creu i Sant Pau. Moreover, he is an Associated Professor of medicine at the Universitat Autònoma de Barcelona and a Former Chairperson of the Spanish Respiratory Society Scientific Committee. On 2021, he is author of more than 60 scientific articles in PubMed. His main research interests include interventional pulmonology, lung cancer, and severe asthma.

PERE J. RIU (Senior Member, IEEE) received the M.Sc. degree in telecommunication engineering and the Ph.D. degree in electronic engineering from the Universitat Politècnica de Catalunya (UPC), Barcelona, Spain, in 1986 and 1991, respectively. He was a Visiting Associate Professor with the Department of Bioengineering, University of Pennsylvania, Philadelphia, PA, USA, in 1997. He is currently a Full Professor of electronics with the Department of Electronic Engineering, UPC. His research interests include electromagnetic compatibility, computational electromagnetics, interaction of EMF with biological tissues, and biomedical instrumentation design with emphasis on electrical bioimpedance techniques, including EIT. These activities are performed within the Centre for Research on Biomedical Engineering (CREB, UPC) and the Institut de Recerca Sant Joan de Déu (IRSJD). He is a member of the Committee on Man and Radiation (COMAR) (IEEE-BMES) and the Vice-President of the International Society for Electrical Bio-Impedance.

JAVIER ROSELL (Senior Member, IEEE) was born in Barcelona, Spain, in June 1959. He received the Ingeniero de Telecomunicación and Doctor Ingeniero de Telecomunicación degrees from the Polytechnic University of Catalonia (UPC), Barcelona, in 1983 and 1989, respectively.

He is currently a Full Professor with the Department of Electronic Engineering, UPC, and the Head of the Research Group, Biomedical Research Center (CREB-UPC). His current research interests include non-invasive and non-obtrusive measurement methods in sports, medical and biological fields, particularly based on bio-electrical impedance spectroscopy and magnetic induction spectroscopy.

RAMON BRAGÓS received the degree in electrical engineering (major in telecommunications engineering) and the Ph.D. degree in electronic engineering from the Technical University of Catalonia (UPC), in 1991 and 1997, respectively. Since 1998, he has been an Associate Professor at the Department of Electronic Engineering, UPC. He belongs to the Electronic and Biomedical Instrumentation Research Group and the Center for Research in Biomedical Engineering (CREB). His main research interests include design of methods and systems for the characterization of biological materials and systems using minimally invasive methods, mainly electrical impedance spectroscopy.

● ● ●

CHAPTER 4: Differentiation Using Minimally-Invasive Bioimpedance Measurements of Healthy and Pathological Lung Tissue through Bronchoscopy

Check for updates

*CORRESPONDENCE
Lexa Nescolarde
✉ lexa.nescolarde@upc.edu

Differentiation using minimally-invasive bioimpedance measurements of healthy and pathological lung tissue through bronchoscopy

Georgina Company-Se[1], Lexa Nescolarde[1]*, Virginia Pajares[2], Alfons Torrego[2], Pere J. Riu[1], Javier Rosell[1] and Ramon Bragós[1]

[1]Department of Electronic Engineering, Universitat Politècnica de Catalunya, Barcelona, Catalonia, Spain, [2]Department of Respiratory Medicine, Hospital de la Santa Creu i Sant Pau, Barcelona, Catalonia, Spain

Purpose: To use minimally-invasive transcatheter electrical impedance spectroscopy measurements for tissue differentiation among healthy lung tissue and pathologic lung tissue from patients with different respiratory diseases (neoplasm, fibrosis, pneumonia and emphysema) to complement the diagnosis at real time during bronchoscopic procedures.

Methods: Multi-frequency bioimpedance measurements were performed in 102 patients. The two most discriminative frequencies for impedance modulus (|Z|), phase angle (PA), resistance (R) and reactance (Xc) were selected based on the maximum mean pair-wise Euclidean distances between paired groups. One-way ANOVA for parametric variables and Kruskal−Wallis for non-parametric data tests have been performed with *post-hoc* tests. Discriminant analysis has also been performed to find a linear combination of features to separate among tissue groups.

Results: We found statistically significant differences for all the parameters between: neoplasm and pneumonia ($p<0.05$); neoplasm and healthy lung tissue ($p<0.001$); neoplasm and emphysema ($p<0.001$); fibrosis and healthy lung tissue ($p\leq0.001$) and pneumonia and healthy lung tissue ($p<0.01$). For fibrosis and emphysema ($p<0.05$) only in |Z|, R and Xc; and between pneumonia and emphysema ($p<0.05$) only in |Z| and R. No statistically significant differences ($p>0.05$) are found between neoplasm and fibrosis; fibrosis and pneumonia; and between healthy lung tissue and emphysema.

Conclusion: The application of minimally-invasive electrical impedance spectroscopy measurements in lung tissue have proven to be useful for tissue differentiation between those pathologies that leads increased tissue and inflammatory cells and those ones that contain more air and destruction of alveolar septa, which could help clinicians to improve diagnosis.

KEYWORDS

lung tissue differentiation, minimally-invasive bioimpedance, bronchoscopy, biopsy, respiratory disease

1. Introduction

Adequate lung sampling is essential to obtain the diagnosis of lung diseases. Respiratory pathologies can affect the lung parenchyma in a diffuse or localized way. The indication of the most appropriate diagnostic method varies depending on the diagnostic possibilities and the distribution of the pathology. Therefore, the correct characterization of the lung tissue is essential in order to guide the collection of lung samples. Although different imaging methods are currently available (chest CT, PET CT or virtual bronchoscopy), these methods are performed prior to the procedure and do not allow real-time guidance for sample collection. For this reason, advanced bronchoscopic techniques have been developed for a few years, such as the use of radial probe endobronchial ultrasound (radial EBUS) or electromagnetic navigation bronchoscopy (ENB), which allow samples to be obtained from the affected areas in real time (1, 2). However, these are high-cost techniques that are not widely available in Interventional Pulmonology units. The developed line of research aims to expand the diagnostic tools currently available in bronchoscopy with the application of an innovative technique based on the use of bioimpedance data to differentiate between tissue states.

The term bioimpedance (Z) is defined as the opposition offered by a biological tissue to an electrical flow. The bioimpedance is composed by two terms: the resistance (R), which describes the opposition to the electrical flow, mainly in the extracellular and intracellular fluids, of the biological tissue, and the reactance (Xc) which describes the opposition produced by the capacitive behavior of the cell membranes (3, 4). The Xc causes a delay between the voltage and the current causing a phase shift, represented by the phase angle (PA) defined as the tan-1 (Xc/R). Finally, the last parameter that can be derived from the first two is the bioimpedance modulus (|Z|) defined as $\sqrt{R^2 + Xc^2}$ (5). When the bioimpedance data is obtained using a broad band of frequencies it is called electrical impedance spectroscopy (EIS) and it is based on the assumption that at low frequencies the electric current flows through the extracellular medium while at high frequencies the electric current is able to flow through the intra and extracellular medium as it is able to penetrate the cell membranes. Hence, it produces a decrease in |Z|, PA, R and Xc (5).

The use of impedance analysis in studies related to medical field is widely extended, especially for studies of body composition. Previous authors have already applied impedance analysis in lung tissue. Toso et al. (6) compared bioimpedance measurements between healthy lung tissue and neoplasm lung tissue by using an impedance plethysmograph at 50 kHz of frequency obtaining a reduced value of Xc while R value was maintained in neoplasm lung tissue as compared to healthy lung tissue. Baarends et al. (7) studied the accuracy in the prediction of body-water compartments using EIS having the isotope dilution as a reference in patients with severe chronic obstructive pulmonary diseases. Orschulik et al. (8) presented a pilot animal study evaluating the possibility of using EIS to detect acute respiratory distress syndrome. Finally, Meroni et al. (9) used bioimpedance measurements to differentiate among multiple tissues and organs, including lung.

To the extent of author's knowledge, there are no studies regarding the application of minimally-invasive lung measurements through bronchoscopy to differentiate among different pathologies and healthy lung tissue apart from the previous studies performed by our research

group. First, Sanchez et al. (10) described, characterized, calibrated and experimentally validated an EIS instrument for performing minimally-invasive bioimpedance measurements through bronchoscopy. Coll et al. (11) performed tissue differentiation between healthy lung tissue, bronchi and pathological lung tissue obtaining statistical differences among the different groups. However, in that first study, pathologies were not differentiated from each other and all pathological tissues were put into the same group. Riu et al. (12) presented a preliminary artificial intelligence predictive algorithm that was able to discriminate between healthy lung tissue and pathological lung tissue automatically. The three studies carried out to date used the 4-electrode method to acquire the bioimpedance data. That method needed to place 4 electrodes in contact with the lung tissue during all the bioimpedance signal recording.

Occasionally, during bronchoscopy, the patient may have cough or movements that reduce the contact of the impedance catheter with the bronchial wall. To improve contact with the lung surface and decrease measurement time, the authors though that by using the 3-electrode method the bioimpedance signals acquisitions would be more feasible for clinicians. For this reason, the authors performed a study, as presented in Company-Se et al. (13), comparing the capacity to differentiate healthy lung tissue from bronchi using the 4-electrode method and the 3-electrode method. In that study the authors concluded that both methods were able to differentiate between both types of tissue. However, the 3-electrode method had more advantages for the clinical practice, deciding to change the method of signal acquisition. Later, Company-Se et al. (14) presented a method, already used in bioimpedance measures performed in hearth (15), to calibrate the 3-electrode bioimpedance measurements in order to increase tissue differentiation capacity by reducing intra-sample data variability. Moreover, in that study tissue differentiation between healthy lung tissue and neoplasm was performed with significant difference obtained. Finally, they studied bioimpedance differences in healthy lung tissue among smoker, ex-smoker and non-smoker patients, without significance among groups.

The aim of this study is to perform tissue differentiation among healthy lung tissue and pathologic lung tissue from patients with different respiratory diseases (neoplasm, fibrosis, pneumonia and emphysema) through minimally-invasive bioimpedance measurements obtained though bronchoscopy.

2. Materials and methods

2.1. Participants

Minimally-invasive EIS measures were performed in 102 patients (age: 66 ± 14 years; weight: 74.5 ± 17.2 kg; BMI: 26.8 ± 4.3 kgm⁻²) with a bronchoscopy prescribed between November 2021 and August 2022 at the "Hospital de la Santa Creu i Sant Pau" in Barcelona.

2.2. EIS measurements

Electrical impedance spectroscopy measures were taken using the 3-electrode method. A complete description of the measurement system is detailed in Company-Se et al. (14). The lung bioimpedance results from the injection of a multisine

current signal (26 frequencies ranging from 1 to 1,000 kHz) between the distal electrode of a tetrapolar catheter (Medtronic 5F RF Marinr) and a skin electrode (3 M Company ref.: 9160F) placed at the level of the ribs. A voltage is induced by the injected current and measured between the distal catheter electrode and a second skin electrode (Ambu BlueSensor VLC ref.: VLC-00-s/10) placed next to the other one. The impedance measures were recorded during a period of 12 s with a sample frequency of 60 spectra per second. Measures were calibrated using a measure of the same patient taken at the bronchi, according to Company-Se et al. (14), to eliminate geometrical factors and reduce intra-group variability.

2.3. Measurement protocol

The patients included were evaluated in Interventional Pulmonology Unit. All of them had a complete blood count with coagulation study and radiological evaluation (chest CT or/ and PET CT). A bronchoscopy was indicated to study of respiratory disease. For bronchoscopy, the upper airway was anaesthetized with topical 2% lidocaine; intravenous sedation was provided throughout the procedure with midazolam, fentanil and/or propofol. The acquisition of the bioimpedance data was carried out by inserting the catheter through a port of the bronchoscope. Depending on the respiratory disease, different diagnostic techniques were performed: bronchoaspiration, bronchoalveolar lavage, bronchial brushing, endobronchial or transbronchial biopsy and/or fine needle aspiration. The endoscopic exploration and diagnostic procedures were indicated accordance with the guidelines.

2.4. Data analysis

The averaged spectra of the minimally-invasive bioimpedance measured through the 12 s acquisition time was used for tissue differentiation among healthy lung tissue, neoplasm, fibrosis, pneumonia and emphysema. Data was obtained between 1 kHz and 1 MHz. Low frequency values (below 15 kHz) were discarded due to electrode effects and high frequency values (above 307 kHz) were discarded due to capacitive coupling errors. To perform tissue differentiation the frequencies of 15 kHz for |Z| and R and 307 kHz for PA and Xc were chosen based on the calculation of the mean pair-wise Euclidean distance between tissue paired groups. Hence, 15 kHz for |Z| and R and 307 kHz for PA and Xc are the two most discriminative frequencies.

Shapiro–Wilk test was used to assess the distribution of normality of the variables (|Z|, PA, R, Xc and the difference between low and high mean bioimpedance values in |Z|, PA, R and Xc). Normally distributed variables are shown as mean ± standard deviation (SD) and 95% confidence interval (CI) of the mean (lower bound – upper bound). The variables non-normally distributed are shown as median (interquartile range, IQR) and minimum – maximum. One-way analysis of variance (ANOVA, normally-distributed data) with Tamhane $t2$ *post-hoc* test was used to determine statistically significant differences in the |Z|, PA, R and the differences between low and high frequencies mean

bioimpedance in |Z|, PA, R and Xc. For non-normally distributed data, Kruskal–Wallis test was used to determine significance in Xc among healthy lung tissue, neoplasm, fibrosis, pneumonia and emphysema.

Discriminant Function Analysis was used to find a linear combination of features that separates healthy lung tissue, neoplasm, fibrosis, pneumonia and emphysema bioimpedance values using the bioimpedance parameters of |Z| and R at 15 kHz and PA and Xc at 307 kHz.

3. Results

The total number of bioimpedance samples obtained were 116 (more than one sample was obtained in a few patients) divided according tissue states: 30 healthy lung (age: 62 ± 18 years; weight: 77.7 ± 25.6 kg; BMI: 26.5 ± 4.4 kgm^{-2}), 29 neoplasm (age: 69 ± 9 years; weight: 74.3 ± 13.9 kg; BMI: 26.4 ± 4.3 kgm^{-2}), 23 emphysema (age: 72 ± 9 years; weight: 72.5 ± 12.3 kg; BMI: 27.3 ± 4.8 kgm^{-2}); 12 fibrosis (age: 73 ± 10 years; weight: 76.9 ± 10.7 kg; BMI: 28.4 ± 2.0 kgm^{-2}) and 22 pneumonia (age: 62 ± 16 years; weight: 68.9 ± 12.0 kg; BMI: 25.8 ± 4.4 kgm^{-2}).

3.1. Box plot

Figure 1 shows the median (central line of each box) and the 25 and 75 percentiles (down and upper extremes of each box) for |Z| and R at 15 kHz and for PA and Xc at 307 kHz for each of the tissue states [neoplasm (6 small cell lung neoplasm and 23 non-small cell lung neoplasm), fibrosis, pneumonia, healthy lung tissue and emphysema]. Dashed lines represent the most extreme points not considered outliers (1.5 times bigger than the interquartile range). Results show an increase in the |Z| and R and a decrease in the PA and Xc as more air content is the tissue.

3.2. Tissue differentiation of minimally-invasive electrical impedance spectroscopy measurements among tissue states

Table 1 lists the descriptive parameters, specified as the mean ± SD, 95% confidence interval for mean (lower bound and upper bound) for normally distributed variables and specified as statistic median (interquartile range, IQR) and minimum – maximum for non-normally distributed variables of |Z|, PA, R and Xc and the results of the one-way ANOVA including the Fisher coefficient (F) and the Kruskal–Wallis test results for the minimally-invasive bioimpedance measures performed in healthy lung tissue ($n = 30$), neoplasm lung tissue ($n = 29$), emphysema ($n = 23$), fibrosis ($n = 12$) and pneumonia ($n = 22$). Both tests show statistical significance ($p < 0.001$) in the |Z|, PA, R and Xc. Fisher coefficient shows higher values in |Z| and R than in PA.

Table 2 shows the Tamhane $t2$ test results for |Z| at 15 kHz, PA at 307 kHz and for R at 15 kHz. Statistical differences are found between: neoplasm and pneumonia, healthy lung tissue and emphysema; fibrosis and healthy lung tissue and emphysema;
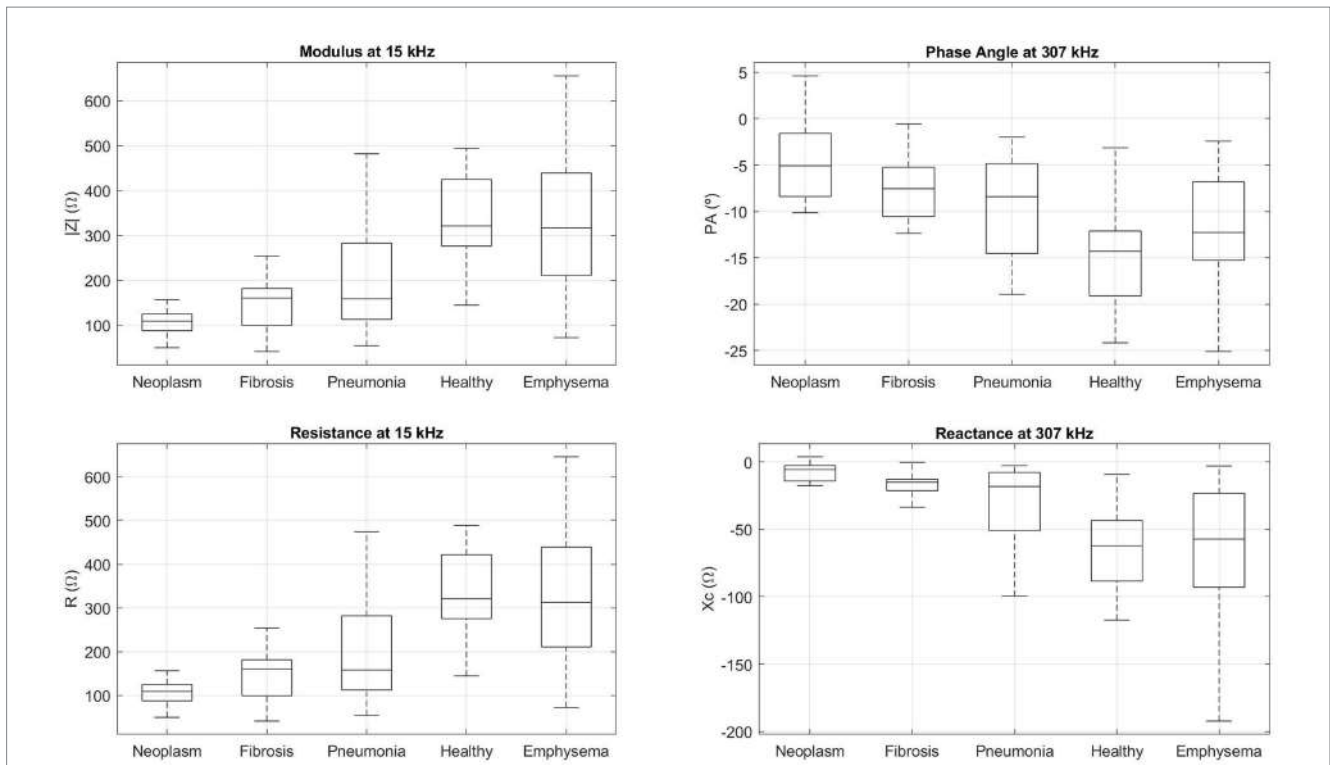
FIGURE 1
Boxplot of the bioimpedance parameters (|Z| and R at 15 kHz and PA and Xc at 307 kHz) for neoplasm, fibrosis, pneumonia, healthy lung tissue and emphysema tissue samples. The central line of each box represents the median of each group, low and upper box lines represent the 25 and 75 percentiles, respectively, and dashed lines belong to the most extreme points which are not considered outliers.

TABLE 1 Descriptions of minimally-invasive bioimpedance measurements for healthy lung tissue, neoplasm, emphysema, fibrosis and pneumonia.

	Healthy ($n=30$)	Neoplasm ($n=29$)	Emphysema ($n=23$)	Fibrosis ($n=12$)	Pneumonia ($n=22$)	One way ANOVA test	
						F	p
$\|Z\|$ (Ω) 15 kHz	356.29 ± 94.15 (296.47–416.11)	114.53 ± 23.24 (99.77–129.30)	340.54 ± 168.19 (233.68–447.40)	149.17 ± 57.62 (112.56–185.78)	199.12 ± 75.27 (151.29–246.95)	30.80	<0.001
PA (°) 307 kHz	-16.02 ± 4.48 [$-18.87 - (-13.18)$]	-4.75 ± 4.35 [$-7.52 - (-1.99)$]	-12.71 ± 6.46 [$-16.82 - (-8.61)$]	-7.29 ± 3.77 [$-9.69 - (-4.89)$]	-9.22 ± 4.52 [$-12.08 - (-6.35)$]	20.52	<0.001
R (Ω) 15 kHz	354.90 ± 93.28 (295.63–414.17)	114.44 ± 23.14 (99.73–129.14)	338.79 ± 166.02 (233.31–444.27)	149.03 ± 57.58 (112.44–185.61)	198.65 ± 75.11 (150.93–246.37)	30.99	<0.001
						Kruskal–Wallis test	
						p	
Xc (Ω) 307 kHz	-73.29 ± 29.42 [$-92.24 - (-54.86)$]	-8.53 ± 7.46 [$-13.27 - (-3.79)$]	-69.88 ± 52.51 [$-103.24 - (-36.51)$]	-15.98 ± 9.30 [$-21.89 - (-10.07)$]	-18.23 (39.35) [$-56.63 - (-3.40)$]	<0.001	

The variables normally distributed are shown as mean ± SD, 95% confidence interval for mean (lower bound and upper bound) while that non-normally distributed data is shown as statistic median (interquartile range, IQR) and minimum-maximum. In addition, the statistic of the Fisher (F) coefficient for variance analysis and the statistical significance (p) are also shown.

pneumonia and healthy lung tissue and emphysema. No statistically significant differences are found between: healthy lung tissue and emphysema; fibrosis and neoplasm; fibrosis and pneumonia.

Table 3 shows the pair to pair comparison results for Xc at 307 kHz as Xc is not normally distributed. Statistically significant differences are found between healthy lung tissue and pneumonia, fibrosis and neoplasm, emphysema and fibrosis and neoplasm and between pneumonia and neoplasm.

3.3. Discriminant analysis of minimally-invasive electrical impedance spectroscopy measurements among tissue states

Table 4 shows the Fisher's linear discriminant functions for lung neoplasm, fibrosis, pneumonia, healthy lung tissue and emphysema bioimpedance measurements and the canonical discriminant

TABLE 2　Tamhane *t2 post-hoc* test results for |Z| at 15kHz, PA at 307kHz and R at 15kHz.

Post-hoc Tamhane t2 test								
|Z| 15kHz (Ω)			R (Ω) 15kHz			PA (°) 307kHz		
		p			*p*			*p*
Healthy	Neoplasm	<0.001	Healthy	Neoplasm	<0.001	Healthy	Neoplasm	<0.001
	Emphysema	1		Emphysema	1		Emphysema	0.17
	Fibrosis	<0.001		Fibrosis	<0.001		Fibrosis	<0.001
	Pneumonia	<0.001		Pneumonia	<0.001		Pneumonia	0.008
Neoplasm	Emphysema	<0.001	Neoplasm	Emphysema	<0.001	Neoplasm	Emphysema	<0.001
	Fibrosis	0.247		Fibrosis	0.248		Fibrosis	0.33
	Pneumonia	0.006		Pneumonia	0.006		Pneumonia	0.002
Emphysema	Fibrosis	<0.001	Emphysema	Fibrosis	<0.001	Emphysema	Fibrosis	0.096
	Pneumonia	0.015		Pneumonia	0.014		Pneumonia	0.979
Fibrosis	Pneumonia	0.64	Fibrosis	Pneumonia	0.649	Fibrosis	Pneumonia	0.618

TABLE 3　Pair to pair comparisons for Xc bioimpedance parameter with significance adjusted by Bonferroni method.

Pair−Pair Comparison Xc (Ω) 307kHz				
		Statistic	*p*	Adjusted *p*
Healthy	Emphysema	−8.31	0.373	1
	Pneumonia	−33.47	<0.001	0.004
	Fibrosis	−45.28	<0.001	0.001
	Neoplasm	−62.08	<0.001	0
Emphysema	Pneumonia	−25.16	0.012	0.121
	Fibrosis	−36.98	0.002	0.02
	Neoplasm	53.77	<0.001	0
Pneumonia	Fibrosis	11.81	0.328	1
	Neoplasm	28.61	0.003	0.026
Fibrosis	Neoplasm	16.80	0.146	1

functions, by Discriminant Function Analysis of the bioimpedance parameters (|Z|, PA and Xc).

4. Discussion

This project developed by the Electronic and Biomedical Instrumentation research group from the Technical University of Catalonia (UPC) and the Interventional Pulmonology Unit from Hospital de la Santa Creu i Sant Pau of Barcelona aims to differentiate among different lung pathologies (neoplasm, fibrosis, pneumonia and emphysema) and healthy lung tissue through minimally-invasive bioimpedance measurements performed directly in lung tissue.

In general terms, in the healthy subject, the lung parenchyma is a histologically heterogeneous structure formed by a network of bronchi and bronchioles that present different subdivisions until generating the alveolar ducts and alveoli where gas exchange occurs. All these structures are surrounded by connective tissue with a reticular structure of collagen and elastic fibers, in which the lymphatic vessels and the capillary of the pulmonary circulation are distributed. In pulmonary pathologies there is an alteration of the pulmonary architecture. The structural changes in the tissues provide a differentiated electrical behavior that will vary according to the tissue involvement and, therefore, could allow differentiating respiratory diseases.

The bioimpedance parameters that can be directly obtained from the bioimpedance measures obtained are the R and the Xc. The first one denotes the behavior of the cellular medium while the second one related to the capacitive behavior of the cell membranes. Two more parameters that can be extracted from the first ones are the |Z| and the PA. While |Z| is highly correlated with the R, the PA is related to Xc (5). To perform tissue differentiation, in this study we have taken into account the four parameters mentioned and have selected the frequency of 15 kHz for |Z| and R and the frequency of 307 kHz for PA and Xc for being the two most discriminative frequencies according to the pair-wise Euclidean distances calculated between pairs of tissue samples. In COPD and specifically in emphysema, the increase in inflammatory cells and oxidative stress produce the secretion of proteases with the capacity to degrade components of the extracellular matrix, which produces direct damage to structural cells and promotes proteolytic degradation of tissues with destruction of alveolar walls (16, 17). The air content present in lungs in proportion to the tissue is higher in this pathology than in the others studied (neoplasm, fibrosis and pneumonia) and also is higher than in healthy lung tissue. In emphysema the data present higher variability and dispersion than in the other tissues studied. This is due to the fact that the sensibility of measure is 2 mm and depending the grade of emphysema the |Z| and R is higher (more air content) or lower. This fact leads to the no differentiation between healthy and emphysema lung tissue.

Considering the above-mentioned, results in Figure 1 show higher values of |Z| and R and lower values of PA and Xc at the tissue samples which have more air content (healthy lung tissue and emphysema). The increase in |Z| and R is due to the non-conductive character of air, as compared with the other tissue samples (neoplasm, fibrosis and pneumonia) in which the proportion of tissue is higher compared to the quantity of air. Related to that condition, the Xc and in

consequence the PA, denotes the additional resistance produced by the cell membranes.

The increase of the Xc values in those pathologies in which there is an increase of tissue denotes the increment of cells present in these tissues (neoplasm and fibrosis). In this way, in neoplasm is produced a proliferation of tumor cells and infiltration of lymphatic and blood vessels. The tumor cells have different histological characteristics and, in general, according to the morphology of the cells, lung cancer is classified in non-small cell lung carcinomas (NSCLCs): adenocarcinoma (ADC) and squamous cell carcinoma (SQCC) and small cell lung cancer (18). On the other hand, idiopathic pulmonary fibrosis belongs to the group of diffuse pulmonary diseases (ILD) that includes a heterogeneous classification of pathologies characterized by thickening of the alveolar septa, proliferation of fibroblasts, collagen deposition and, in advanced phases, of the disease, pulmonary fibrosis (19).

For tissue differentiation among neoplasm, fibrosis, pneumonia, healthy lung tissue and emphysema one-way ANOVA test for parametric parameters (|Z|, PA and R) and Kruskal–Wallis test for the non-parametric Xc have been performed. One-way ANOVA test determines differences among different groups means using their variances to determine if their means are equally distributed or not. Hence, a $p > 0.05$ concludes that the distributions of the different groups are equal based on their means. To determine which of the parameters (|Z|, PA or R) have more significance, Fisher coefficient (F) is used, which is defined as the ratio between the variance between samples and the variance within samples. Then, as larger the F, as higher the significance in that variable (20). Also, Kruskal–Wallis test determines differences among groups based on mean ranks (21). Then, according to the results obtained in Table 1, there are statistically significant differences ($p < 0.001$) among tissue samples in |Z|, PA, R and Xc. The significance obtained is higher in |Z| and R than in PA according to the value of the Fisher coefficient obtained. Therefore, a significance higher in |Z| and R means that the most important element for tissue differentiation among the tissue states studied seems to be the proportion of air present in the extracellular medium as compared to the amount of tissue.

Regarding the *post-hoc* tests results (Tables 2, 3), results show statistical significant differences between neoplasm and pneumonia ($p < 0.05$) in |Z|, PA, R and Xc; neoplasm and healthy lung tissue ($p < 0.001$) in |Z|, PA, R and Xc; neoplasm and emphysema ($p < 0.001$) in |Z|, PA, R and Xc; fibrosis and healthy lung tissue ($p \leq 0.001$) in |Z|, PA, R and Xc; fibrosis and emphysema ($p < 0.05$) in |Z|, R and Xc; pneumonia and healthy lung tissue ($p < 0.01$) in |Z|, PA, R and Xc; and between pneumonia and emphysema ($p < 0.05$) in |Z| and R. No statistically significant differences ($p > 0.05$) are found between neoplasm and fibrosis; fibrosis and pneumonia; and between healthy lung tissue and emphysema.
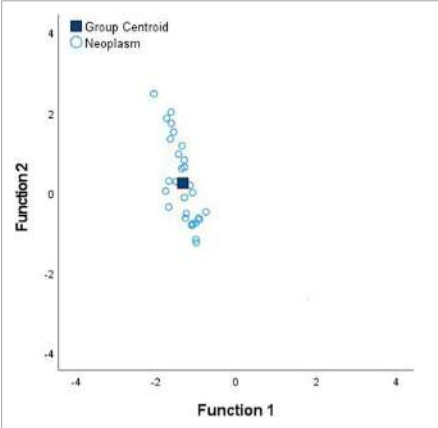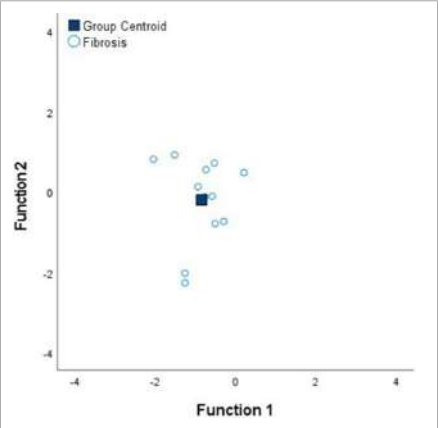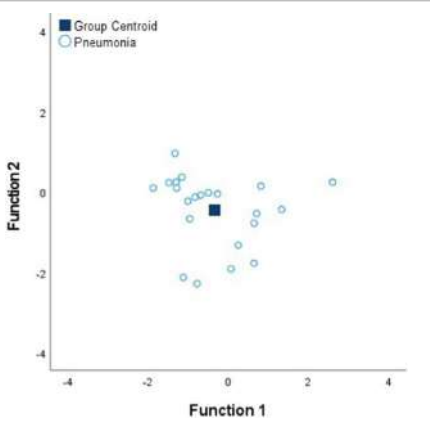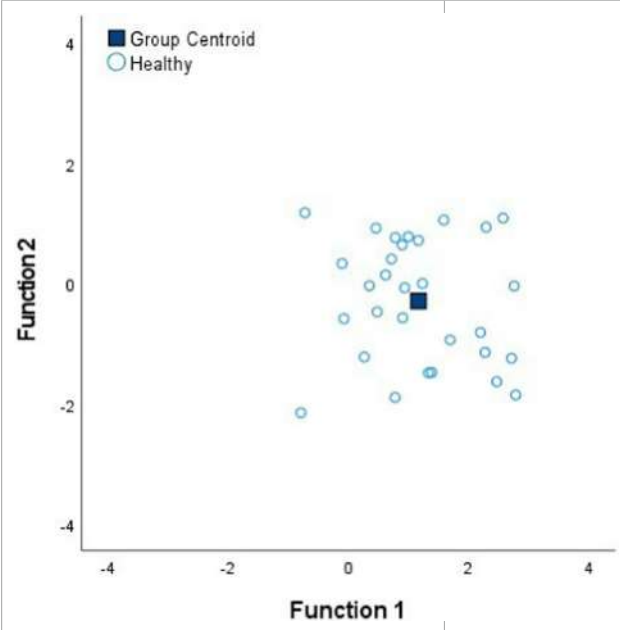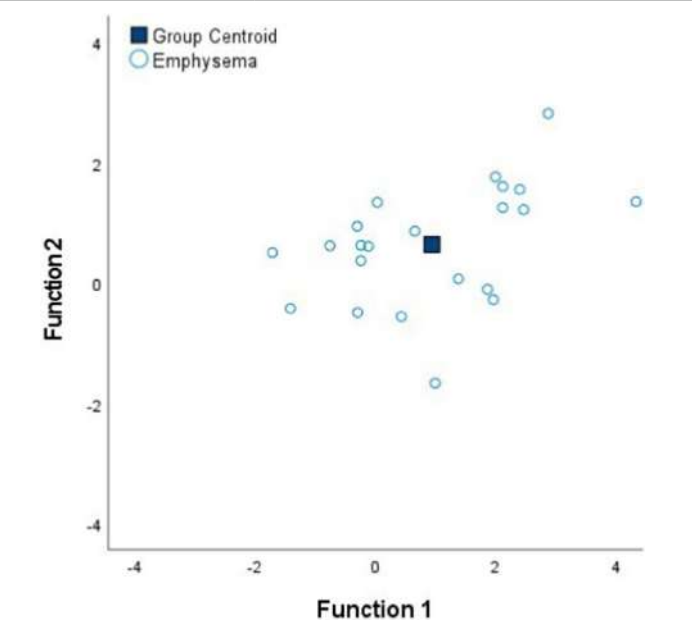
In summary, as we have described above, neoplasm is characterized by a cell growth and an increase of vascularization and fibrosis is characterized by an increase of tissue in the pathological region despite not being over-vascularized. This similitude of increment of tissue in the pathological region and, in consequence, a decrease in air proportion, lowers the bioimpedance |Z| and R and increases the Xc and PA (Figure 1; Table 1). Despite the over-vascularization of the neoplasm tissue, which lowers slightly the |Z| and R and increases slightly the Xc and PA, the similitude in both

pathologies regarding the increment of tissue and, in turn, cell concentration makes not possible to distinguish through minimally-invasive bioimpedance measures between both pathologies. In pneumonia, the inflammatory response is initially characterized by a congestive phase with vascular hyperemia followed by an exudative phase in which the presence of neutrophils and fibrin increases, which can completely occupy the alveolar spaces (22) which decreases the impedance |Z| and R as compared to healthy lung tissue as the quantity of air decreases. However, pneumonia presents higher proportion of air than fibrosis which makes the |Z| and R higher in pneumonia than in fibrosis. Despite the differences between these two pathologies, the characteristic of lung condensation hinders the differentiation between both pathologies.

In complement to the statistical tests performed (one-way ANOVA and Kruskal–Wallis) and following with the tissue differentiation, we have performed a discriminant analysis among the different tissue states (neoplasm, fibrosis, pneumonia, healthy lung tissue and emphysema). Each tissue type obtains a Fisher's linear discriminant function that aims to find a linear function that maximizes the distance between classes of the projected data means and minimizes the projected within-class variance. The generalization of Fisher's discriminant function is the canonical discriminant function which have maximum discriminant power to classify among multiple groups. The canonical discriminant functions are vectors of canonical variables composed by linear combinations of the original variables (23). According to the results obtained in Table 4, the graphics of the individual tissue type distributions show an increase in the data dispersion as higher is the air proportion in lungs. Moreover, the results of the graphic where all the tissue types are represented show a higher separation between neoplasm and emphysema and neoplasm and healthy lung tissue (as in Figure 1). Moreover, discriminant analysis shows little distance between neoplasm and fibrosis and between fibrosis and pneumonia, which is in accordance to the results obtained in the statistical tests (Tables 2, 3). Moreover, canonical discriminant functions show that in the first function the |Z| have more importance than the PA and the Xc while in the second function the variable which has more importance is the PA.

The differentiation among the different tissue states using the mean impedance values obtained from the 12 s duration of acquisition signals at 15 kHz for |Z| and R and at 307 kHz for PA and Xc have been proved to be useful for the differentiation between neoplasm and pneumonia, neoplasm and healthy lung tissue, neoplasm and emphysema, fibrosis and healthy lung tissue, fibrosis and emphysema, pneumonia and healthy lung tissue and pneumonia and emphysema. However, it has not been proved to be useful to differentiate between neoplasm and fibrosis, fibrosis and pneumonia and healthy lung tissue and emphysema. As discussed in Company-Se et al. (13) the 3-electrode method was more suitable for the minimally-invasive lung tissue measurements than the 4-electrode method. Furthermore, as also stated in Company-Se et al. (13) the two-electrode method (the simplest method) that only uses the tip of the catheter and an external electrode was discarded because this last method has higher interpatient variability due to non-related lung tissue characteristics factors. Moreover, this last method depends on sweat regulation and skin hydration. Despite the reduction of the data variability through calibration, the data variability continues to

TABLE 4 Fisher's linear discriminant functions for neoplasm, fibrosis, pneumonia, healthy and emphysema lung bioimpedance samples and canonical discriminant functions for the bioimpedance parameters (|Z|, PA and Xc).

Fisher's linear discriminant function

| $F_{Neoplasm} = 0.03\%|Z| - 0.15\%PA + 0.10\%Xc - 3.22$ | $F_{Fibrosis} = 0.04\%|Z| - 0.29\%PA + 0.12\%Xc - 4.36$ | $F_{Pneumonia} = 0.04\%|Z| - 0.39\%PA + 0.12\%Xc - 5.38$ |

Fisher's linear discriminant function

| $F_{Healthy} = 0.05\%|Z| - 0.36\%PA + 0.12\%Xc - 9.59$ | $F_{Emphysema} = 0.06\%|Z| - 0.06\%PA + 0.10\%Xc - 8.37$ |

(Continued)

be high. This is due to the different respiratory patterns observed in the different patients. While some patients remain still during the signal acquisition, others produce apneas, cough or even movement, affecting the mean values of the signals. In future studies, bronchoscopy will be performed in patients which would undergo general anesthesia in order to study if it affects to the reduction of data variability.
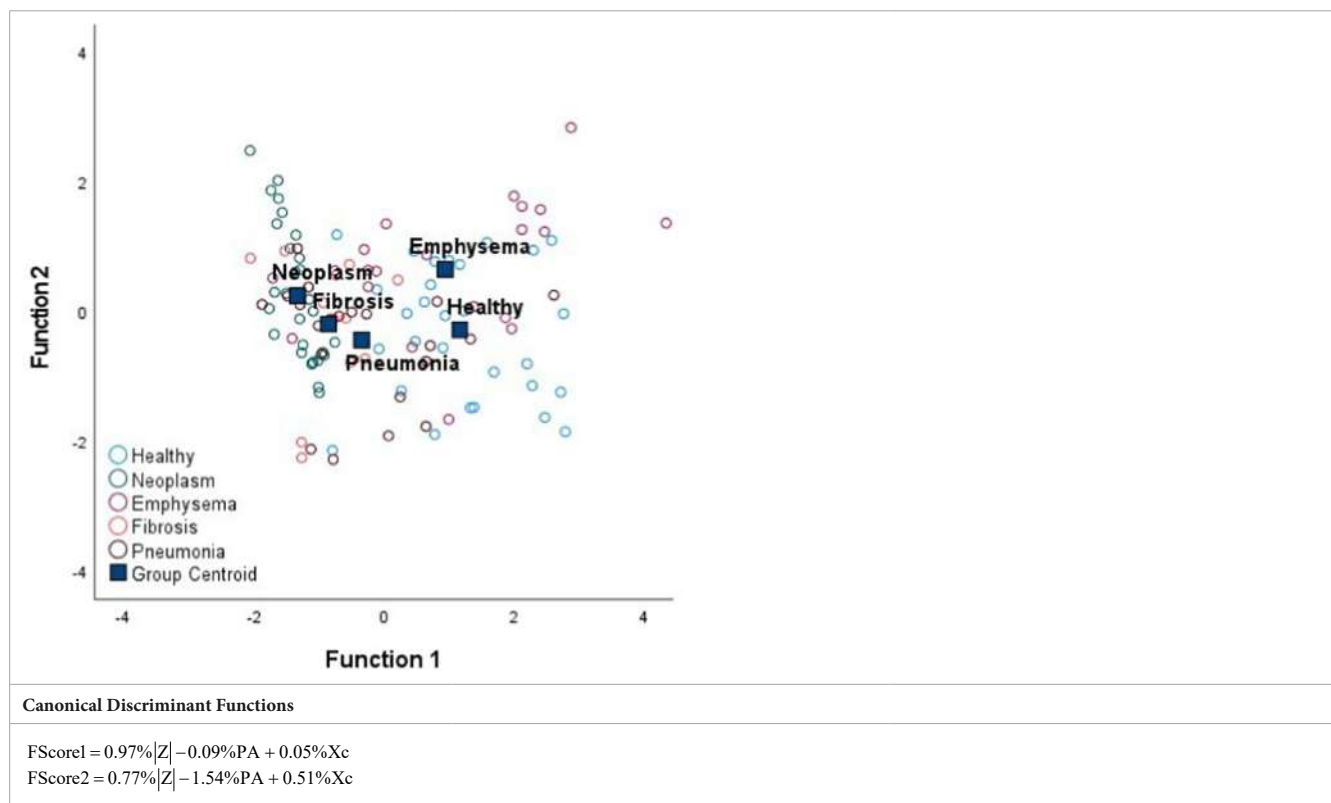
4.1. Contribution

The minimally-invasive bioimpedance measurements is a complementary method to bronchoscopy procedure for real time diagnosis through tissue differentiation for respiratory diseases.

The major contribution is the capability to differentiate between those pathologies that leads increased tissue and inflammatory cells and those ones that contain more air and destruction of alveolar septa.

4.2. Limitation

To validate minimally-invasive bioimpedance as a method for real time diagnosis through tissue differentiation for respiratory diseases, it is necessary to perform studies that compare standardized procedures that allow real-time localization of pulmonary lesions, such as electromagnetic navigation bronchoscopy (ENB) or radial EBUS.

TABLE 4 (Continued)

Canonical Discriminant Functions

$FScore1 = 0.97\%|Z| - 0.09\%PA + 0.05\%Xc$
$FScore2 = 0.77\%|Z| - 1.54\%PA + 0.51\%Xc$

5. Conclusion

The use of minimally-invasive bioimpedance measurements have been proven to be useful for tissue differentiation among lung pathologies and healthy lung tissue. Statistical differences have been found between groups by using the two most discriminative frequencies. Bioimpedance has proven to differentiate between those pathologies that leads increased tissue and inflammatory cells and those ones that contain more air and destruction of alveolar septa.

Data availability statement

The raw data supporting the conclusions of this article will be made available by the authors, without undue reservation.

Ethics statement

The studies involving human participants were reviewed and approved by "Hospital de la Santa Creu i Sant Pau" (CEIC-73/2020). The patients/participants provided their written informed consent to participate in this study.

Author contributions

RB, VP, PR, JR, GC-S, AT, and LN designed the experiments and revised the paper and approved the final version of the

manuscript. GC-S, VP, and AT performed the experiments. LN and GC-S performed the data processing, analyzed the data, drafted the manuscript and prepared the tables and figures. All authors contributed to the article and approved the submitted version.

Conflict of interest

The authors declare that the research was conducted in the absence of any commercial or financial relationships that could be construed as a potential conflict of interest.

Publisher's note

All claims expressed in this article are solely those of the authors and do not necessarily represent those of their affiliated organizations, or those of the publisher, the editors and the reviewers. Any product that may be evaluated in this article, or claim that may be made by its manufacturer, is not guaranteed or endorsed by the publisher.

References

1. Herth FJF, Eberhardt R, Becker HD, Ernst A. Endobronchial ultrasound-guided transbronchial lung biopsy in fluoroscopically invisible solitary pulmonary nodules: a prospective trial. *Chest*. (2006) 129:147–50. doi: 10.1378/chest.129.1.147

2. Folch EE, Pritchett MA, Nead MA, Bowling MR, Murgu SD, Krimsky WS, et al. Electromagnetic navigation bronchoscopy for peripheral pulmonary lesions: one-year results of the prospective, multicenter NAVIGATE study. *J Thorac Oncol*. (2019) 14:445–58. doi: 10.1016/j.jtho.2018.11.013

3. Lukaski HC, Vega Diaz N, Talluri A, Nescolarde L. Classification of hydration in clinical conditions: indirect and direct approaches using bioimpedance. *Nutrients*. (2019) 11:809. doi: 10.3390/nu11040809

4. Khalil S, Mohktar M, Ibrahim F. The theory and fundamentals of bioimpedance analysis in clinical status monitoring and diagnosis of diseases. *Sensors*. (2014) 14:10895–928. doi: 10.3390/s140610895

5. Lukaski HC. Biological indexes considered in the derivation of the bioelectrical impedance analysis. *Am J Clin Nutr*. (1996) 64:397S–404S. doi: 10.1093/ajcn/64.3.397S

6. Toso S, Piccoli A, Gusella M, Menon D, Bononi A, Crepaldi G, et al. Altered tissue electric properties in lung cancer patients as detected by bioelectric impedance vector analysis (2000) 16:120–4. doi: 10.1016/s0899-9007(99)00230-0,

7. Baarends EM, Van Marken Lichtenbelt WD, Wouters EFM, Schols AMWJ. Body-water compartments measured by bio-electrical impedance spectroscopy in patients with chronic obstructive pulmonary disease. *Clin Nutr*. (1998) 17:15–22. doi: 10.1016/S0261-5614(98)80038-1

8. Orschulik J, Hochhausen N, Santos SA, Czaplik M, Leonhardt S, Walter M. Detection of Acute Respiratory Distress Syndrome Using Sectoral Bioimpedance Spectroscopy – A Pilot Study. (2018). doi: 10.18154/RWTH-CONV-224905

9. Meroni D, Bovio D, Frisoli PA, Aliverti A. Measurement of electrical impedance in different ex-vivo tissues In: . *2016 38th Annual International Conference of the IEEE Engineering in Medicine and Biology Society (EMBC)*. Orlando, FL, USA: IEEE (2016). 2311–4.

10. Sanchez B, Vandersteen G, Martin I, Castillo D, Torrego A, Riu PJ, et al. In vivo electrical bioimpedance characterization of human lung tissue during the bronchoscopy procedure. A feasibility study. *Med Eng Phys*. (2013) 35:949–57. doi: 10.1016/j.medengphy.2012.09.004

11. Guich NC, Bardia RB, Muñoz-Fernández AM, Ruiz VP, Torrego A, PJR Costa. Espectrometría de Impedancia Eléctrica en Tejido Pulmonar. XXXIV Congreso Anual de la Sociedad Española de Ingeniería Biomédica (2016).

12. Riu PJ, Company G, Bragos R, Rosell J, Pajares V, Torrego A. Minimally invasive real-time electrical impedance spectroscopy diagnostic tool for lung parenchyma pathologies In: . *2020 42nd Annual International Conference of the IEEE Engineering in Medicine and Biology Society (EMBC)*. Montreal, QC, Canada: IEEE (2020). 5077–80.

13. Company-Se G, Nescolarde L, Pajares V, Torrego A, Riu PJ, Rosell J, et al. Minimally invasive lung tissue differentiation using electrical impedance spectroscopy: a comparison of the 3- and 4-electrode methods. *IEEE Access*. (2022) 10:7354–67. doi: 10.1109/ACCESS.2021.3139223

14. Company-Se G, Nescolarde L, Pajares V, Torrego A, Riu PJ, Rosell J, et al. Effect of calibration for tissue differentiation between healthy and neoplasm lung using minimally invasive electrical impedance spectroscopy. *IEEE Access*. (2022) 10:103150–63. doi: 10.1109/ACCESS.2022.3209809

15. Amorós-Figueras G, Jorge E, Alonso-Martin C, Traver D, Ballesta M, Bragós R, et al. Endocardial infarct scar recognition by myocardial electrical impedance is not influenced by changes in cardiac activation sequence. *Heart Rhythm*. (2018) 15:589–96. doi: 10.1016/j.hrthm.2017.11.031

16. Núñez-Naveira L, Montero-Martínez C, Ramos-Barbón D. Oxidación, inflamación y modificaciones estructurales. *Arch Bronconeumol*. (2007) 43:18–29. doi: 10.1016/S0300-2896(07)71169-9

17. Halpin DMG, Criner GJ, Papi A, Singh D, Anzueto A, Martinez FJ, et al. Global initiative for the diagnosis, management, and prevention of chronic obstructive lung disease. The 2020 GOLD science committee report on COVID-19 and chronic obstructive pulmonary disease. *Am J Respir Crit Care Med*. (2021) 203:24–36. doi: 10.1164/rccm.202009-3533SO

18. Travis WD, Brambilla E, Noguchi M, Nicholson AG, Geisinger K, Yatabe Y, et al. Diagnosis of lung cancer in small biopsies and cytology: implications of the 2011 International Association for the Study of Lung Cancer/American Thoracic Society/European Respiratory Society classification. *Arch Pathol Lab Med*. (2013) 137:668–84. doi: 10.5858/arpa.2012-0263-RA

19. Travis WD, Costabel U, Hansell DM, King TEJ, Lynch DA, Nicholson AG, et al. An official American Thoracic Society/European Respiratory Society statement: update of the international multidisciplinary classification of the idiopathic interstitial pneumonias. *Am J Respir Crit Care Med*. (2013) 188:733–48. doi: 10.1164/rccm.201308-1483ST

20. Illowsky B, Dean S. Introductory Statistics. (2013), 913.

21. Dodge Y. *The Concise Encyclopedia of Statistics. 1st* ed. New York: Springer (2008). 616 p.

22. Cillóniz C, Ewig S, Polverino E, Marcos MA, Esquinas C, Gabarrús A, et al. Microbial aetiology of community-acquired pneumonia and its relation to severity. *Thorax*. (2011) 66:340–6. doi: 10.1136/thx.2010.143982

23. Peña D. *Análisis de Datos Multivariantes*, Spain: McGraw-Hill Interamericana de España SL (2002). 560 p.

CHAPTER 5: Application of Machine Learning Classification Algorithms in Lung Electrical Impedance Spectroscopy Measurements

Work in Progress – Under Review

Title: Application of Machine Learning Classification Algorithms in Lung Electrical Impedance Spectroscopy Measurements

Authors: Georgina Company-Se, Lexa Nescolarde, Virginia Pajares, Albert Rafecas, Pere J. Riu, Javier Rosell and Ramon Bragós

Journal:

Quartile:

Application of Machine Learning Classification Algorithms in Lung Electrical Impedance Spectroscopy Measurements

Georgina Company-Se[1], Virginia Pajares[2], Albert Rafecas[2], Pere J. Riu[1], Javier Rosell[1], Ramon Bragós[1], Lexa Nescolarde*[1]

[1]Department of Electronic Engineering, Universitat Politècnica de Catalunya, Barcelona, 08034 Spain

[2]Department of Respiratory Medicine, Hospital de la Santa Creu i Sant Pau, Barcelona, 08041 Spain

This work involved human subjects or animals in its research. Approval of all ethical and experimental procedures and protocols was granted by the Ethics Committee on Clinical Investigation of the Hospital de la Santa Creu i Sant Pau, Barcelona, Spain, under Application No. CEIC-73/2010.

E-mail: lexa.nescolarde@upc.edu

Word Count: 4924

ABSTRACT

PURPOSE: to apply classification algorithms using minimally-invasive EIS measurements obtained through bronchoscopy to perform multiple-class lung tissue classification among neoplasm, fibrosis, pneumonia, healthy lung tissue and emphysema.

METHODS: Machine Learning classification algorithms (Decision Tree, Random Forest, KNN, Naïve Bayes and Gradient Boosting) were implemented using the mean averaged spectra of the bioimpedance |Z| and PA obtained from 15 kHz to 307 kHz of neoplasm (n = 29), fibrosis (n = 12), pneumonia (n = 22), healthy lung tissue (n = 30) and emphysema (n = 23). Confusion matrix was used to visualize the results of the classification algorithm. Classification report was obtained to evaluate the metrics of each algorithm for each of the different output classes (neoplasm, fibrosis, pneumonia, healthy lung tissue and emphysema).

RESULTS: Decision tree and Naïve Bayes algorithms obtained a classification accuracy higher than

60% with a recall of 86% and 100% for neoplasm class respectively. Healthy lung tissue and neoplas classes presented higher classification accuracy.

CONCLUSION:

The application of Machine Learning classification algorithms presents an opportunity to help minimally-invasively in the diagnosis of lung diseases for real-time tissue characterization. Promising results have been obtained by the possible classification and thus, differentiation, of neoplasm with respect to fibrosis (two pathologies with similar bioimpedance values).

Keywords: classification, machine learning, minimally-invasive bioimpedance, bronchoscopy, respiratory disease.

1. INTRODUCTION

The diagnosis of lung diseases requires tissue characterization and, in most occasions, it is necessary obtain lung samples to establish the correct final diagnosis. The actual imaging methods of diagnosis of lung diseases [Chest computed tomography (Chest-CT), Positron emission tomography combined with CT (PET/CT) or virtual bronchoscopy are adequate to guide the diagnosis but they have limited value as they do not allow real time guidance for the collection of lung tissue samples.

In recent years, new bronchoscopic techniques have been developed for sampling characterization in real time such as the radial probe endobronchial ultrasound (radial EBUS) or the electromagnetic navigation bronchoscopy (ENB) [1], [2]. The high cost of these novel techniques hinders their availability in Interventional Pulmonology units.

To complement the actual methods of diagnosis, the combination of electrical impedance spectroscopy (EIS) measurements with the application of artificial intelligence algorithms could help for the lung tissue differentiation. The bioimpedance (Z) is defined as the opposition of the tissue to the flow of an electrical current applied. When alternating current is applied, the bioimpedance is frequency-dependent and when a wide-range of frequencies is used to measure bioimpedance then EIS is performed. The Z is composed by two terms, the resistance (R) and the reactance (Xc). R describes the behavior of the extracellular and intracellular medium while Xc describes the capacitive behavior of the cell membranes [3]–[5]. From R and Xc two more parameters are extracted: the impedance modulus (|Z|) defined as $\sqrt{R^2 + Xc^2}$ and the phase angle (PA) defined as $\tan^{-1}(\frac{Xc}{R})$, that represents the lag of the current behind the voltage [3]. The principle of EIS is that at low frequencies the current circulates through the extracellular medium only and at high frequencies the current is able to penetrate the cell membranes, thus it circulates through the intra and extracellular medium [3].

Previous studies evaluate the use of bioimpedance for tissue characterization in lungs. Toso *et al.* [6] studied the differences between healthy and lung neoplasm. Baarends *et al.* [7] predicted body

water compartments of patients with chronic obstruction pulmonary diseases. And Meroni *et al*. [8] studied bioimpedance differences among different organs, including lungs.

To the extent of the authors knowledge, the are no studies regarding the application of minimally invasive EIS for lung tissue differentiation apart from the studies performed by our research group. Sanchez *et al*. [9] presented a feasibility study to validate an EIS measurement device evaluating the accuracy and calibration process for the instrument. Later, Coll *et al*. [10] performed tissue differentiation using minimally-invasive EIS for the differentiation among healthy lung tissue, bronchi and pathological tissue (no pathologies differentiation) using the frequency of 11 kHz and 33 kHz and obtaining differences among groups. Riu *et al*. [11] introduced a Machine Learning classification algorithm to differentiate between healthy lung tissue and other lung tissue (grouping bronchi and pathological tissue) and obtained promising results. All of these studies were performed using the 4-electrode method to acquire bioimpedance measurements. However, due to the limitation of ensuring the contact of the 4 electrodes during the signal acquisition in a trabecular structure, the authors evaluated the possibility to perform tissue differentiation and signal acquisition using the 3-electrode method. As evaluated in Company-Se *et al*. [12]. The capacity of tissue differentiation of both methods (4- and 3-electrode methods) was similar. However, the clinical feasibility of the 3-electrode method was greater. The authors changed to the 3-electrode method to acquire minimally-invasive bioimpedance measurements. Company-Se *et al*. [13] presented a calibration method using bronchi measures to reduce data variability and increase tissue state separation and differentiation capacity. The method was similar to the one used in Amorós-Figueras *et al*. [14]. Finally, Company-Se *et al*. [15] performed tissue differentiation among neoplasm, fibrosis, pneumonia, healthy lung tissue and emphysema using the two most discriminative frequencies (15 kHz for |Z| and R and 307 kHz for PA and Xc). They found statistically significant differences for all the parameters between: neoplasm and pneumonia; neoplasm and healthy lung tissue; neoplasm and emphysema; fibrosis and healthy lung tissue and pneumonia and healthy lung tissue. For fibrosis and emphysema only in |Z|, R and

Xc; and between pneumonia and emphysema only in |Z| and R. They did not find statistically statistically significant differences between neoplasm and fibrosis; fibrosis and pneumonia; and between healthy lung tissue and emphysema.

The application of Machine Learning algorithms presents an opportunity to predict outcomes and develop new methods of diagnostic as well as improve prognostics [16].

The use of artificial intelligence for clinical data analysis has raise importance in recent years. Raj V *et al*. [17] applied logistic regression to classify between control subjects and patients with temporal lobe epilepsy. Cikes *et al*. [18] used K-means clustering algorithm to divide into groups patients having heart failure to identify responders to cardiac resynchronization therapy. Soujanya Chilla *et al*. [19] implemented multiple classification algorithms to identify schizophrenic subjects from healthy. Papp *et al*. [20] applied Random Forest to classify between low and high risk of prostate cancer. Rastegar *et al.* [21] utilized multiple classification algorithms to distinguish between three groups of bone mineral loss (healthy, osteopenia and osteoporosis) using radiomics.

To the best of the authors knowledge, this is the first study describing the application of Machine Learning classification algorithms to differentiate among lung tissue states by using electrical impedance spectroscopy measurements.

The aim of this study is to apply different Machine Learning algorithms (Decision Tree, Random Forest, K-Nearest Neighbours (KNN), Naïve Bayes and Gradient Boosting) to perform multiple-class lung tissue classification among neoplasm, fibrosis, pneumonia, healthy lung tissue and emphysema using minimally-invasive EIS measurements obtained through bronchoscopy.

2. MATERIALS AND METHODS

2.1 Participants

Minimally invasive EIS measurements were performed between November 2021 and August 2022 in 102 patients (Age: 66 ± 14 yr; Weight: 74.5 ± 17.2 kg; BMI: 26.8 ± 4.3 kgm-2) with a bronchoscopy prescribed at the "Hospital de la Santa Creu i Sant Pau" of Barcelona. A total number of 116

samples were obtained divided in: 30 healthy lung, 29 neoplasm, 23 emphysema, 12 fibrosis and 22 pneumonia.

Ethics approval was obtained from the "Hospital de la Santa Creu i Sant Pau" (CEIC-73/2020) according to principles of the Declaration of Helsinki for experiments with human being. All patients proved signed informed consent.

2.2 EIS measurements

Minimally-invasive EIS using the 3-electrode method bioimpedance measurements are obtained through the injection of a multisine current signal (from 1 kHz to 1000 kHz) between a distal tetrapolar catheter electrode and a skin electrode. The voltage induced by the injected current is measured between the distal electrode and a second skin electrode. Impedance signal acquisition time was 12 seconds using a sample frequency of 60 spectra per second. Measures were calibrated according to Company-Se *et al*. [13]. The complete description of the impedance device is at Company-Se *et al*. [13].

2.3 Measurement protocol

Minimally-invasive EIS measurements were acquired though a bronchoscopy. Radiological images (CT or PET/CT) are taken in each patient before bronchoscopy following the diagnostic process. The catheter used to obtain the bioimpedance data is inserted through the working channel of the bronchoscope. Patients are placed in a supine position during the bioimpedance acquisition with the upper airways anaesthetized. Moreover, intravenous sedation is also provided. Biopsy was obtained to confirm the neoplasm diagnosis.

2.4 Data analysis

Decision Tree, Random Forest, KNN, Naïve Bayes and Gradient Boosting classification algorithms were implemented to the bioimpedance measurements. To apply the classification algorithm the mean averaged spectra of the bioimpedance |Z| and PA obtained from 15 kHz to 307 kHz of neoplasm, fibrosis, pneumonia, healthy lung tissue and emphysema were used. Frequencies below 15 kHz and above 307 kHz were discarded due to electrode and capacitive coupling errors. The mean

impedance spectrum was plotted for data visualization. The dataset for algorithms implementation was divided using 75% for training and 25% for testing.

Confusion matrix was used to evaluate visually the results of the classification algorithm. Finally, classification report was obtained to evaluate the metrics of each algorithm and for each of the different output classes (neoplasm, fibrosis, pneumonia, healthy lung tissue and emphysema).
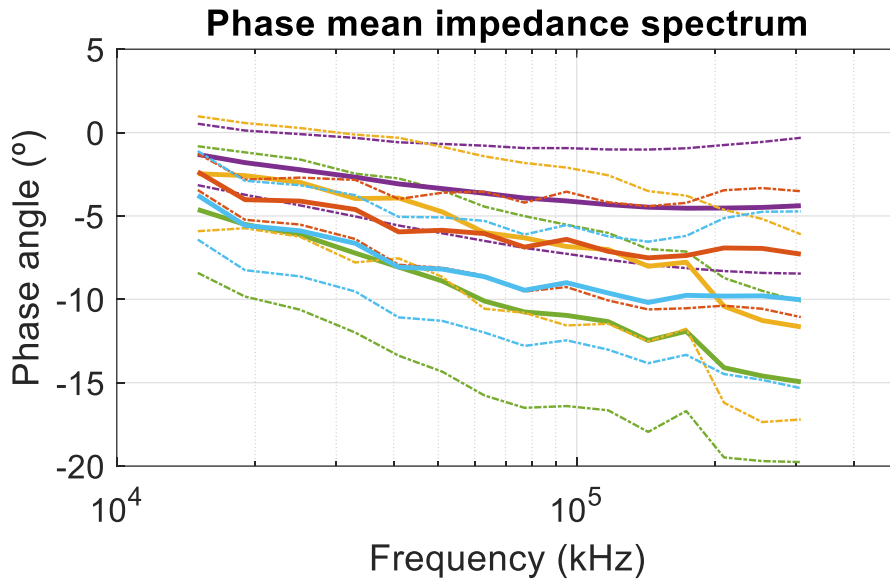
3. RESULTS

3.1 Impedance |Z| and PA Mean Impedance Spectrum

Figure 1 shows the mean impedance spectra of the modulus (a) and phase angle (b) for neoplasm (purple), fibrosis (orange), pneumonia (blue), healthy lung tissue (green) and emphysema (yellow) along all the frequencies (15 kHz to 307 kHz). The continuous line represents de mean while the dashed and pointed lines represent the ±SD. Tissues with higher air proportion (emphysema and healthy lung tissue) present higher values in bioimpedance modulus. Tissues with increased cell concentration (neoplasm) present higher phase angle values.
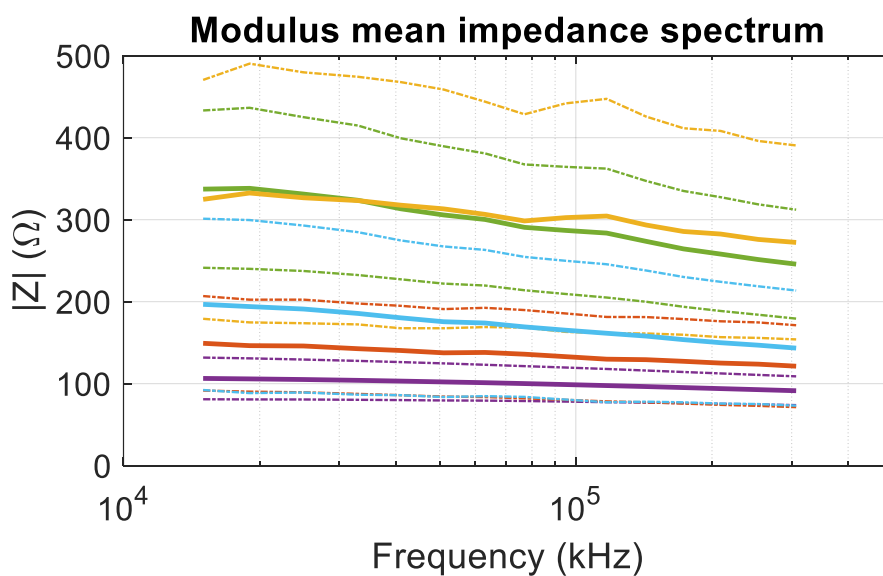

(a)

(b)

Figure 1. Mean impedance spectrum of |Z| (a) and phase angle (b) for all the frequency range. Purple: neoplasm; Orange: fibrosis; Blue: pneumonia; Green: healthy lung tissue; Yellow: emphysema.

**3.2 Confusion matrix for multi-class classification results**

Figure 2 shows the confusion matrix for the predictions over the test set for the multiple classification algorithms implemented (Decision Tree, Random Forest, KNN, Naïve Bayes and Gradient Boosting). Vertical axis represents the true label while the horizontal label represents the predicted label.
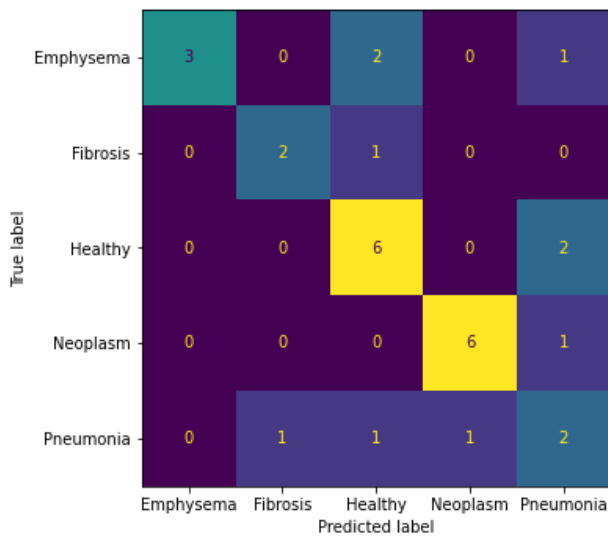
a) Decision Tree
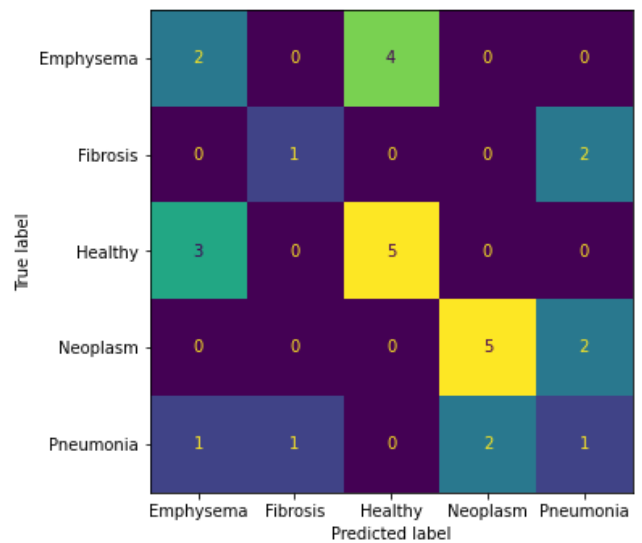
b) Random Forest

c) KNN

d) Naïve Bayes

e) Gradient Boosting

Figure 2. Confusion matrix results for Decision Tree (a), Random Forest (b), KNN (c), Naïve Bayes (d) and Gradient Boosting (e) for lung tissue classification among neoplasm, fibrosis, pneumonia, healthy lung tissue and emphysema.

3.3 Classification reports for multi-class classification algorithms

Table 1 shows the classification reports for the different Machine Learning classification algorithms implemented (Decision T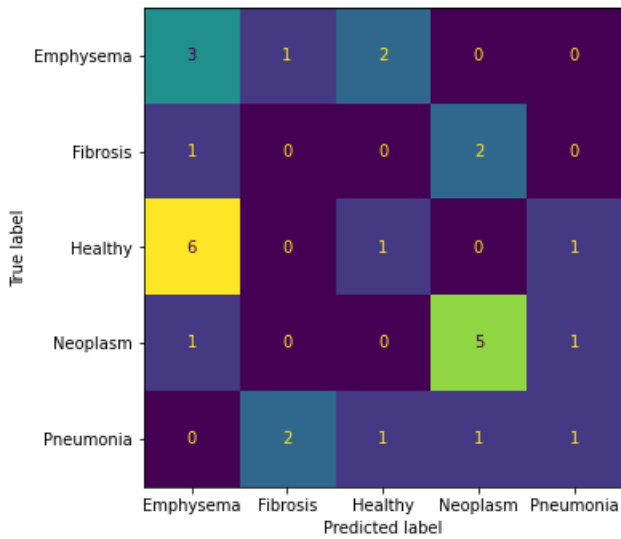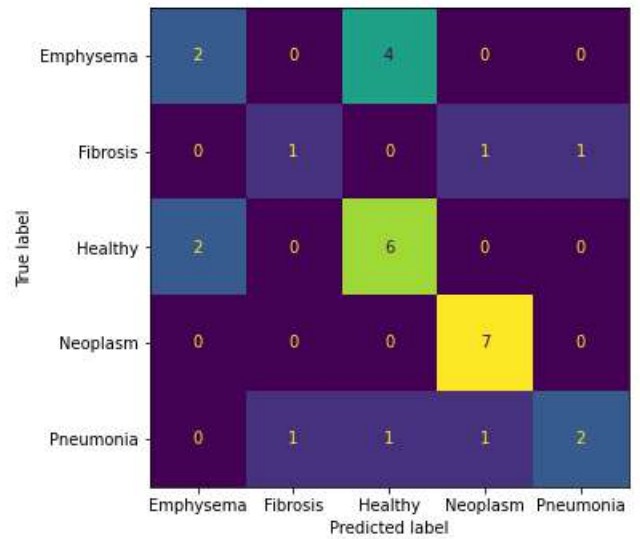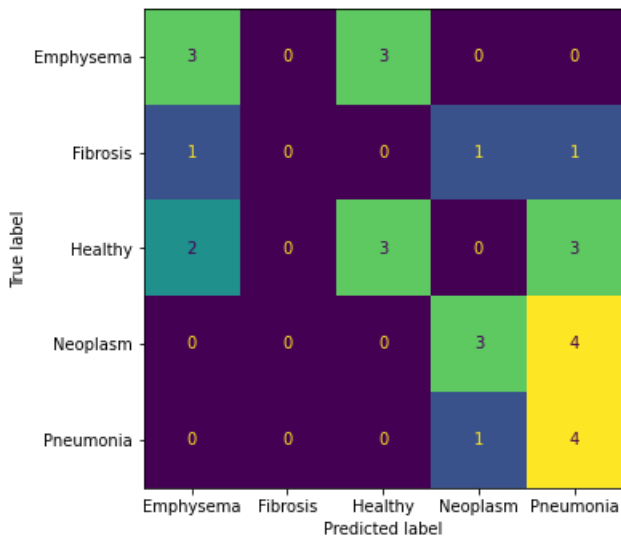ree, Random Forest, KNN, Naïve Bayes and Gradient Boosting). The number of samples used for training have been 87 (75% of the dataset) while the number of samples used for testing have been 29 (25% of the dataset) distributed by 6 samples of emphysema, 3 samples of fibrosis, 8 samples of healthy lung tissue, 7 samples of neoplasm and 5 samples of pneumonia.

Table 1. Classification report for the different Machine Learning classification algorithms (Decision Tree, Random Forest, KNN, Naïve Bayes and Gradient Boosting).

	Decision Tree			Random Forest			KNN		
	Precision	Recall	F1-score	Precision	Recall	F1-score	Precision	Recall	F1-score
Emphysema	1.00	0.50	0.67	0.33	0.33	0.33	0.27	0.50	0.35
Fibrosis	0.67	0.67	0.67	0.50	0.33	0.40	0.00	0.00	0.00
Healthy	0.60	0.75	0.67	0.56	0.62	0.59	0.25	0.12	0.17
Neoplasm	0.89	0.86	0.86	0.71	0.71	0.71	0.62	0.71	0.67
Pneumonia	0.33	0.40	0.36	0.20	0.20	0.20	0.33	0.20	0.25
Accuracy training			1.00			0.98			0.70
Accuracy testing			0.66			0.48			0.34
	Naïve Bayes			Gradient Boosting					
	Precision	Recall	F1-score	Precision	Recall	F1-score			
Emphysema	0.50	0.33	0.40	0.50	0.50	0.50			
Fibrosis	0.50	0.33	0.40	0.00	0.00	0.00			
Healthy	0.55	0.75	0.63	0.50	0.38	0.43			
Neoplasm	0.78	1.00	0.88	0.60	0.43	0.50			
Pneumonia	0.67	0.40	0.50	0.33	0.80	0.47			
Accuracy training			0.62			0.84			
Accuracy testing			0.62			0.45			

4. DISCUSION

This project evaluates the possible implementation of Machine Learning classification algorithms for classification of electrical impedance spectroscopy measures performed in lung tissue. Under normal conditions, the function of the lungs and structures of respiratory system is to facilitate gas exchange. Oxygen gets transported through the alveoli into the capillary network, where it can enter the arterial system. Different pathologies can affect to the respiratory system such as emphysema,

neoplasm, fibrosis or pneumonia. Each of these disorders have their own anatomical and histological changes, thus differences in bioimpedance values are expected (**Fig. 1**) [22].

In the previous studies [12], [13], [15], the authors discarded the frequencies below 15 kHz and above 307 kHz due to electrode and capacitive errors respectively. The electrode errors are produced due to the impedance of the electrode, which have a capacitive component. Given the unknown electrode impedance, the influence in the tissue is lower as higher is the value of the impedance parameter. The capacitive errors produced at high frequencies affect differently the tissues as the pathologic cells produce changes in the tissue, thus, varying the Xc of the tissue. The frequencies of 15 kHz and 307 kHz were the most discriminative ones according to the pair-wise Euclidean distance among groups [15]. In this present study, all the frequencies between the frequency range of 15 kHz to 307 kHz have been used for the implementation of the classification algorithms.

Results in **Fig. 1** show an increase in the mean impedance values in those tissues with higher air content, such as healthy lung tissue or emphysema, with respect to those tissues with a decrease in air content, such as neoplasm or fibrosis. Emphysema is characterized by a destruction of the alveoli walls [23] that increases the volume of air and decreases the presence of tissue. These pathological changes increase the module impedance. On the other hand, neoplasm is characterized by an increase in cell concentration as well as tissue vascularization [23] which lowers the module impedance.

For the application of the classification algorithms, the mean values of |Z| and PA for all the patients have been taken into consideration, discarding the resistance and reactance values to avoid dependency of the data. The learning problem consist on dividing the data into a training set and a test set. The percentage of splitting is not fixed and although it is usually to use 80% for training and 20% for testing it is not any fixed rule for this partition. Due to the relatively small data available in this application, the percentage for training have been decreased slightly to 75%, then the percentage for testing have been 25%. With the training data the algorithm is trained and learns a model to classify the data. The test data is used to check if the algorithm is able to generalize with never seen data, and thus, adapts well to the objective of the task [24].

To evaluate the performance of the algorithms implemented, the classification report for all the algorithms have been obtained. In the classification report the precision, the recall and the F1-score metrics are visualized. Precision indicates how many of the samples predicted as positive are truly positive (for example, how many of the samples predicted as neoplasm are actually neoplasm). This metric is important specially when no false positives are desired. On the other hand, the recall metric measures how many of the positive samples are captured by the positive predictions. The recall is specially used for avoiding false negatives. In our case it is especially important as false negatives have a direct impact in the rapid and correct diagnosis of patients. To complement the precision and recall metrics, the F1-score is defined as $2 * \frac{precision*recall}{precision+recall}$ [24].

The first algorithm implemented have been the Decision Tree. This algorithm is widely used due to its simplicity. It basically consists on learning a hierarchy of if/else questions that finally lead to a decision. The algorithm builds a hierarchical partition that is repeated until each of the classes are separated from each other. Although its easy implementation, this algorithm is prone to overfitting, a situation in which the algorithms adapts to the training set (high training set accuracy) but is not able to generalize (low training set accuracy) [24], [25]. This algorithm has a precision and a recall of 86% for neoplasm tissue and a recall of 75% for healthy samples. The accuracy of 100% for the training set and the accuracy of 66% for the test set may indicate the overfitting of the data (**Table 1**). However, this difference in accuracies can not be concluded to be due to overfitting, as it could be also due to the small number of samples for the test set, especially for fibrosis (n=3).

To address the possible condition of overfitting, and related to Decision Tree algorithm, Random Forest algorithm is also implemented. This algorithm consists on the implementation of multiple Decision Trees different one from the others that enables the creation of a more robust model than the Decision Tree algorithm. In addition, Random Forest is promoted to be one of the best classification algorithms [24], [25]. The number of Decision Trees applied to the Random Forest algorithm has been optimized (n=10) in order to obtain the best training and test sets accuracy. The higher recall and precision metrics have been obtained in neoplasm samples (71%) followed by healthy

tissue samples with a recall of 62% and a precision of 56%. The overall accuracy of the test set for the Random Forest algorithm obtained has been 48% (**Table 1**). Although this algorithm is promoted to be one of the best classification algorithms, for our data Decision Tree is more accurate. This is possible due to the fact that the number of samples available for training is relatively small (n=87 divided among neoplasm, fibrosis, pneumonia, healthy lung tissue and emphysema). Partitions of the training data into different groups, or different trees, may not be suitable for training the algorithm. It should be necessary to increase the number of samples for the implementation of this algorithm.

KNN algorithm has also been implemented. This algorithm classifies new data points according to the information of the K nearest neighbors. Then, the number of neighbors has been optimized (n=3) in order to obtain the best test accuracy. This algorithm obtains a recall of 71% and a precision of 62% for neoplasm samples. The overall accuracy of the test set obtained is 34% while in the training set the higher accuracy obtained have been 69% (**Table 1**). This algorithm seems not suitable for our data.

The next classification algorithm implemented have been the Naïve Bayes algorithm. There are three types of Naïve Bayes classifier, the Bernoulli, the Multinomial and the Gaussian. The last one is the one used for our application as it is the one used for continuous data while Bernoulli assumes data to be binary and Multinomial Naïve Bayes assumes count data. The principle of the Gaussian Naïve Bayes algorithm is that it makes predictions comparing each data point against the statistics (mean and standard deviation) of each of the classes for the best matching [24]. This algorithm has obtained a recall of 100% and a precision of 78% for neoplasm samples. The overall accuracy of the algorithm is 62% both, for the training and the test sets (**Table 1**).

Finally, the last algorithm implemented has been the Gradient Boosting. Similarly to the Random Forest algorithm, Gradient Boosting algorithm consists on building trees to a manner that each tree tries to solve the mistakes of the previous tree. The learning rate parameter, which controls how the tree corrects the mistakes of the previous tree, has been optimized (learning rate = 0.1) to obtain the higher accuracy in the test set while maintaining a high accuracy for the test set. The higher recall

13

obtained in this algorithm has been for pneumonia with an 80%. However, its precision has been 33%. The accuracy of the test set obtained has been 45% while the obtained for the training set has been 84% (**Table 1**).

In the previous study performed by Company-Se *et al.* [15] the authors did not find statistically significant differences between neoplasm and fibrosis. However, in this study, especially in the Naïve Bayes and the Decision Tree algorithms, confusion matrices (**Figure 2**) show that neoplasm samples are correctly identified and classified.

The sample size used for the application of the algorithms is 116, which is considered small for non-medical applications. However, for clinical applications, the number of samples seems adequate as compared with previous author's publications. In addition, the accuracy obtained is similar to previous clinical studies applying Machine Learning [17], [19]–[21].

The results are promising and have high clinical importance. Neoplasm and fibrosis are not statistically significant different, due to their similarities in the bioimpedance parameters values [15]. However, by using Machine Learning classification algorithms, the results show that no neoplasm sample would be diagnosed as fibrosis. Moreover, neoplasm samples are correctly classified, specially using the Naïve Bayes (7 out of 7 samples correctly classified) and the Decision tree (6 out of 7 samples correctly classified) algorithms. However, it is necessary to continue increasing the number of samples, both for training and testing, for improving classification accuracy for all the tissue types. For the moment, it seems that the more suitable algorithms for our data could be the Naïve Bayes and the Decision Tree algorithms.

CONTRIBUTION

The application of Machine Learning classification algorithms to minimally-invasive bioimpedance data of lung tissue is a complementary method to bronchoscopy procedure for real time tissue characterization through tissue classification.

LIMITATION

To validate the application of Machine Learning algorithm in minimally-invasive bioimpedance lung measurements as a method for real time tissue characterization, it is necessary to increase the sample size to train the algorithm more efficiently.

CONCLUSIONS

The application of Machine Learning classification algorithms are promising tools for the future of the medicine. They present an opportunity to help minimally-invasively in the diagnosis of diseases and in the real-time tissue characterization. In this study, promising results have been obtained by the possible classification and thus, differentiation, of neoplasm with respect to fibrosis, two pair tissue samples with similar impedance parameters values which no statistically significant differences between them. The authors believe that with an increase of the sample size the accuracy of the overall test set and the accuracy of each class will increase. In future studies the authors aim to increase the sample size of the bioimpedance database as well as to implement multiple classification algorithms to increase the classification accuracy and to continue evaluating the implementation of classification Machine Learning algorithms for real-time tissue differentiation using bioimpedance parameters.

DATA AVAILABILITY STATEMENT

The raw data supporting the conclusions of this article will be made available by the authors, without undue reservation.

ETHICS STATEMENT

Ethics approval was obtained from the "Hospital de la Santa Creu i Sant Pau" (CEIC-73/2020) according to principles of the Declaration of Helsinki for experiments with human being. All patients proved signed informed consent.

AUTHOR CONTRIBUTIONS

RB, VP, PR, JR, GC, AR and LN designed the experiments; GC, VP and AR performed the experiments; LN and GC performed the data processing, analyzed the data, drafted the manuscript and prepared the tables and figures. Finally, RB, VP, PR, JR, GC, AR and LN revised the paper and approved the final version of the manuscript.

REFERENCES

[1]   F. J. F. Herth, R. Eberhardt, H. D. Becker, and A. Ernst, 'Endobronchial ultrasound-guided transbronchial lung biopsy in fluoroscopically invisible solitary pulmonary nodules: a prospective trial.', *Chest*, vol. 129, no. 1, pp. 147–150, Jan. 2006, doi: 10.1378/chest.129.1.147.

[2]   E. E. Folch *et al.*, 'Electromagnetic Navigation Bronchoscopy for Peripheral Pulmonary Lesions: One-Year Results of the Prospective, Multicenter NAVIGATE Study', *J. Thorac. Oncol.*, vol. 14, no. 3, pp. 445–458, Mar. 2019, doi: 10.1016/j.jtho.2018.11.013.

[3]   H. C. Lukaski, 'Biological indexes considered in the derivation of the bioelectrical impedance analysis', *Am. J. Clin. Nutr.*, vol. 64, no. 3, pp. 397S-404S, Sep. 1996, doi: 10.1093/ajcn/64.3.397S.

[4]   H. C. Lukaski, N. Vega Diaz, A. Talluri, and L. Nescolarde, 'Classification of Hydration in Clinical Conditions: Indirect and Direct Approaches Using Bioimpedance', *Nutrients*, vol. 11, no. 4, p. 809, Apr. 2019, doi: 10.3390/nu11040809.

[5]   S. Khalil, M. Mohktar, and F. Ibrahim, 'The Theory and Fundamentals of Bioimpedance Analysis in Clinical Status Monitoring and Diagnosis of Diseases', *Sensors*, vol. 14, no. 6, pp. 10895–10928, Jun. 2014, doi: 10.3390/s140610895.

[6]   S. Toso *et al.*, 'Altered Tissue Electric Properties in Lung Cancer Patients as Detected by Bioelectric Impedance Vector Analysis', p. 5.

[7]   E. M. Baarends, W. D. Van Marken Lichtenbelt, E. F. M. Wouters, and A. M. W. J. Schols, 'Body-water compartments measured by bio-electrical impedance spectroscopy in patients with chronic obstructive pulmonary disease', *Clin. Nutr.*, vol. 17, no. 1, pp. 15–22, Feb. 1998, doi: 10.1016/S0261-5614(98)80038-1.

[8]   D. Meroni, D. Bovio, P. A. Frisoli, and A. Aliverti, 'Measurement of electrical impedance in different ex-vivo tissues', in *2016 38th Annual International Conference of the IEEE Engineering in Medicine and Biology Society (EMBC)*, Orlando, FL, USA: IEEE, Aug. 2016, pp. 2311–2314. doi: 10.1109/EMBC.2016.7591192.

[9]   B. Sanchez *et al.*, 'In vivo electrical bioimpedance characterization of human lung tissue during the bronchoscopy procedure. A feasibility study', *Med. Eng. Phys.*, vol. 35, no. 7, pp. 949–957, Jul. 2013, doi: 10.1016/j.medengphy.2012.09.004.

[10] N. C. Guich, R. B. Bardia, A. M. Muñoz-Fernández, V. P. Ruiz, A. Torrego, and P. J. R. Costa, 'Espectrometría de impedancia eléctrica en tejido pulmonar', p. 4, 2016.

[11] P. J. Riu, G. Company, R. Bragos, J. Rosell, V. Pajares, and A. Torrego, 'Minimally Invasive Real-Time Electrical Impedance Spectroscopy Diagnostic Tool for Lung Parenchyma Pathologies', in *2020 42nd Annual International Conference of the IEEE Engineering in Medicine & Biology Society (EMBC)*, Montreal, QC, Canada: IEEE, Jul. 2020, pp. 5077–5080. doi: 10.1109/EMBC44109.2020.9175860.

[12] G. Company-Se *et al.*, 'Minimally Invasive Lung Tissue Differentiation Using Electrical Impedance Spectroscopy: A Comparison of the 3- and 4-Electrode Methods', *IEEE Access*, vol. 10, pp. 7354–7367, 2022, doi: 10.1109/ACCESS.2021.3139223.

[13] G. Company-Se *et al.*, 'Effect of Calibration for Tissue Differentiation Between Healthy and Neoplasm Lung Using Minimally Invasive Electrical Impedance Spectroscopy', *IEEE Access*, vol. 10, pp. 103150–103163, 2022, doi: 10.1109/ACCESS.2022.3209809.

[14] G. Amorós-Figueras *et al.*, 'Endocardial infarct scar recognition by myocardial electrical impedance is not influenced by changes in cardiac activation sequence', *Heart Rhythm*, vol. 15, no. 4, pp. 589–596, Apr. 2018, doi: 10.1016/j.hrthm.2017.11.031.

[15] G. Company-Se *et al.*, 'Differentiation Using Minimally-Invasive Bioimpedance Measurements of Healthy and Pathological Lung Tissue through Bronchoscopy', *Front. Med.*, 2023, doi: 10.3389/fmed.2023.1108237.

[16] M. May, 'Eight ways machine learning is assisting medicine', *Nat. Med.*, vol. 27, no. 1, pp. 2–3, Jan. 2021, doi: 10.1038/s41591-020-01197-2.

[17] K. R. V *et al.*, 'Machine learning detects EEG microstate alterations in patients living with temporal lobe epilepsy', *Seizure*, vol. 61, pp. 8–13, Oct. 2018, doi: 10.1016/j.seizure.2018.07.007.

[18] M. Cikes *et al.*, 'Machine learning-based phenogrouping in heart failure to identify responders to cardiac resynchronization therapy', *Eur. J. Heart Fail.*, vol. 21, pp. 74–85, 2019, doi: 10.1002/ejhf.1333.

[19] G. S. Chilla, L. Y. Yeow, Q. H. Chew, K. Sim, and K. N. B. Prakash, 'Machine learning classification of schizophrenia patients and healthy controls using diverse neuroanatomical markers and Ensemble methods', *Sci. Rep.*, vol. 12, no. 1, p. 2755, Feb. 2022, doi: 10.1038/s41598-022-06651-4.

[20] L. Papp *et al.*, 'Supervised machine learning enables non-invasive lesion characterization in primary prostate cancer with [68Ga]Ga-PSMA-11 PET/MRI', *Eur. J. Nucl. Med. Mol. Imaging*, vol. 48, no. 6, pp. 1795–1805, Jun. 2021, doi: 10.1007/s00259-020-05140-y.

[21] S. Rastegar *et al.*, 'Radiomics for classification of bone mineral loss: A machine learning study', *Diagn. Interv. Imaging*, vol. 101, no. 9, pp. 599–610, Sep. 2020, doi: 10.1016/j.diii.2020.01.008.

[22] S. E. Weinberger, B. A. Cockrill, and J. Mandel, *Principles of pulmonary medicine*, 7th ed. Elsevier, 2019.

[23] G. D. Hammer and S. J. McPhee, *Pathophysiology of disease, an introduction to clinical medicine*, Eight. McGraw-Hill Education.

[24] A. C. Müller and S. Guido, *Introduction to Machine Learning with Python, A Guide for Data Scientists*, First. United States of America: O'Reilly Media, 2017.

[25] R. C. Deo, 'Machine Learning in Medicine', *Circulation*, vol. 132, no. 20, pp. 1920–1930, Nov. 2015, doi: 10.1161/CIRCULATIONAHA.115.001593.

CHAPTER 6: DISCUSSION AND CONCLUSIONS

This thesis, initiated in the frame of the research project: Z-LUNG (RTI2018-098116-B-C21) aimed to study bioimpedance differences in lung tissue according to its state. Four pathologies, with different mechanisms from each other were included in the study: lung neoplasm, fibrosis, pneumonia and emphysema. In addition, healthy lung tissue was also included.

Before performing all the measurements to accomplish the main objective of the thesis, a prior study was performed. Preliminary measurements were taken to study the most efficient way to acquire the EIS measurements; with the 4-electrode method or with the 3-electrode method. The first method had been used in the previous studies performed by Sanchez et al. [51], Coll *et al.* [28] and Riu *et. al* [52] while the second had been used for cardiac applications by Amorós *et al.* [50] both methods with good tissue differentiation for their applications. The first article of the thesis (Chapter 2) shows the study of the comparison between the 4-electrode method and the 3-electrode method using minimally-invasive lung bioimpedance measurements for the differentiation between healthy lung tissue and bronchi. Although both methods show high statistically significant differences between tissues ($P < 0.001$) the Fisher Coefficient showed higher values for |Z| and Xc in the 4-electrode method while the value in PA parameter was higher in the 3-electrode method. The value of the coefficient for R was similar between both methods. Furthermore, during bronchoscopy patients cough and move so the acquisition of the measurements using the 4-electrode method present higher difficulties than the 3-electrode method. Due to the similarity in the tissue differentiation, the authors then decided to change from the 4-electrode method to the 3-electrode method for the EIS measurements acquisition. This also simplifies the operation and reduces the cost of the catheters.

During the acquisition of the measurements, an intermediate study was performed with the objective of deciding if calibrating the data to reduce the patient geometry effects would increase tissue differentiation or not. In this study (Chapter 3) two analysis were performed: 1) Study if there were statistically significant differences between smoker, non-smoker and ex-smoker people and 2) study if calibration increase tissue differentiation by differentiating calibrated and non-calibrated data between healthy lung

tissue and neoplasm. No significant differences ($P > 0.05$) were found related to the smoking condition meaning that this condition should not influence the tissue differentiation. Regarding the tissue differentiation between healthy and neoplasm lung tissue statistically significant differences ($P < 0.001$) ere found in |Z|, PA, R and Xc both in the calibrated and the non-calibrated data. However, the statistic of the tests was higher in the calibrated data. Calibration demonstrated to reduce data variability and increase tissue state separation capability. For this reason, calibration has been implemented in the third study (Chapter 4) as more pathologies with similar mechanisms from each other have been included.

In the third study (Chapter 4) the differentiation using bioimpedance measurements among neoplasm, fibrosis, pneumonia, healthy lung tissue and emphysema was performed. Data was acquired using the 3-electrode method according to Chapter 2 and calibrated according to Chapter 3. The two most discriminative frequencies (15 kHz for |Z| and R and 307 kHz for PA and Xc) were selected to perform the tissue differentiation. Statistically significant differences for all the parameters between: neoplasm and pneumonia ($P < 0.05$); neoplasm and healthy lung tissue ($P < 0.001$); neoplasm and emphysema ($P < 0.001$); fibrosis and healthy lung tissue ($P \leq 0.001$) and pneumonia and healthy lung tissue ($P < 0.01$) were found. For fibrosis and emphysema ($P < 0.05$) only in |Z|, R and Xc; and between pneumonia and emphysema ($P < 0.05$) only in |Z| and R. No statistically significant differences ($P > 0.05$) were found between neoplasm and fibrosis; fibrosis and pneumonia; and between healthy lung tissue and emphysema. In general, the study showed differences between those pathologies that lead to tissue increase and inflammation of cells (neoplasm, fibrosis and pneumonia) and those pathologies that lead to destruction of alveolar septa (emphysema).

Finally, in the last study (Chapter 5) different Machine Learning algorithms have been applied to the bioimpedance measurements for the classification amount the different types of tissue included in the studies. Despite taking into account that the main limitation for the application of the classification algorithms have been the small sample size (specially for fibrosis), the algorithms have been optimized through parameter tuning and grid search to obtain the best accuracy and also avoid as much as possible overfitting. Although some algorithms provide better performance than others (as discussed in Chapter 5), the most relevant result is that the classification capacity of the algorithms

por the neoplasm samples is high. With classic statistical methods, there was not statistical difference between neoplasm and fibrosis. However, using Machine Learning, the algorithms were capable of classify neoplasm samples with high accuracy. This could, with further validation and training of the algorithms, provide a real-time electronic biopsy to help clinicians in the correct sample location of biopsies during bronchoscopies.

The different studies performed go towards the implementation of EIS measurements for real-time tissue characterization to complement the actual methods of diagnostic (chest CT, PET/CT or virtual bronchoscopy). Although the actual diagnosis method do not allow real time guidance for sample collection, advanced bronchoscopic techniques have been developed for a few years, such as the radial probe endobronchial ultrasound (radial EBUS) or electromagnetic navigation bronchoscopy (ENB). The high-cost of the new techniques makes its availability difficult in the Interventional Pulmonology units so EIS measurements could be a low economic cost alternative.

Although positive results have been obtained in the study, it is also important to remark the limitations and difficulties encountered during the project. The main limitation, has been the pandemic of Covid-19. The study was initiated in January of 2020 and it was not possible to go to the hospital before the lockdown. After the lockdown we went for 2 weeks to the hospital between Covid-19 waves and managed to performed the preliminary measurements from Chapter 2. It was not until November of 2021 when the measurement campaign started. Having started earlier, the sample size would be higher, specially those pathologies with lower incidence in the population such as fibrosis. However, we have managed to study tissue differences. With an increase in the sample size the algorithms of machine learning could be trained and tested better.

Finally, it is important to comment that the title of the thesis is: "Temporal and frequency differentiation of healthy and pathological lung tissue through minimally invasive electrical impedance spectroscopy". However, any temporal tool has been applied for the moment. The initial hypothesis was that according to tissue state the amplitude of the EIS bioimpedance time signal would change due to respiratory modulation (as presented in the International Conference of Bioelectromagnetism, Electrical Bioimpedance and Electrical Impedance Tomography 2022 (Annex 2)). As also remarked in the Chapter 2, during bronchoscopy patients cough and move although some patients move more and some patients move less. The high movement artifacts and the higher differences in the

respiratory patterns (some patients cough, some produced apneas…) make not possible to implement temporal tools as differences in amplitude did not showed the real state of the tissue. For this reason, a second project has been initiated called ELUNG "Biopsia Pulmonar Electrónica Guiada por Broncoscopia de Navegación Electromagnética" (PID2021-128602OB-C21). During Electromagnetic navigation patients are anaesthetized so the movements produced during bronchoscopy will be eliminated and temporal analysis will be able to be performed.

In conclusion, tissue differentiation has been performed with positive results. The implementation of this technique to complement the actual methods of diagnosis needs further validation by increasing the sample size and training the machine learning algorithms. However, EIS bioimpedance measurements performed with 3-electrode method and calibrated according to Chapter 3 have demonstrated to discriminate between several lung pathologies.

REFERENCES

[1] S. M. Levine and D. D. Marciniuk, 'Global Impact of Respiratory Disease', *Chest*, vol. 161, no. 5, pp. 1153–1154, May 2022, doi: 10.1016/j.chest.2022.01.014.

[2] T. M. Dempsey and P. D. Scanlon, 'Pulmonary Function Tests for the Generalist: A Brief Review.', *Mayo Clin. Proc.*, vol. 93, no. 6, pp. 763–771, Jun. 2018, doi: 10.1016/j.mayocp.2018.04.009.

[3] M. Silva, G. Milanese, V. Seletti, A. Ariani, and N. Sverzellati, 'Pulmonary quantitative CT imaging in focal and diffuse disease: current research and clinical applications.', *Br. J. Radiol.*, vol. 91, no. 1083, p. 20170644, Feb. 2018, doi: 10.1259/bjr.20170644.

[4] S. Candemir and S. Antani, 'A review on lung boundary detection in chest X-rays.', *Int. J. Comput. Assist. Radiol. Surg.*, vol. 14, no. 4, pp. 563–576, Apr. 2019, doi: 10.1007/s11548-019-01917-1.

[5] A. Mouton, R. D. Pitcher, and T. S. Douglas, 'Computer-aided detection of pulmonary pathology in pediatric chest radiographs.', *Med. Image Comput. Comput.-Assist. Interv. MICCAI Int. Conf. Med. Image Comput. Comput.-Assist. Interv.*, vol. 13, no. Pt 3, pp. 619–625, 2010, doi: 10.1007/978-3-642-15711-0_77.

[6] J. Dimastromatteo, E. J. Charles, and V. E. Laubach, 'Molecular imaging of pulmonary diseases.', *Respir. Res.*, vol. 19, no. 1, p. 17, Jan. 2018, doi: 10.1186/s12931-018-0716-0.

[7] E. A. Kazerooni, 'High-Resolution CT of the Lungs', *Am. J. Roentgenol.*, vol. 177, no. 3, pp. 501–519, Sep. 2001, doi: 10.2214/ajr.177.3.1770501.

[8] F. G. Meinel *et al.*, 'Diagnosing and Mapping Pulmonary Emphysema on X-Ray Projection Images: Incremental Value of Grating-Based X-Ray Dark-Field Imaging', *PLOS ONE*, vol. 8, no. 3, pp. 1–9, Mar. 2013, doi: 10.1371/journal.pone.0059526.

[9] D. E. Ost *et al.*, 'Diagnostic Yield and Complications of Bronchoscopy for Peripheral Lung Lesions. Results of the AQuIRE Registry.', *Am. J. Respir. Crit. Care Med.*, vol. 193, no. 1, pp. 68–77, Jan. 2016, doi: 10.1164/rccm.201507-1332OC.

[10] J. S. Wang Memoli, P. J. Nietert, and G. A. Silvestri, 'Meta-analysis of guided bronchoscopy for the evaluation of the pulmonary nodule.', *Chest*, vol. 142, no. 2, pp. 385–393, Aug. 2012, doi: 10.1378/chest.11-1764.

[11] S. Grimnes, *Bioimpedance and bioelectricity basics*. Boston, MA: Elsevier, 2014.

[12] P. L. Shah, F. J. Herth, Y. G. Lee, and G. J. Criner, *Essentials of Clinical Pulmonology*. CRC Press, 2020.

[13] D. S. Zander and C. F. Farver, *Pulmonary Pathology: a volume in the series Foundations in diagnoistic pathology*. Churchill Livingstone Elsevier.

[14] S. E. Weinberger, B. A. Cockrill, and J. Mandel, *Principles of pulmonary medicine*, 7th ed. Elsevier, 2019.

[15] G. D. Hammer and S. J. McPhee, *Pathophysiology of disease, an introduction to clinical medicine*, Eight. McGraw-Hill Education.

[16] J. Sauleda, B. Núñez, E. Sala, and J. Soriano, 'Idiopathic Pulmonary Fibrosis: Epidemiology, Natural History, Phenotypes', *Med. Sci.*, vol. 6, no. 4, p. 110, Nov. 2018, doi: 10.3390/medsci6040110.

[17] K. C. Meyer and S. D. Nathan, Eds., *Idiopathic Pulmonary Fibrosis: A Comprehensive Clinical Guide*. in Respiratory Medicine. Cham: Springer International Publishing, 2019. doi: 10.1007/978-3-319-99975-3.

[18] *Introduction to Bronchoscopy*, 2nd ed. Cambridge University Press, 2017. doi: 10.1017/9781316084182.

[19] M. Mondoni *et al.*, 'Bronchoscopic sampling techniques in the era of technological bronchoscopy', *Pulmonology*, vol. 28, no. 6, pp. 461–471, Nov. 2022, doi: 10.1016/j.pulmoe.2020.06.007.

[20] P. Mazzone, P. Jain, A. C. Arroliga, and R. A. Matthay, 'Bronchoscopy and needle biopsy techniques for diagnosis and staging of lung cancer', *Clin. Chest Med.*, vol. 23, no. 1, pp. 137–158, Mar. 2002, doi: 10.1016/S0272-5231(03)00065-0.

[21] S. Khalil, M. Mohktar, and F. Ibrahim, 'The Theory and Fundamentals of Bioimpedance Analysis in Clinical Status Monitoring and Diagnosis of Diseases', *Sensors*, vol. 14, no. 6, pp. 10895–10928, Jun. 2014, doi: 10.3390/s140610895.

[22] G. Martinsen, S. Grimnes, and H. P. Schwan, 'INTERFACE PHENOMENA AND DIELECTRIC PROPERTIES OF BIOLOGICAL TISSUE', 2002.

[23] R. Pethig and D. B. Kell, 'The passive electrical properties of biological systems: their significance in physiology, biophysics and biotechnology', *Phys. Med. Biol.*, vol. 32, no. 8, pp. 933–970, Aug. 1987, doi: 10.1088/0031-9155/32/8/001.

[24] H. P. Schwan, 'Electrical properties of tissues and cell suspensions: mechanisms and models', in *Proceedings of 16th Annual International Conference of the IEEE*

Engineering in Medicine and Biology Society, Baltimore, MD, USA: IEEE, 1994, pp. A70–A71. doi: 10.1109/IEMBS.1994.412155.

[25] M. Ibrani, L. Ahma, and E. Hamiti, 'The Age-Dependence of Microwave Dielectric Parameters of Biological Tissues', in *Microwave Materials Characterization*, S. Costanzo, Ed., InTech, 2012. doi: 10.5772/51400.

[26] H. C. Lukaski, 'Biological indexes considered in the derivation of the bioelectrical impedance analysis', *Am. J. Clin. Nutr.*, vol. 64, no. 3, pp. 397S-404S, Sep. 1996, doi: 10.1093/ajcn/64.3.397S.

[27] H. C. Lukaski, N. Vega Diaz, A. Talluri, and L. Nescolarde, 'Classification of Hydration in Clinical Conditions: Indirect and Direct Approaches Using Bioimpedance', *Nutrients*, vol. 11, no. 4, p. 809, Apr. 2019, doi: 10.3390/nu11040809.

[28] N. C. Guich, R. B. Bardia, A. M. Muñoz-Fernández, V. P. Ruiz, A. Torrego, and P. J. R. Costa, 'Espectrometría de impedancia eléctrica en tejido pulmonar', p. 4, 2016.

[29] K. S. Cole and R. H. Cole, 'Dispersion and Absorption in Dielectrics I. Alternating Current Characteristics', *J. Chem. Phys.*, vol. 9, no. 4, pp. 341–351, Dec. 2004, doi: 10.1063/1.1750906.

[30] D. A. Dean, T. Ramanathan, D. Machado, and R. Sundararajan, 'Electrical Impedance Spectroscopy Study of Biological Tissues.', *J. Electrost.*, vol. 66, no. 3–4, pp. 165–177, Mar. 2008, doi: 10.1016/j.elstat.2007.11.005.

[31] P. Héroux and M. Bourdages, 'Monitoring living tissues by electrical impedance spectroscopy.', *Ann. Biomed. Eng.*, vol. 22, no. 3, pp. 328–337, Jun. 1994, doi: 10.1007/BF02368239.

[32] J. Estrela da Silva, J. P. Marques de Sá, and J. Jossinet, 'Classification of breast tissue by electrical impedance spectroscopy', *Med. Biol. Eng. Comput.*, vol. 38, no. 1, pp. 26–30, Jan. 2000, doi: 10.1007/BF02344684.

[33] K. Yoon *et al.*, 'Electrical impedance spectroscopy and diagnosis of tendinitis.', *Physiol. Meas.*, vol. 31, no. 2, pp. 171–182, Feb. 2010, doi: 10.1088/0967-3334/31/2/004.

[34] E. Gersing, 'Impedance spectroscopy on living tissue for determination of the state of organs', *Bioelectrochem. Bioenerg.*, vol. 45, no. 2, pp. 145–149, 1998, doi: https://doi.org/10.1016/S0302-4598(98)00079-8.

[35]   F. Mellert *et al.*, 'Detection of (reversible) myocardial ischemic injury by means of electrical bioimpedance.', *IEEE Trans. Biomed. Eng.*, vol. 58, no. 6, pp. 1511–1518, Jun. 2011, doi: 10.1109/TBME.2010.2054090.

[36]   S. Kun, B. Ristić, R. A. Peura, and R. M. Dunn, 'Algorithm for tissue ischemia estimation based on electrical impedance spectroscopy.', *IEEE Trans. Biomed. Eng.*, vol. 50, no. 12, pp. 1352–1359, Dec. 2003, doi: 10.1109/TBME.2003.819846.

[37]   C. Skourou, P. J. Hoopes, R. R. Strawbridge, and K. D. Paulsen, 'Feasibility studies of electrical impedance spectroscopy for early tumor detection in rats.', *Physiol. Meas.*, vol. 25, no. 1, pp. 335–346, Feb. 2004, doi: 10.1088/0967-3334/25/1/037.

[38]   R. J. Halter, A. Hartov, J. A. Heaney, K. D. Paulsen, and A. R. Schned, 'Electrical impedance spectroscopy of the human prostate.', *IEEE Trans. Biomed. Eng.*, vol. 54, no. 7, pp. 1321–1327, Jul. 2007, doi: 10.1109/TBME.2007.897331.

[39]   V. S. Teixeira, T. Barth, V. Labitzky, U. Schumacher, and W. Krautschneider, 'Electrical Impedance Spectroscopy for Characterization of Prostate PC-3 and DU 145 Cancer Cells.', *Annu. Int. Conf. IEEE Eng. Med. Biol. Soc. IEEE Eng. Med. Biol. Soc. Annu. Int. Conf.*, vol. 2019, pp. 6485–6489, Jul. 2019, doi: 10.1109/EMBC.2019.8856627.

[40]   W. Homola, T. Fuchs, P. Baranski, A. Zimmer, M. Zimmer, and M. Pomorski, 'Use of electrical impedance spectroscopy as an adjunct to colposcopy in a pathway of cervical intraepithelial neoplasia diagnostics.', *Ginekol. Pol.*, vol. 90, no. 11, pp. 628–632, 2019, doi: 10.5603/GP.2019.0107.

[41]   J. A. Tidy *et al.*, 'Accuracy of detection of high-grade cervical intraepithelial neoplasia using electrical impedance spectroscopy with colposcopy.', *BJOG Int. J. Obstet. Gynaecol.*, vol. 120, no. 4, pp. 400–10; discussion 410-411, Mar. 2013, doi: 10.1111/1471-0528.12096.

[42]   S. L. Hillary, B. H. Brown, N. J. Brown, and S. P. Balasubramanian, 'Use of Electrical Impedance Spectroscopy for Intraoperative Tissue Differentiation During Thyroid and Parathyroid Surgery.', *World J. Surg.*, vol. 44, no. 2, pp. 479–485, Feb. 2020, doi: 10.1007/s00268-019-05169-7.

[43]   S. P. Desai, A. Coston, and A. Berlin, 'Micro-Electrical Impedance Spectroscopy and Identification of Patient-Derived, Dissociated Tumor Cells.', *IEEE Trans.*

Nanobioscience, vol. 18, no. 3, pp. 369–372, Jul. 2019, doi: 10.1109/TNB.2019.2920743.

[44]   S. Gabriel, R. W. Lau, and C. Gabriel, 'The dielectric properties of biological tissues: III. Parametric models for the dielectric spectrum of tissues', *Phys. Med. Biol.*, vol. 41, no. 11, p. 2271, Nov. 1996, doi: 10.1088/0031-9155/41/11/003.

[45]   S. Toso *et al.*, 'Altered Tissue Electric Properties in Lung Cancer Patients as Detected by Bioelectric Impedance Vector Analysis', p. 5.

[46]   D. M. Nierman, D. I. Eisen, E. D. Fein, E. Hannon, J. I. Mechanick, and E. Benjamin, 'Transthoracic bioimpedance can measure extravascular lung water in acute lung injury.', *J. Surg. Res.*, vol. 65, no. 2, pp. 101–108, Oct. 1996, doi: 10.1006/jsre.1996.0350.

[47]   J. Orschulik, N. Hochhausen, S. A. Santos, M. Czaplik, S. Leonhardt, and M. Walter, 'Detection of Acute Respiratory Distress Syndrome using Sectoral Bioimpedance Spectroscopy – a Pilot Study', p. 4, doi: 10.18154/RWTH-CONV-224905.

[48]   E. Jorge, G. Amorós-Figueras, T. García-Sánchez, R. Bragós, J. Rosell-Ferrer, and J. Cinca, 'Early detection of acute transmural myocardial ischemia by the phasic systolic-diastolic changes of local tissue electrical impedance', *Am. J. Physiol.-Heart Circ. Physiol.*, vol. 310, no. 3, pp. H436–H443, Feb. 2016, doi: 10.1152/ajpheart.00754.2015.

[49]   G. Amorós-Figueras, E. Jorge, T. García-Sánchez, R. Bragós, J. Rosell-Ferrer, and J. Cinca, 'Recognition of Fibrotic Infarct Density by the Pattern of Local Systolic-Diastolic Myocardial Electrical Impedance', *Front. Physiol.*, vol. 7, Aug. 2016, doi: 10.3389/fphys.2016.00389.

[50]   G. Amorós-Figueras *et al.*, 'Endocardial infarct scar recognition by myocardial electrical impedance is not influenced by changes in cardiac activation sequence', *Heart Rhythm*, vol. 15, no. 4, pp. 589–596, Apr. 2018, doi: 10.1016/j.hrthm.2017.11.031.

[51]   B. Sanchez *et al.*, 'In vivo electrical bioimpedance characterization of human lung tissue during the bronchoscopy procedure. A feasibility study', *Med. Eng. Phys.*, vol. 35, no. 7, pp. 949–957, Jul. 2013, doi: 10.1016/j.medengphy.2012.09.004.

[52]   P. J. Riu, G. Company, R. Bragos, J. Rosell, V. Pajares, and A. Torrego, 'Minimally Invasive Real-Time Electrical Impedance Spectroscopy Diagnostic Tool

for Lung Parenchyma Pathologies', in *2020 42nd Annual International Conference of the IEEE Engineering in Medicine & Biology Society (EMBC)*, Montreal, QC, Canada: IEEE, Jul. 2020, pp. 5077–5080. doi: 10.1109/EMBC44109.2020.9175860.

[53]   M. May, 'Eight ways machine learning is assisting medicine', *Nat. Med.*, vol. 27, no. 1, pp. 2–3, Jan. 2021, doi: 10.1038/s41591-020-01197-2.

[54]   A. C. Müller and S. Guido, *Introduction to Machine Learning with Python, A Guide for Data Scientists*, First. United States of America: O'Reilly Media, 2017.

[55]   R. C. Deo, 'Machine Learning in Medicine', *Circulation*, vol. 132, no. 20, pp. 1920–1930, Nov. 2015, doi: 10.1161/CIRCULATIONAHA.115.001593.

[56]   S. Dinç and R. S. Aygün, 'Evaluation of Hyperspectral Image Classification Using Random Forest and Fukunaga-Koontz Transform', in *Machine Learning and Data Mining in Pattern Recognition*, P. Perner, Ed., in Lecture Notes in Computer Science, vol. 7988. Berlin, Heidelberg: Springer Berlin Heidelberg, 2013, pp. 234–245. doi: 10.1007/978-3-642-39712-7_18.

[57]   S. Zeadally, E. Adi, Z. Baig, and I. A. Khan, 'Harnessing Artificial Intelligence Capabilities to Improve Cybersecurity', *IEEE Access*, vol. 8, pp. 23817–23837, 2020, doi: 10.1109/ACCESS.2020.2968045.

[58]   G. Amorós-Figueras *et al.*, 'Electrophysiological and histological characterization of atrial scarring in a model of isolated atrial myocardial infarction.', *Front. Physiol.*, vol. 13, p. 1104327, 2022, doi: 10.3389/fphys.2022.1104327.

[59]   G. Amoros-Figueras *et al.*, 'A closed-chest model of selective atrial myocardial infarction for the study of induced electrophysiological and structural derangements', *Eur. Heart J.*, vol. 43, no. Supplement_2, Oct. 2022, doi: 10.1093/eurheartj/ehac544.2907.

[60]   G. Amoros-Figueras *et al.*, 'Real-time electrophysiological characterization of acute and chronic radiofrequency ablation lesions', *Eur. Heart J.*, vol. 43, no. Supplement_2, Oct. 2022, doi: 10.1093/eurheartj/ehac544.2972.

ANNEX 1

CONFERENCE PAPERS DERIVED FROM THE THESIS

TITLE: "Aplicación de un algoritmo de inteligencia artificial en datos de espectroscopia de impedancia eléctrica para la clasificación de tejidos pulmonares".

AUTHORS: Albert Rafecas Codern, Georgina Company Se, Lexa Nescolarde, Virginia Pajares Ruiz, Alfons Torrego Fernández, Javier Rosell Ferrer, Pere J. Riu Costa, Ramon Bragós Bardia.

CONFERENCE: 56° Congreso Nacional de la Sociedad Española de Neumología y Cirugía Torácica (SEPAR)

YEAR: 2023

TITLE: Relaxation differences using EIS through bronchoscopy of healthy and pathological lung tissue

AUTHORS: Georgina Company-Se, Lexa Nescolarde, Virginia Pajares, Alfons Torrego, Albert Rafecas, Javier Rosell, Pere J. Riu, and Ramon Bragós

CONFERENCE: 45th Annual International Conference of the IEEE Engineering in Medicine and Biology Society

YEAR:2023

TITLE: Using Temporal Electrical Impedance Spectroscopy Measures to Differentiate Lung Pathologies with the 3-Electrode Method

AUTHORS: Georgina Company-Se, Lexa Nescolarde, Javier Rosell, Pere J. Riu, Virginia Pajares, Alfons Torrego and Ramon Bragós

CONFERENCE: Proceedings of the International Conference of Bioelectromagnetism, Electrical Bioimpedance and Electrical Impedance Tomography.

YEAR: 2022

TITLE: "Viabilidad de la Medición de la Impedáncia Eléctrica Pulmonar Mediante Broncoscopia".

AUTHORS: Albert Rafecas Codern, Georgina Company Se, Esther Palonés Femenia, Lexa Nescolarde Selva, Alfons Torrego Fernández, Javier Rosell Ferrer, Virginia Pajares Ruiz, Pere J. Riu Costa, Marta Navarro Colom, Ramon Bragós Bardia

CONFERENCE: 55° Congreso Nacional de la Sociedad Española de Neumología y Cirugía Torácica (SEPAR)

YEAR: 2022

CONFERENCE PAPERS AND ARTICLES NON-DIRECTLY DERIVED FROM THE THESIS

TITLE: Electrophysiological and histological characterization of atrial scarring in a model of isolated atrial myocardial infarction [58].

AUTHORS: Gerard Amorós-Figueras, Sergi Casabella-Ramon, Georgina Company-Se, Dabit Arzamendi, Esther Jorge, Alvaro Garcia-Osuna, Yolanda Macías, Damián Sánchez-Quintana, Javier Rosell-Ferrer, José M. Guerra and Juan Cinca

JOURNAL: Frontiers in Physiology

DOI: 10.3389/fphys.2022.1104327

YEAR: 2022

TITLE: A closed-chest model of selective atrial myocardial infarction for the study of induced electrophysiological and structural derangements [59].

AUTHORS: G. Amoros-Figueras, S. Casabella, G. Company, D. Arzamendi, Y. Macias, E. Jorge, D. Sanchez-Quintana, J. Rosell-Ferrer, J.M. Guerra, J. Cinca

JOURNAL: European Heart Journal

DOI: https://doi.org/10.1093/eurheartj/ehac544.2907

YEAR: 2022

TITLE: Real-time electrophysiological characterization of acute and chronic radiofrequency ablation lesions [60]

AUTHORS: G. Amoros-Figueras, S. Casabella, Z. Moreno-Weidmann, G. Company, E. Jorge, J. Rosell-Ferrer, J. Cinca, J.M. Guerra

JOURNAL: European Heart Journal

DOI: https://doi.org/10.1093/eurheartj/ehac544.2972

YEAR: 2022

TITLE: Minimally-Invasive Real-Time Electrical Impedance Spectroscopy Diagnostic Tool for Lung Parenchyma Pathologies [52].

AUTHORS: Pere J Riu, Georgina Company, Ramon Bragós, Javier Rosell, Virginia Pajares and Alfons Torrego

CONFERENCE: 42nd Annual International Conference IEEE Engineering in Medicine and Biology Society

DOI: 10.1109/EMBC44109.2020.9175860

YEAR: 2020

ANNEX 2: Using temporal electrical impedance spectroscopy measures to differentiate lung pathologies with the 3-electrode method

Title: Using temporal electrical impedance spectroscopy measures to differentiate lung pathologies with the 3-electrode method

Authors: Georgina Company-Se, Lexa Nescolarde, Javier Rosell, Pere J. Riu, Virginia Pajares, Alfons Torrego and Ramon Bragós

Congress: International Conference of Bioelectromagnetism, Electrical Bioimpedance, and Electrical Impedance Tomography 2022

Using temporal electrical impedance spectroscopy measures to differentiate lung pathologies with the 3-electrode method

Georgina Company-Se[1], Lexa Nescolarde[1], Javier Rosell[1], Pere J. Riu[1], Virginia Pajares[2], Alfons Torrego[2] and Ramon Bragós[1]

[1]Department of electronic engineering, Universitat Politècnica de Catalunya, Barcelona, Spain
[2]Department of Respiratory Medicine, Hospital de la Santa Creu i Sant Pau, Barcelona, Spain

Correspondence: Georgina Company-Se, e-mail: georgina.company@upc.edu

Abstract– Minimally invasive lung bioimpedance measurements could serve in the future diagnosis of lung pathologies complementing biopsies and imaging techniques. Through the electrical impedance spectroscopy (EIS) technique using the 3-electrode method, distinction of lung pathologies could be possible depending on the state of the tissue. Since now, only averaged information has been used for the analysis of bioimpedance data in lungs. The aim of this study is to use temporal information to evaluate changes in the impedance signal due to the mechanism of ventilation and perfusion produced by the lungs. Preliminary results show: 1) correlation between ventilation and perfusion with the bioimpedance signal and 2) changes in the amplitude of the bioimpedance time signal depending on the pathology. As conclusion, together with cycled averaged data, temporal data could be useful for lung pathologies distinction.

Keywords: lung; electrical impedance spectroscopy (EIS); modulation; bronchoscopy.

1. Introduction

Lung pathologies present different histological results. Some pathologies lead to an increase of cell concentration and extracellular matrix in lung tissue while others lead to the destruction of the lung parenchyma. Moreover, other lung pathologies lead to the increase of mucous that hinders the passage of air in the respiratory tract. Electrical impedance spectroscopy (EIS) offers an opportunity to differentiate lung disorders based on the different patterns associated with each of them. Moreover, changes in the blood perfusion and changes in the ventilatory movement of the tissue (two phenomena present during the acquisition of lung bioimpedance measures) may help to differentiate these lung pathologies.

In previous studies, Sanchez *et al.* observed the effect of the ventilation and the perfusion of the blood present in the alveoli in the EIS measurements taken using the 4-electrode method [2]. However, the 4-electrode method, as discussed in Company-Se *et al.* [1] when measuring lung tissue is more difficult for the clinicians than the measurement of bioimpedance data with the 3-electrode method due to the difficulty of ensuring the contact of the 4 electrodes with the tissue target. Also, the capacity of tissue differentiation is the same on both methods. For this reason, EIS lung measurements using the 3-electrode method are being taken in the current project during a bronchoscopy process.

The aim of this study is to demonstrate the effect of the ventilation and the perfusion mechanisms in the bioimpedance signal in preliminary measurements.

2. Materials and methods

Participants

Minimally invasive EIS lung measurements are being taken in patients for whom a bronchoscopy is indicated at the "Hospital de la Santa Creu i Sant Pau" using the 3-electode method in bronchi, healthy lung tissue and in pathological tissue if applied (neoplasm, emphysema, pneumonia and fibrosis). Ethics approval has been obtained from the Ethics

Committee of Hospital de la Santa Creu i Sant Pau (CEIC-73/2010) according to principles of the declaration of Helsinki. All patients participating in the study have provided signed informed consent.

Measurement system

To acquire the bioimpedance measures, a tetrapolar catheter, 115 cm long with a diameter of 1.65 mm (5 F) is being used (Medtronic 5F RF Marinr steerable catheter with electrode separation 2/5/2 mm). Also, two skin electrodes (Ambu BlueSensor VLC ref: VLC-00-s/10 and 3M Company ref: 9160F) placed on the right side of the patients at the level of the ribs are being used.

The measurement system consists of an optically insulated battery powered patient interface (including the impedance front end), a rugged PC platform based on a National Instruments PXI system and an analog-optical interface to connect the PXI with the insulated front end. An arbitrary waveform generator generates a multisine excitation signal which is a broadband signal composed of 26 frequencies between 1 kHz and 1 MHz.

To acquire the bioimpedance measurements, only the electrode located at the tip of the catheter is used to inject the current and to detect the potential while the low current and the low potential electrodes correspond to the two skin electrodes. A more detailed explanation of the measurement system is included in Company-Se *et al.* [1].

To acquire the ventilation and the ECG signals the polygraphy monitoring device Embletta MPR from Natus, with a thoracic inductive band, is used.

Measurement protocol

Records of 12 seconds of bioimpedance measurements (60 spectra/s) are obtained by inserting the catheter through the bronchoscope working channel. Patients are placed in a supine position during the process. Topical 2% lidocaine is used to anaesthetise the upper airway as well as intravenous sedation is provided through the procedure. Prior to bronchoscopy, computed tomography (CT) of the thorax was performed as part of the diagnostic process of respiratory diseases and to guide the bronchoscopy procedures.

Data extraction

To compare the effect of the ventilation and the perfusion on the bioimpedance signal a 30-points double-pass moving-average filter is applied to the signal to extract the ventilatory modulation. The difference between the original signal and the signal filtered is supposed to be the modulation corresponding to the perfusion.

3. Results

Efect of the ventilatory and perfusion modulations in the bioimpedance signal

Figure 1 shows the 12 seconds acquisition of the bioimpedance magnitude signal at 33 kHz, in blue, as well as the breathing, in black, and electrocardiographic (ECG), in red, signals.
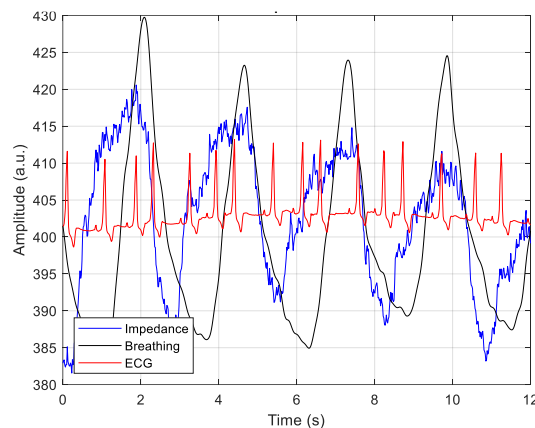

Figure 1. Superposition of the 12 seconds impedance signal at 33 kHz with the ventilation and ECG signals in a healthy lung tissue location

Figure 2 shows the power spectral density of the impedance signal (blue) after applying the 30-points double-pass moving-average filter and the ventilation signal (orange).
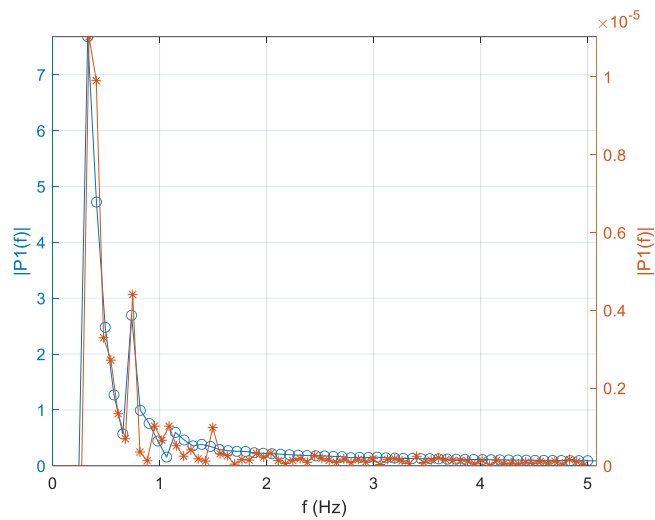
Figure 2. Power spectral density of the bioimpedance signal after applying a 30-points double-pass moving-average filter (blue, peak at 0.33 Hz) and power spectral density of the ventilation signal (orange, peak at 0.33 Hz).

Figure 3 shows the power spectral density of the signal after making the difference between the original signal and the signal resulting of the application of the 30-points double-pass moving-average filter (blue), considered to be the perfusion signal, and the power spectral density of the ECG signal (orange).
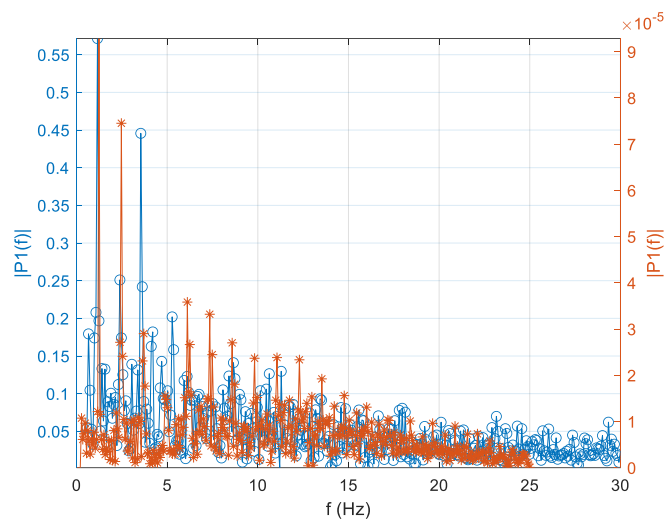

Figure 3. Power spectral density of the perfusion signal (blue, peak at 1.2 Hz) and ECG signal (orange, peak at 1.2 Hz).

Changes in amplitude of the bioimpedance signal based on different states of the tissue

Figure 4 shows amplitude changes due to ventilation depending on the state of the tissue measured at 33 kHz from 3 different cases (healthy tissue, pneumonia and neoplasic tissue). Healthy tissue shows a higher breathing modulation than neoplasic lung tissue which, in turn, shows higher breathing modulation than the area of lung with pneumonia. Also, different ventilatory frequencies and shapes are visible.
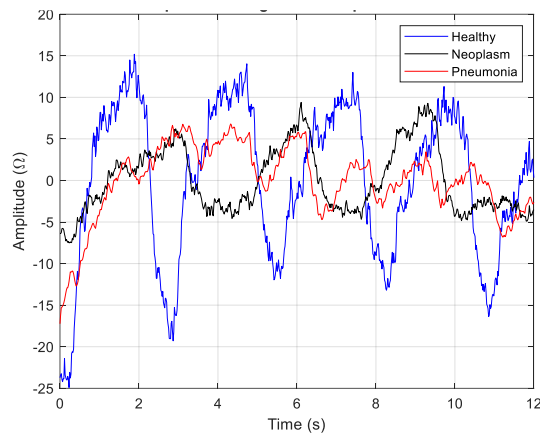
Figure 4. Amplitude changes in bioimpedance signals at 33 kHz from different patients and different tissue states.

4. Discussion

Electrical impedance spectroscopy can represent an opportunity to differentiate lung pathologies in order to complement the actual diagnostic processes. Together with averaged impedance results, temporal information could be useful to improve the tissue differentiation through changes in amplitude and shape of the signals acquired due to the effect of the ventilation and the perfusion.

The effect of the modulation is easily observable while the effect of the perfusion is not (Figure 1). The comparison between the spectrum of the signal considered to be the breathing modulation and the spectrum of the breathing signal (Figure 2) show a high frequency component at the same frequency (between 0.3 and 0.4 Hz) validating the existing modulation due to the inhalation and exhalation of the patients during the acquisition of the measure.

The effect of the perfusion is not so easily observable. This effect is demonstrated in the power spectrum of the two signals, the one representing the perfusion extracted from the bioimpedance signal and the ECG. In both cases there is a high frequency component in the 1.2 Hz corresponding to the cardiac rhythm.

The presence or absence of these two modulations could be used in the future to distinguish between different tissue states. An absence of breathing modulation could represent that the tissue measured is rigid while a high modulation of perfusion could represent the presence of neoplasic tissue, due to the nature of this pathology. These changes have also been demonstrated on Figure 4 in which the amplitude of the neoplasic tissue due to breathing is lower than the amplitude for healthy tissue. This phenomenon is due to the higher concentration of cells in the neoplasic tissue and, in consequence, the lower concentration of air. We have also seen that the amplitude of the signal related to breathing in lung with pneumonia is lower than the amplitude of the neoplasic tissue signal. This phenomenon could be due to the excessive concentration of mucous, which hinders the air flowing through the ventilatory ways.

5. Conclusions

Ventilatory and perfusion modulations are present in the bioimpedance signal and could be a tool to distinguish between different lung pathologies.

References

[1]   Company-Se G, Nescolarde L, Pajares V, Torrego A, Riu P J, Rosell J and Bragós R 2022 Minimally Invasive Lung Tissue Differentiation Using Electrical Impedance Spectroscopy: A Comparison of the 3- and 4-Electrode Methods *IEEE Access* **10** 7354–67

[2]   Sanchez B, Vandersteen G, Martin I, Castillo D, Torrego A, Riu P J, Schoukens J and Bragos R 2013 In vivo electrical bioimpedance characterization of human lung tissue during the bronchoscopy procedure. A feasibility study *Med. Eng. Phys.* **35** 949–57

ANNEX 3: Relaxation differences using EIS through bronchoscopy of healthy and pathological lung tissue

Title: Relaxation differences using EIS through bronchoscopy of healthy and pathological lung tissue

Authors: Georgina Company-Se, Lexa Nescolarde, Virginia Pajares, Alfons Torrego, Albert Rafecas, Javier Rosell, Pere J. Riu, and Ramon Bragós

Conference: 45th Annual International Conference of the IEEE Engineering in Medicine and Biology Society

Relaxation differences using EIS through bronchoscopy of healthy and pathological lung tissue

Georgina Company-Se, Lexa Nescolarde*, Virginia Pajares, Alfons Torrego, Albert Rafecas, Javier Rosell, *Member, IEEE,* Pere J. Riu, *Member, IEEE* and Ramon Bragós

Abstract— The use of electrical impedance spectroscopy for lung tissue differentiation is an opportunity for the improvement of clinical diagnosis. The aim of this work is to distinguish among different lung tissue states by evaluating the differences among impedance spectrum parameters between two separate frequencies (15 kHz and 307 kHz) in the beta dispersion region. In previous studies we have used single frequency measurements for tissue differentiation. Differences ($P < 0.05$) are found between those tissues that undergo an increase in tissue density (neoplasm and fibrosis) and those tissues that lead to tissue destruction (emphysema). Electrical impedance spectroscopy shows its utility for lung tissue differentiation for diagnosis improvement among pathologies with different tissue structure. Further studies are necessary for the differentiation among those tissue states that are more similar to each other.

Clinical Relevance— Expand the diagnostic tools currently available in bronchoscopy by using minimally-invasive bioimpedance measurements to differentiate between lung patterns.

I. INTRODUCTION

The diagnosis of peripheral lung lesions in patients who are suspected of having lung cancer remains a challenge. The measurement of Electrical Impedance Spectroscopy (EIS) could allow the differentiation of pathological tissue and help in the choice of the specific sampling location and allow the selection of the biopsy area in real time.

Bioimpedance (Z) is defined as the opposition that the tissue offers to the flow of an electrical current administrated. When the administrated current is alternating current the bioimpedance is frequency dependent. When several frequencies into a wide range of frequency is used to measure bioimpedance then EIS is performed. The Z has a resistance (R) component, which is the opposition produced by the extracellular and intracellular medium and a reactance (Xc) component, produced by the capacitive behavior of the cell membranes. From these two terms, the bioimpedance module (|Z|) defined as $\sqrt{R^2 + Xc^2}$ and the bioimpedance phase angle (PA) described as $\tan^{-1}(\frac{Xc}{R})$ can be extracted. PA is produced because the capacitance causes a lag between the current and the voltage [1]–[3].

Due to the capacitive behavior of the cell membranes, between the tens of kHz and the tens of MHz the biological tissue produces a relaxation, called beta-dispersion [4]. Beta dispersion produces a drop in the permittivity (ε) with an associated increase in conductivity [5]. Moreover, depending on the tissue properties the beta dispersion produces variations [6].

The aim of this study is to differentiate among different lung tissue states (neoplasm, fibrosis, pneumonia, healthy lung tissue and emphysema) by evaluating differences among impedance parameters in the beta-dispersion region of each of the tissues through minimally-invasive EIS acquired through a bronchoscopy process.

II. MATERIALS AND METHODS

A. Participants

Minimally invasive EIS measurements were carried out in a total number of 102 patients (Age: 66 ± 14 yr; Weight: 74.5 ± 17.2 kg; BMI: 26.8 ± 4.3 kgm-2) with a bronchoscopy prescribed between November 2021 and August 2022 at the "Hospital de la Santa Creu i Sant Pau" of Barcelona. The number of samples divided per classes obtained were: 30 healthy lung, 29 neoplasm, 23 emphysema, 12 fibrosis and 22 pneumonia.

Ethics approval was obtained from the "Hospital de la Santa Creu i Sant Pau" (CEIC-73/2020) according to principles of the Declaration of Helsinki for experiments with human being. All patients proved signed informed consent.

B. EIS measurements

Minimally-invasive EIS measurements acquired through the 3-electrode method were obtained by injecting a multisine current signal (from 1 kHz to 1000 kHz) between a distal tetrapolar catheter electrode and a skin electrode. The injection of current induces a voltage that is measured between the distal electrode and a second skin electrode. Impedance signal is acquired using a sample frequency of 60 spectra per second during 12 seconds. A complete description of the impedance measurement system and of the calibration procedure can be found at Company-Se et al [7].

C. Measurement protocol

Minimally-invasive EIS measurements were acquired though a bronchoscopy. Radiological evaluation (chest CT or/ and PET CT) was performed before bronchoscopy. The upper airway was anaesthetized and intravenous sedation was

F. A., S. B.*, S.F, S.G and E.H authors are with the Department of Electronics Engineering, Universitat Politècnica de Catalunya, Barcelona, 08034 Spain (corresponding author to provide phone: +34 934137286; e-mail: lexa.nescolarde@upc.edu).

T. C F. D and F.E Authors are with the Department of Respiratory Medicine, Hospital de la Santa Creu i Sant Pau, Barcelona, 08041 Spain

provided. The acquisition of the bioimpedance data was carried out by inserting the catheter through a port of the bronchoscope. Endoscopic exploration and diagnostic procedures were indicated accordance with the guidelines.

D. Data analysis

The averaged spectra of the minimally-invasive bioimpedance measured through the 12 seconds acquisition time was used for data visualization among healthy lung tissue, neoplasm, fibrosis, pneumonia and emphysema. Data was obtained between 1 kHz and 1 MHz although 15 kHz to 307 kHz was the frequency range chosen to visualize the bioimpedance data. Low frequency values (below 15 kHz) and high frequency values (above 307 kHz) were discarded due to electrode effects and capacitive coupling induced errors respectively.

While in Company-Se et al [7] absolute values of the impedance parameters were used to differentiate between tissue states, in the current study, to perform tissue differentiation the difference between low (15 kHz) and high (307 kHz) frequency mean bioimpedance values were calculated for |Z|, PA, R and Xc.

Shapiro-Wilk test was used to assess the distribution of normality of the variables (the difference between low and high mean bioimpedance values in |Z|, PA, R and Xc). Normally distributed variables are shown as mean $\pm$ standard deviation (SD) and 95% confidence interval (CI) of the mean (lower bound – upper bound). One-way analysis of variance (ANOVA) with Tamhane t2 post-hoc test was used to determine statistically significant differences in the differences between low and high frequencies mean bioimpedance in |Z|, PA, R and Xc.

III. RESULTS

A. Multi-frequency response for minimally-invasive lung tissue measurements

Fig.1 to **Fig. 4** shows the mean impedance spectrum for bioimpedance |Z|, PA, R and Xc respectively for the frequency range of 15 kHz to 307 kHz for neoplasm (black), fibrosis (red), pneumonia (blue), healthy lung tissue (green) and emphysema (pink). Mean is represented by the continuous line and $\pm$SD is represented by dashed lines. Impedance |Z|, PA, R and Xc show higher differences between low and high frequencies in healthy lung tissue and emphysema.
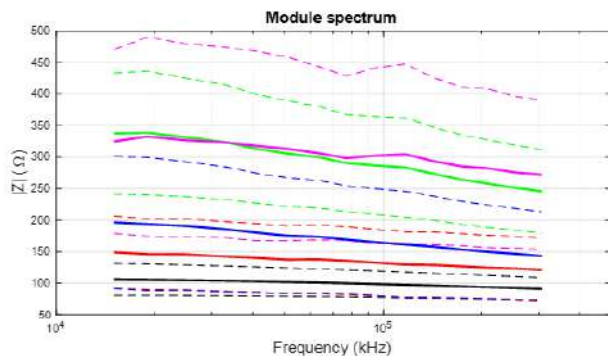

Figure 1. Modulus mean impedance spectrum for neoplasm (black), fibrosis (red), pneumonia (blue), healthy lung tissue (green) and

emphysema (pink). Mean is represented by the continuous line while $\pm$SD is represented with dashed lines.
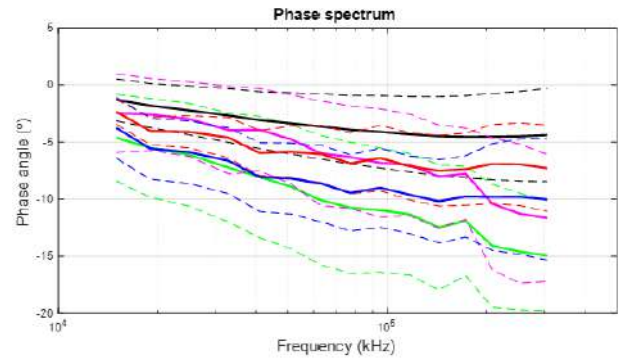

Figure 2. Phase angle mean impedance spectrum for neoplasm (black), fibrosis (red), pneumonia (blue), healthy lung tissue (green) and emphysema (pink). Mean is represented by the continuous line while $\pm$SD is represented with dashed lines.

Figure 3. Resistance mean impedance spectrum for neoplasm (black), fibrosis (red), pneumonia (blue), healthy lung tissue (green) and emphysema (pink). Mean is represented by the continuous line while $\pm$SD is represented with dashed lines.

Figure 4. Reactance mean impedance spectrum for neoplasm (black), fibrosis (red), pneumonia (blue), healthy lung tissue (green) and emphysema (pink). Mean is represented by the continuous line while $\pm$SD is represented with dashed lines.
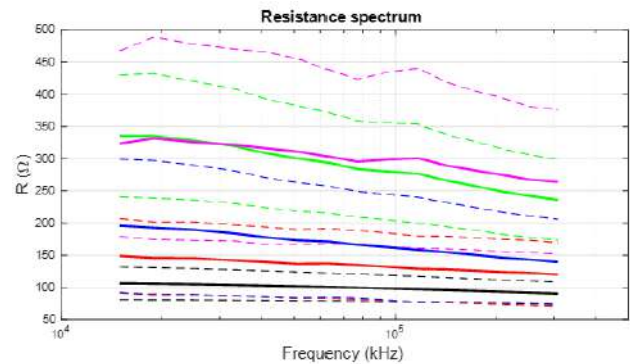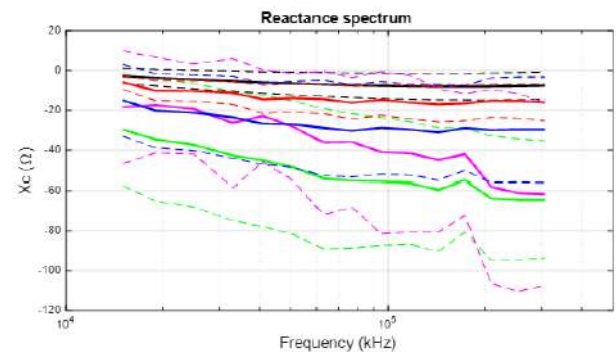
B. Differentiation of minimally-invasive electrical impedance spectroscopy bioimpedance measurements among tissue states from the differences between high and low frequency values

Table 1 lists the descriptive parameters, specified as the mean $\pm$ SD, 95% confidence interval for mean (lower bound

Table 1. Descriptions of minimally-invasive bioimpedance measurements for healthy lung tissue, neoplasm, emphysema, fibrosis and pneumonia. The variables normally distributed are shown as mean ± SD, 95% confidence interval for mean (lower bound and upper bound) while that non-normally distributed data is shown as statistic median (interquartile range, IQR) and minimum-maximum. In addition, the statistic of the Fisher (F) coefficient for variance analysis and the statistical significance (P) are also shown.

	Mean ± SD 95% CI (lower bound – upper bound)					F	P
	Healthy (n= 30)	Neoplasm (n= 29)	Emphysema (n= 23)	Fibrosis (n= 12)	Pneumonia (n= 22)		
Diff |Z| (Ω)	90.91 ± 55.82 (55.44 – 126.37)	17.84 ± 13.73 (9.12 – 26.56)	65.56 ± 63.15 (25.44 – 105.68)	27.91 ± 14.57 (18.66 – 37.17)	52.20 ± 29.69 (33.34 – 71.06)	12.73	<.001
Diff PA (°)	12.20 ± 3.05 (10.26 – 14.14)	4.37 ± 2.14 (3.01 – 5.73)	9.95 ± 2.99 (8.06 – 11.85)	5.42 ± 2.92 (3.57 – 7.27)	5.85 ± 4.43 (3.03 – 8.66)	15.24	<.001
Diff R (Ω)	100.69 ± 59.12 (63.13 – 138.25)	18.36 ± 14.14 (9.37 – 27.34)	74.13 ± 71.34 (28.80 – 119.46)	28.98 ± 15.30 (19.26 – 38.71)	54.55 ± 31.99 (34.22 – 74.87)	13.47	<.001
Diff Xc (Ω)	48.30 ± 27.85 (30.60 – 65.99)	6.83 ± 3.67 (4.50 – 9.17)	44.18 ± 24.53 (28.60 – 59.77)	10.58 ± 6.86 (6.22 – 14.94)	15.21 ± 15.12 (5.60 – 24.81)	15.68	<.001

and upper bound) of the difference between the mean values of |Z|, PA, R and Xc at 15 kHz and 307 kHz and the results of the one-way ANOVA including the Fisher coefficient (F) for healthy lung tissue (n = 30), neoplasm lung tissue (n = 29), emphysema (n = 23), fibrosis (n = 12) and pneumonia (n = 22). One-way ANOVA test shows statistical significance (P < 0.001) for the four parameters. Higher Fisher coefficient is obtained in PA and Xc.

Table 2 shows the Tamhane t2 test results for the multiple comparison test evaluating the difference in the mean values of |Z|, PA, R and Xc between the lowest frequency (15 kHz) and the highest frequency (307 kHz). Statistical differences are found between the following groups: healthy and neoplasm; healthy and fibrosis; healthy and pneumonia; emphysema and fibrosis; emphysema and pneumonia; neoplasm and emphysema; neoplasm and pneumonia. No statistical differences are found between healthy and emphysema; neoplasm and fibrosis and between fibrosis and pneumonia in any of the four parameters (|Z|, PA, R and Xc).

IV. DISCUSSION

This study aims to evaluate differences among different lung tissue states (neoplasm, fibrosis, pneumonia, healthy lung tissue and emphysema) through differences into the beta dispersion region.
Beta dispersion, produced between tens of kHz and tens of MHz, is due to the interfacial polarization of cell membranes, that act as barriers for the passive transport of ions between the ionic solutions that are present inside and outside the cells [4], [8]. When current penetrates the cell membranes (when frequency increases) causes reactance and phase angle to increase and resistance and modulus to decrease [1] (**Fig. 1** to **Fig. 4**). As also seen in **Fig 1** to **Fig 4**, changes in cell membranes due to lung disorders produce changes in the

mean impedance spectrum obtained producing different changes in the beta dispersions based on the tissue states. Neoplasm (black) and fibrosis (red) results in a flattened spectrum, as compared with healthy lung tissue (green) and emphysema (pink).

The beta dispersion produces differences in mean impedance values between high and low frequencies, producing significant differences (P < 0.001) in |Z|, PA, R and Xc (**Table 1**). Tamhane t2 post-hoc test showed significant differences between: neoplasm and pneumonia (|Z|, R), healthy lung tissue (|Z|, PA, R and Xc) and emphysema (|Z|, PA, R and Xc); fibrosis and healthy lung tissue (|Z|, PA, R and Xc) and emphysema (PA and Xc); pneumonia and healthy lung tissue (PA, R and Xc) and emphysema (Xc). Non-significant differences were found (P > 0.05) between fibrosis and neoplasm; fibrosis and pneumonia and between healthy lung tissue and emphysema. Healthy lung tissue and emphysema have more air content than others patterns. In emphysema, the increase in inflammatory cells and oxidative stress produce the secretion of proteases which produces direct damage to structural cells and destruction of alveolar walls. The air content present in lungs in proportion to the tissue is higher compared to neoplasm, fibrosis and pneumonia. Neoplasm is characterized by a cell growth and an increase of vascularization and fibrosis is characterized by an increase of tissue non-over-vascularized. The similitude in both pathologies regarding the increment of tissue and, in turn, cell concentration makes not possible to distinguish through minimally-invasive bioimpedance measures between both pathologies. In pneumonia, the inflammatory response is initially characterized by a congestive phase with vascular hyperemia followed by an exudative phase in which the presence of neutrophils and fibrin increases, which can completely occupy the alveolar spaces. Despite the clinical differences between pneumonia and fibrosis, there are several pathological phases that could hide the differences.

Table 2. Tamhane t2 post-hoc test results for the difference between low and high frequency of the mean impedance parameters (|Z|, PA, R and Xc)

Post hoc Tamhane t2 test							
			P				**P**
Diff |Z| (Ω)	Healthy	Neoplasm	<.001	**Diff PA (°)**	Healthy	Neoplasm	<.001
		Emphysema	0.129			Emphysema	0.876
		Fibrosis	<.001			Fibrosis	<.001
		Pneumonia	0.063			Pneumonia	0.028
	Neoplasm	Emphysema	0.025		Neoplasm	Emphysema	<.001
		Fibrosis	0.161			Fibrosis	0.896
		Pneumonia	0.002			Pneumonia	0.296
	Emphysema	Fibrosis	0.336		Emphysema	Fibrosis	0.023
		Pneumonia	1			Pneumonia	0.398
	Fibrosis	Pneumonia	0.113		Fibrosis	Pneumonia	0.99
			P				**P**
Diff R (Ω)	Healthy	Neoplasm	<.001	**Diff Xc (Ω)**	Healthy	Neoplasm	<.001
		Emphysema	0.18			Emphysema	0.999
		Fibrosis	<.001			Fibrosis	<.001
		Pneumonia	0.038			Pneumonia	0.005
	Neoplasm	Emphysema	0.015		Neoplasm	Emphysema	<.001
		Fibrosis	0.159			Fibrosis	0.441
		Pneumonia	0.002			Pneumonia	0.091
	Emphysema	Fibrosis	0.207		Emphysema	Fibrosis	<.001
		Pneumonia	1			Pneumonia	0.012
	Fibrosis	Pneumonia	0.106		Fibrosis	Pneumonia	0.826

V. Conclusion

In conclusion, the study of differences in impedance parameters at separated frequencies into the beta dispersion region due to changes in lung tissue states can be used for the differentiation among different lung pathologies. The difference in the impedance parameters in the beta dispersion region is higher between those pathologies that lead to an increase of tissue (neoplasm and fibrosis) and those pathologies that lead to higher air content in lungs (emphysema). The use of minimally-invasive bioimpedance measurements to differentiate between lungs patterns aims to expand the diagnostic tools currently available in bronchoscopy. However, further studies are necessary for the differentiation among the lung disorders that are more similar to each other.

Acknowledgment

References

[1] H. C. Lukaski, 'Biological indexes considered in the derivation of the bioelectrical impedance analysis', *Am. J. Clin. Nutr.*, vol. 64, no. 3, pp. 397S-404S, Sep. 1996, doi: 10.1093/ajcn/64.3.397S.

[2] H. C. Lukaski, N. Vega Diaz, A. Talluri, and L. Nescolarde, 'Classification of Hydration in Clinical Conditions: Indirect and Direct Approaches Using Bioimpedance', *Nutrients*, vol. 11, no. 4, p. 809, Apr. 2019, doi: 10.3390/nu11040809.

[3] S. Khalil, M. Mohktar, and F. Ibrahim, 'The Theory and Fundamentals of Bioimpedance Analysis in Clinical Status Monitoring and Diagnosis of Diseases', *Sensors*, vol. 14, no. 6, pp. 10895–10928, Jun. 2014, doi: 10.3390/s140610895.

[4] H. P. Schwan, 'Electrical properties of tissues and cell suspensions: mechanisms and models', in *Proceedings of 16th Annual International Conference of the IEEE Engineering in Medicine and Biology Society*, Baltimore, MD, USA, 1994, pp. A70–A71. doi: 10.1109/IEMBS.1994.412155.

[5] G. Martinsen, S. Grimnes, and H. P. Schwan, 'INTERFACE PHENOMENA AND DIELECTRIC PROPERTIES OF BIOLOGICAL TISSUE', 2002.

[6] H. P. Schwan and S. Takashima, 'Electrical Conduction and Dielectric Behavior in Biological Systems', in *digital Encyclopedia of Applied Physics*, Wiley-VCH Verlag GmbH & Co. KGaA, Ed. Weinheim, Germany: Wiley-VCH Verlag GmbH & Co. KGaA, 2003, p. eap106. doi: 10.1002/3527600434.eap106.

[7] G. Company-Se *et al.*, 'Effect of Calibration for Tissue Differentiation Between Healthy and Neoplasm Lung Using Minimally Invasive Electrical Impedance Spectroscopy', *IEEE Access*, vol. 10, pp. 103150–103163, 2022, doi: 10.1109/ACCESS.2022.3209809.

[8] S. Grimnes, *Bioimpedance and bioelectricity basics*. Boston, MA: Elsevier, 2014.